Development of Novel Signal Amplified-Virus Sensing Platform using Tunable Localized Surface Plasmon Resonance and Electrochemically Active Liposome

THESIS

Development of Novel Signal Amplified-Virus Sensing Platform using Tunable Localized Surface Plasmon Resonance and Electrochemically Active Liposome

June 2020

Graduate School of Science and Technology

Department of Bioscience

Shizuoka University

Fahmida Nasrin

TABLE OF CONTENTS

LIST OF FIGURES

LIST OF TABLES

LIST OF ABBREVIATIONS

Ab	Antibody
APTES	(3-Aminopropyl) tiethoxysilane
AuNPs	Gold nanoparticles
BSA	Bovine serum albumin
CdO	Cadmium oxide
ChikVE1	Chikungunya virus E1 protein
DI water	Deionized water
DLS	Dynamic light scattering
DOPC	1-palmitoyl-2-oleoyl-sn-glycero-3-phosphocholine
DOPG	1,2-dioleoyl-sn-glycero-3-phospho-(1'-rac-glycerol)
DPV	Differential pulse voltammetry
DSPE	1,2-distearoyl-sn-glycero-3-phosphoethanolamine-N [amino(polyethylene glycol)-2000] (ammonium salt)
EDC	N-(3-dimethylaminopropyl)-N-ethylcarbodiimide
EDS	Energy-dispersive X-ray spectroscopy
fg	femto gram
HDA	Hexadecylamine
$HAuCl_4$	Chloroauric acid
HEV-LP	Hepatitis E virus-like particle
KOH	Potassium hydroxide
LOD	Limit of detection
LSPR	Localized surface plasmon resonance
MB	Methylene blue
mM	mili molar
MNP	Magnetic nanoparticle
NHS	*N*-hydroxysuccinimide
nm	Nanometer
ODE	1-octadecene
NoV	Norovirus
NoV-LP	Norovirus-like particle

OA	Oleic acid
ODE	1-Octadecene
PBS	Phosphate-buffered saline
pg	pico gram
QDs	Quantum dots
S	Sulfur
Se	Selenium
SPR	Surface plasmon resonance
Te	Tellurium
TEM	Transmission electron microscopy
TGA	Thioglycolic acid
TOP	Trioctylphosphine
TOPO	Trioctylphosphine oxide
WSSV	White spot syndrome virus
XPS	X-ray photoelectron spectroscopy
XRD	X-ray diffraction
ZnO	Zinc oxide
11-MUDA	11-mercaptoundecanoic acid
-SH	Thiol group
$-NH_2$	Amine group
-COOH	Carboxyl group

ABSTRACT

The ongoing research in nanotechnology is emerging in the most challenging field of virus sensing as life undergoes to threatened due to the rapid spread of several viral infections recently. Precise and sensitive methods for virus detection are in high demand for the diagnosis and control of diseases. The key to highly sensitive detection methods should be reliable in the early stage of infection, which may improve the probability of survival. To improve sensitivity, proper signal amplification of target needs where the system can generate strong indication for easy detection even in the presence of a few virus particles.

The main aim of this thesis is to develop various biosensing platforms by using different nanocomposites along with their application in the sensing field, which further leads to virus detection. The study includes the synthesis, characterization of nanocomposites, and applications in developing biosensors for virus detection. Different sensing mechanisms are adequately explained and shown by schematic illustrations. The presented work in this thesis can give some new ideas for the development of biosensors for virus detection.

In this work, the limitations of the sensing process have overcome without compromising its advantages. Here, the work has focused on the optical and electrochemical sensing process by incorporating different nanoparticles like quantum dots (QDs), gold nanoparticles (AuNPs), etc. and established various techniques for sensing target analytes with high specificity, sensitivity, and low detection limit. Therefore, to find out the simplicity and reliable method of biosensing was the first and foremost goal of this work.

The whole work about this thesis describes five chapters (**Chapter 2, 3, 4, 5,** and **6)** along with the introduction (**Chapter 1**) and conclusion (**Chapter 7**).

Chapter 2 describes the detail about the chemicals, materials, virus samples, different antibodies used in this whole work. Used instruments in this study for the characterization and analysis of the nanoparticles and nanocomposites, along with the sensing procedures, were introduced.

Chapter 3 describes the concepts, principles, and detection mechanisms for virus sensing using plasmonic and electrochemical methods.

Chapter 4 describes the construction and application of a new method of the virus sensing system. In this work, the CdSeTeS QDs/AuNPs nanocomposite was employed to induce localized surface plasmon resonance (LSPR) of gold nanoparticles (AuNPs) and fluorescent quantum dots

(QDs). While adding the target virus into the solution, the steric hindrance between AuNPs and QDs induced LSPR signal for the virus detection. This method applied to norovirus-like particles (NoV-LPs) and a clinical sample of norovirus (NoV) detection, which exhibited a 100-fold higher sensitivity than the commercially available ELISA kit. Therefore, the developed biosensor showed ultrasensitive detectability at a femtogram level of the target virus.

Chapter 5 describes the preparation and application of a tunable biosensor for virus detection based on the designed LSPR and optimized the distance between fluorescent CdZnSeS/ZnSeS QDs and AuNPs in a controlled way. Different lengths of peptide chains were designed and employed for creating the distance between these two nanoparticles which is the crucial point to generate surface plasmon effect towards virus detection. In this case, binding of target virus on the nanocomposite initiates steric hindrance on the LSPR, and therefore, amplified the signal. A highly sensitive biosensor has been developed for entrapping different concentrations of the influenza virus with a very low limit of detection.

Chapter 6 describes the advancement of a new model of dual-functional signal amplification method to detect viruses by using the combination of a fluorescent and a redox indicator dye encapsulated liposome. Amine functionalized liposomes have been constructed containing hydrophobic fluorescent QDs in the lipid bilayer and centrally filled with methylene blue (MB) as a redox indicator. In the presence of the target, the dual functional liposome can form a sandwich structure with the virus and APTES-coated Fe_3O_4 magnetic nanoparticles (MNP) and magnetically separate the target virus from its analyte medium. After the external burst out of the liposome, the released QDs and MB generate the fluorescence and electrochemical signal, respectively. This amplified signal can give the indirect quantification of the target virus.

Chapter 7 summarizes all the results found in the presented work and includes a discussion about further research scope in this field.

Overall, the scope of the thesis encompasses the development of different nanocomposites and applicability of the proposed sensors for the detection of several viruses in a wide range of sensing platforms, which can give some new ideas. Based on the obtained results, these proposed biosensors can be a good alternative in the large potential window of the application on monitoring disease and point-of-care of infectious viral diseases.

CHAPTER 1

INTRODUCTION

1. Introduction

1.1 Prelude

A wide range of optical biosensors in various fields emerging from environmental safety, drug design, food industry, clinical diagnosis has been developed by optically sensitive nanocomposite in the recent progress of nanotechnology (Zhou *et al.*, 2013). In the last decade, several biosensors that have developed exponentially in the combination of nanotechnology as the label-free and real-time detection of biological and chemical materials are in high demand (Anh *et al.*, 2017; Dutta Chowdhury *et al.*, 2017). There are a lot of limitations to performing these sensing systems in real applications. In the serological system, the analysis for antibody detection may present false results or incorrect data interpretations (Tate and Ward, 2004). There is a lack of sensitivity in immunofluorescence assays whereas detection by culture system is time-consuming. Therefore, the development of fast, sensitive, and cost-effective sensing platforms is in high demand for virus detection.

This presented thesis work mainly focuses on the extensively emerging field of biosensing applications. The advancements in biological and medical research such as quantitative or qualitative measurements, analysis of biomolecules, purification, etc. have been accelerated in the last two decades (Gerard *et al.*, 2002; Ramanathan *et al.*, 2005; Xia *et al.*, 2010). Additionally, nanoparticles used to develop biosensors having exclusive properties of optical activity may establish their nanocomposites highly suitable for sensing applications. Numerous approaches have been presented to develop biosensor in the last two decades by using the surface and interfacial properties of different nanomaterials by reaching a proper combination (Chowdhury *et al.*, 2014; Chowdhury *et al.*, 2018; Ganganboina and Doong, 2018; Monošík *et al.*, 2012). Different nanocomposites can be used in a variety of applications in the practical field such as

biosensors, drug delivery systems, biomedical imaging, etc. These nanomaterials and their nanocomposites are gaining attractions in these application areas due to the optical and physical properties along with easy processability and lower cost.

In this thesis, the work has been focused on the development of optical and electrochemical biosensor for the establishment of some new ideas for virus sensing. Localized surface plasmon resonance (LSPR) based biosensors has emerged significantly as their fabrication process is easy to carry out and it requires a very low number of samples to make a drastic change in fluorescent intensities, fast and containing low limit of detection (Gowri and Sai, 2016; Jeon *et al.*, 2018; Kulakovich *et al.*, 2002; Liu *et al.*, 2015). However, sometimes the applicability of these methods is restricted due to their sensitivity as a little change in the formation of nanocomposites may affect the sensing mechanism. Therefore, it is extremely needed to optimize the process by investigating more intensely to get excellent repeatability.

It is established that a metallic nanoparticle combined with the properties of surface plasmon resonance can be an excellent option to observe the change of fluorescence of adjacent quantum dots (QDs) fluorophores with improved sensitivity (Takemura *et al.*, 2017). Due to the optical properties of QDs including broad absorption, narrow emission, biocompatibility, etc., they have been widely used in the development of various biosensors (Anderson and Chan, 2008; Bruchez *et al.*, 1998; Chan and Nie, 1998).

Additionally, the development of dual-functional biosensors has been emerged as an advancement in the field of sensing application which can combine two or more detection methods in a single platform and ensures better sensitivity and reliability for detection (Chuong *et al.*, 2017; Peng *et al.*, 2019; Xiong *et al.*, 2018). Therefore, it is necessary to work and develop dual-functional biosensors to overcome the limitations and challenges in the conventional methods.

However, keeping all the challenges in mind, the present thesis encompasses the synthesis, characterization of different nanoparticles and utilizing these nanocomposites in developing optical and electrochemical biosensors after optimizing all the probable parameters including size, concentration, etc. for the best sensing performance. Overall, it is very advantageous to generate some new ideas and develop various methods of biosensing systems easily and cost-effectively which may overcome the challenges in a real application.

1.2 Nanomaterials

A nanostructured material can be defined as an object containing at least one dimension which is less than a hundred nanometers. For example, nanotextured surfaces of graphene have only one dimension on the nanoscale range which is between 0.1 and 100 nm. Again, the nanotubes such as different conducting polymers, metal oxide nanorods, etc. have two dimensions on the nanoscale range where the diameter of the tube is between 0.1 and 100 nm, whereas the length can be greater enough. Finally, spherical nanoparticles such as quantum dots, gold nanoparticles, etc., have three dimensions in the nanoscale range in 0.1 and 100 nm for each dimension.

The nanomaterials have special characteristic properties which are,

(1) their large fraction of surface can be exposed in reaction,

(2) contains high surface area compared to the volume,

(3) their spatial confinement, and finally,

(4) the imperfections are very reduced.

Therefore, there are several advantages to use nanomaterials in the nanocomposites. First, the nanostructures can be closely packed together due to their very small particle size. Therefore, the higher surface area and volume capacity can be used for application by accelerating interactions

between them. All these properties and advantages make the nanomaterials extremely useful for their application in various fields like biosensors, drug delivery systems, biomedical imaging, etc. (**Fig. 1.1**).

When a material dimension is in nano size, the surface to volume ratios is significantly increased. Therefore, the corner atoms form bonds with the highest affinity with the analyte molecules by the edge and on a plane surface. For this reason, it provides great importance in the sensing and catalytic application. Nanocomposites can play role in extremely high biological and chemical reactivity due to their small particle size. Therefore, the exceptional chemical and physical properties of nanocomposites open new opportunities for application in a biosensor.

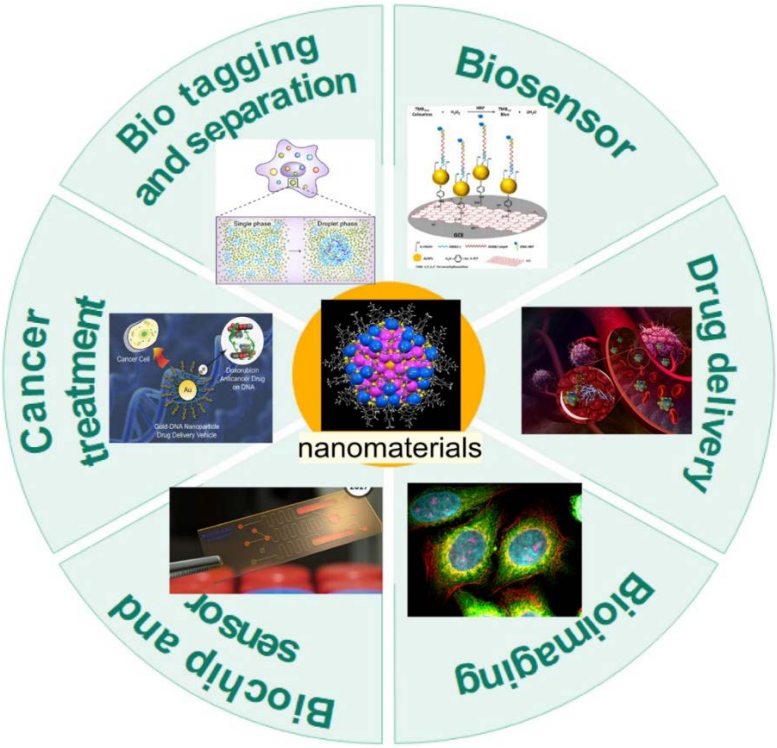

Fig. 1.1 Different nanocomposites can be used in a variety of applications in the practical field such as biosensors, drug delivery systems, biomedical imaging, etc.

1.2.1 Gold nanoparticles (AuNPs)

AuNPs are noble metal nanoparticles in biosensing application which are widely used (Li *et al.*, 2010) because of their optical and electronic properties, biocompatibility, and easy to produce and modify (Biju, 2014).

Surface plasmon resonance (SPR) is the most interesting optical characteristic of AuNPs where irradiation with one specific wavelength of light causes an electron oscillation in the conduction band. When the incident wavelength is greater than particle size, propagation of the oscillating electrons cannot occur along the surface. Therefore, the polarization of electron density occurred on one side of the particle. This phenomenon (Hao *et al.*, 2004; Mulvaney, 1996) is strongly dependent on the nanoparticle including shape and size along with the dielectric constant of its environment (Kelly *et al.*, 2003). For this reason, it is a huge advantage for bioanalytic as it will make a change of the oscillation frequency and thereafter, the color change of AuNPs can easily be observed with a bare eye. As a consequence, a wide range of efficient colorimetric biosensors have been developed for detecting analytes (Liu and Lu, 2004; Oldenburg *et al.*, 2002; Reynolds *et al.*, 2000; Xu *et al.*, 2009).

Using SPR transduction of gold nanoparticles has also proved to be beneficial in bioanalysis. This phenomenon depends on the change of dielectric constant of its environment of surface plasmon where the detection can be observed based on the changes of intensity, angle, state of the light reflection (Guo, 2012; Wijaya *et al.*, 2011). AuNPs also can be used for labeling by attachment with antibodies or DNA strands and in this case, the signal can be enhanced by several orders of magnitudes (Zeng *et al.*, 2013) which is a very convincing approach for application.

Another powerful ability of AuNPs is to detect a single molecule by forming a transduction platform. By sensing the refractive index obtained from localized surface plasmon resonance

(LSPR) can be coupled with enzyme-linked immunosorbent assay (ELISA) using AuNPs of 60 nm sizes (Chen *et al.*, 2011). The benefit of using AuNPs is also confirmed for the highly sensitive biosensing methods of surface-enhanced Raman spectroscopy (SERS). Biosensors constructed of the surface plasmon supported signal amplification (Moskovits, 1978), the detection limits become as low as to the single-molecule level (Hossain *et al.*, 2009; Lim *et al.*, 2011; Nie and Emory, 1997; Saha *et al.*, 2012).

Besides the above supreme properties of gold nanoparticles, they also can transfer electrons in a variety of electroactive biological materials. This phenomenon is often used in the biosensing of the redox enzyme where it needs to catalyze the oxidation or reduction of the analyte. In this case, AuNPs act as the electron shuttle to the redox center of the enzyme by electron transfer in the redox reaction of the electrode.

AuNPs are one of the most promising nanomaterials for use in bioanalytic and a wide range of research fields for their outstanding properties which can also be tuned and adjusted. Depending on the application purpose, any desired size and shape of AuNPs can be obtained using different synthesis techniques (**Fig. 1.2**). With the different morphologies obtained by different synthesis, it may vary resulting in different properties of AuNPs such as catalytic, optical, and electronic behavior (Eustis and El-Sayed, 2006).

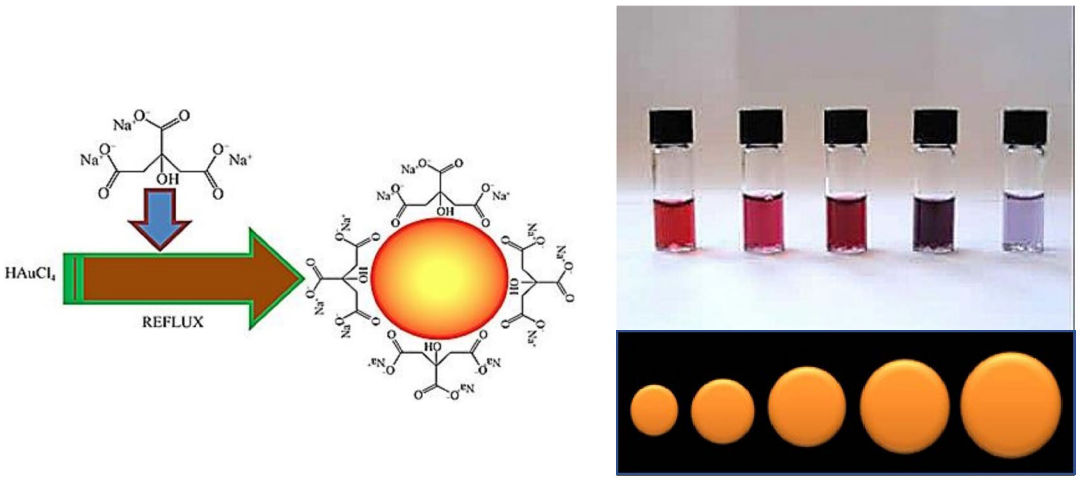

Fig. 1.2 Synthesis of citrate stabilized gold nanoparticle (Ghosh and Chattopadhyay, 2013) and changing color depending on size (Hansen *et al.*, 2005). (Reprinted, with permission from Scientific Research and ACS publications, respectively)

1.2.2 Inorganic quantum dots (QDs)

Semiconductor quantum dots (QDs) are one of the most useful nanoparticles as they characterize a unique optical property including high quantum yield, narrow emission, broad excitation, and photochemical stability and can emit different color and emission wavelength depending on size (**Fig. 1.3**). It can be used as a fluorescent dye in a wide range of biomedical research and labeling along with in vitro or in vivo imaging.

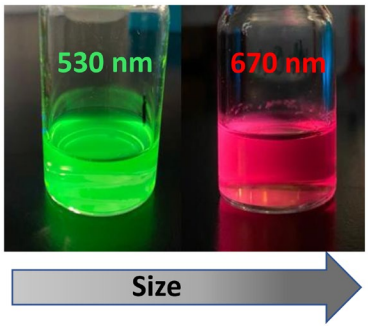

Fig. 1.3 Depending on size, QDs emit different color and an emission wavelength.

QDs are a prominent luminescent semiconducting nanocrystal used for bioanalytic. QDs are mostly studied which are based on cadmium chalcogen elements (S, Se, Te) and provide a size-dependent narrow emission spectrum along with a large absorption spectrum (Murray *et al.*, 1993; Park *et al.*, 2007; Reiss *et al.*, 2009). Due to this, QDs enable multiplexed analysis efficiently by using optical transduction (Geißler *et al.*, 2010; Petryayeva and Algar, 2014). Moreover, as core/shell QDs (**Fig. 1.4**) have high photochemical stability, therefore, they can overcome the structural defect and enhance their photostability and quantum yields (Dabbousi *et al.*, 1997; Jaiswal *et al.*, 2003).

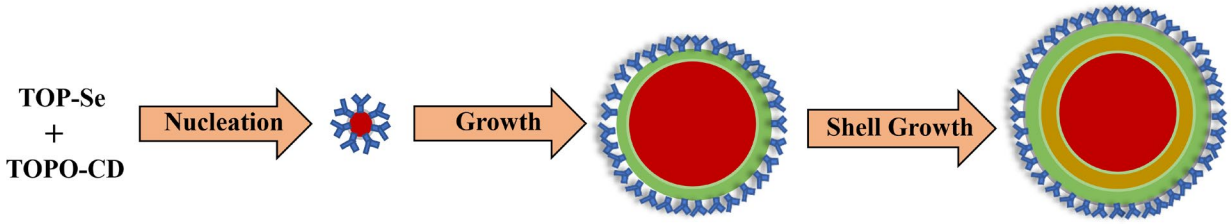

Fig. 1.4 Colloidal synthesis of CdSe QDs nanoparticles. A cadmium precursor dissolved in the tri-n-octylphosphine oxide (TOPO) and a selenium precursor dissolved in tri-n-octylphospine (TOP), initiates the rapid nucleation of CdSe nanoparticles at high temperature. Then, the particle growth occurred and reached at desired size, and collected by precipitation.

Nowadays, biocompatible coatings can be obtained on QDs (Biju *et al.*, 2010) which can provide functional groups for bioreceptor conjugation. Therefore, any kind of biomolecule can be bound to these QDs without hampering its advantages.

In Förster (Fluorescence) Resonance Energy Transfer (FRET) phenomenon, quenching of fluorescence of QDs was observed (Clapp *et al.*, 2006) in which the quenching effect depends on the non-radiative energy transfer between the donor (QD) and the acceptor. After that, when the

quencher is removed, it revealed to the original state of QD fluorescence. This phenomenon is commonly used for sensing applications of optical DNA and oligonucleotide (Freeman *et al.*, 2013; Zhang *et al.*, 2005).

Gold nanoparticles are excellent acceptor and can quench QD very strongly. The distance between QD and the quencher is the key factor in the detection principles. Another effect that can enhance the optical signal is it can interact with the surface plasmon property on gold surfaces which can excite QDs following to light emission (Wei *et al.*, 2009). Another report confirmed that various combined forms of gold and QDs can be beneficial for strong enhancement signals in an SPR imaging-based biosensor (Malic *et al.*, 2011).

Overall, the above-described principles and examples suggest that QDs is a promising alternative material to organic fluorophores and the combination of different nanoparticles along with their specific characteristic properties can make a promising way in the area of biosensors with new and highly sensitive techniques.

1.3 Localized surface plasmon resonance (LSPR)

Surface plasmon resonance (SPR) biosensors are very common in the fields of biochemistry, biotechnology, bioengineering, etc. where they can be used as detection probes for ion sensing, infectious diseases, protein-DNA interactions, binding events and other biological surface modifications (Campbell and Kim, 2007; Eum *et al.*, 2003; Jeong *et al.*, 2008; Lee *et al.*, 2015; Patskovsky *et al.*, 2008; Yeom *et al.*, 2013). Additionally, LSPR biosensor has been revised from this SPR mechanism which has recently made extreme interest in the wide range of research areas.

The development in nano-optics has open the new way for the fabrication of label-free and highly sensitive optical transducers by using the mechanism of LSPR from metal nanostructures

in recent years (Sepúlveda *et al.*, 2009). The most commonly used optical biosensors are based on the SPR changes in thin gold films (Homola, 2008). As the metal nanostructures have exclusive optical properties that can be applied to connect with their LSPR which can be defined as the optical phenomenon where the collective oscillations of the electron can be generated in the metal nanostructures that are bounded by a dielectric (Bohren and Huffman, 1983). Such noble metal nanostructures are, for example, gold or silver nanoparticles. Among these, a silver nanoparticle can provide larger and more intense LSPR, but AuNPs are mostly used because of their chemical stability which favors its application in biosensing.

LSPR is based on the extinction or measurements of scattering on the metal nanostructures. When a light beam interacts with metal nanostructures, then absorption occurred of some portion of the incident photons and some portions are scattered. Therefore, the excited LSPR induces enhancement due to the absorption and scattering. Generally, this intense and prominent change of LSPR can be simply detected by optical spectroscopy, therefore, this system has become an attractive tool for sensing applications (Sepúlveda *et al.*, 2009).

As the AuNPs are one of excellent metal nanostructure as an acceptor and can highly quench QD, the distance between QD and gold nanostructure is the key point for the detection mechanism. According to previously reported LSPR-based phenomena, closely positioned (<5 nm) acceptor and QD cause quenching of LSPR, while 6 – 12 nm distance between two nanoparticles shows enhancement of LSPR and after certain distances (>12 nm) it shows no effect on LPSR (Feng *et al.*, 2015; Li *et al.*, 2016; Nasrin *et al.*, 2020; Nasrin *et al.*, 2018). (**Fig. 1.5**).

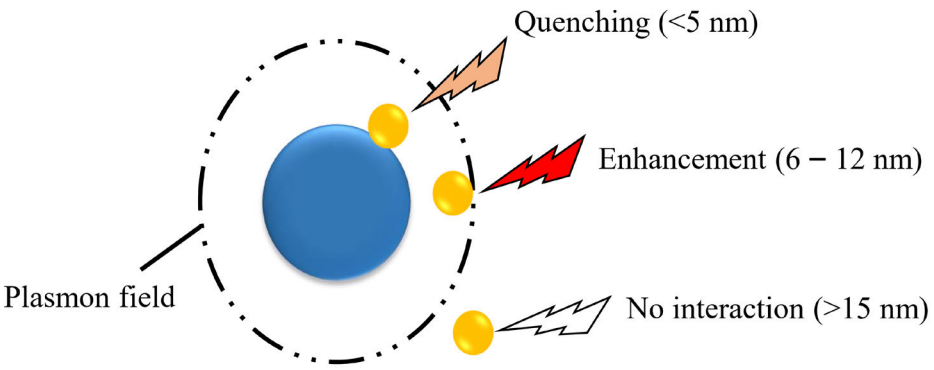

Fig. 1.5 Optical properties of distance-dependent LSPR where specific distance is responsible for the effect.

The combination of LSPR along with fluorescent molecules has been introduced as a well-established phenomenon for biosensing application in recent years (Acimovic *et al.*, 2014; Adegoke *et al.*, 2017; Brolo, 2012; Jeon *et al.*, 2018; Satija *et al.*, 2015; Takemura *et al.*, 2017). The fluorescent intensities of the fluorophore can be influenced in a controlled manner by the adjacent metal nanoparticles such as Ag, Au, Pt, etc. which depends on the size, shape, and concentration of the nanostructure (Brolo, 2012; Feng *et al.*, 2008; Oh *et al.*, 2017; Saha *et al.*, 2012; Singh and Strouse, 2010; Wu *et al.*, 2018). Similarly, a combination of fluorescent QDs with AuNPs has been improved the sensing performance (Adegoke *et al.*, 2017; Ganganboina and Doong, 2018; Schreiber *et al.*, 2014; Shi *et al.*, 2015).

Therefore, AuNPs plays the crucial role by generating SPR in various LSPR-based sensing system by influencing the fluorescence of QDs, whereas altering the distance between them can generate variation in the detection signal. It is already established that in LSPR mechanism, when QDs and AuNPs are combined in a very near distance, quenching of LSPR occurred and while maintaining a certain distance between them, a drastic change of fluorescence enhancement can

be observed and finally, when these two duos are far apart, there is no LSPR effect (Feng *et al.*, 2015; Li *et al.*, 2016; Nasrin *et al.*, 2020; Nasrin *et al.*, 2018). (**Fig. 1.6**).

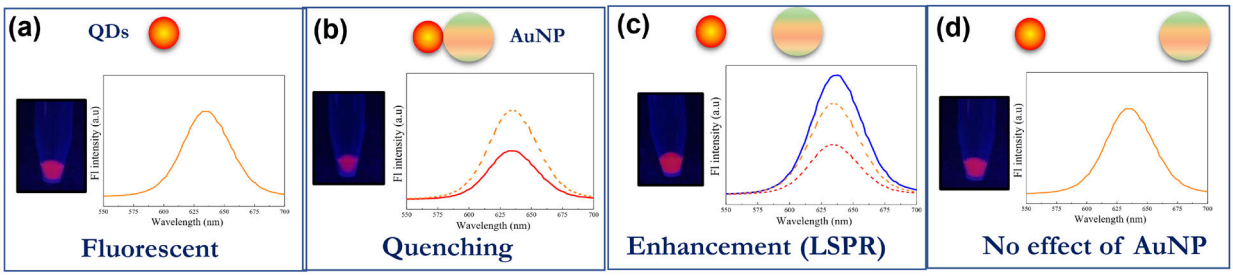

Fig. 1.6 Distance-dependent LSPR phenomena. **(a)** Fluorescence of an individual QDs, **(b)** Fluorescence quenching due to close position of QD and AuNP, **(c)** Fluorescence enhancement at a certain distance of QD and AuNP, **(d)** No effect on LSPR for far distance.

It has been noticed that by changing the distance between metal nanostructures containing SPR effect and inorganic fluorescent molecules like QDs along with optimizing various parameters, a promising biosensing platform can be developed by using this LSPR-based phenomenon.

1.4 Biosensor

The biosensor is defined as a transducer or probe which includes a biological component as the main functional element for the detection of biomolecule qualitatively or quantitatively (Cornell *et al.*, 1997; Thévenot *et al.*, 2001). Certain biochemical reactions are used in biosensors which are mediated by immunosystems, isolated enzymes, tissues, whole cells, or organelles to detect specific chemical components by optical, thermal, or electrical signals (Aberl and Kößlinger, 1998; Rogers, 2006).

Biosensors are comprised of mainly three parts:

1. A biological element e.g. microorganisms, tissues, enzymes, organelles, enzymes, antibodies, cell receptors, nucleic acids, etc.

2. A detector element, or transducer such as optical, electrochemical or piezoelectric, etc. which converts the signal generated from the interaction of the biological element with the target analyte into another signal which can be easily readable and quantified.

3. A signal processor or electronics which are principally responsible for the reading and analysis of the results in the most accessible way.

Generally, a biosensor generates a digital electronic signal which depends on the concentration of a specific target or set of biochemicals/chemicals proportionally. Biosensor devices are rapid, specific and, simple to operate that can be easily fabricated. The generated biochemical signal can be converted to an electronic signal by the transducer as presented in **Fig. 1.7**. An electrical device generates the signal in a way that can be easily amplified, analyzed, displayed, and stored. The biosensors incorporated with biomolecules in the formed nanocomposites are characterized via several measurements of electronic and spectroscopic ways to confirm the immobilization process.

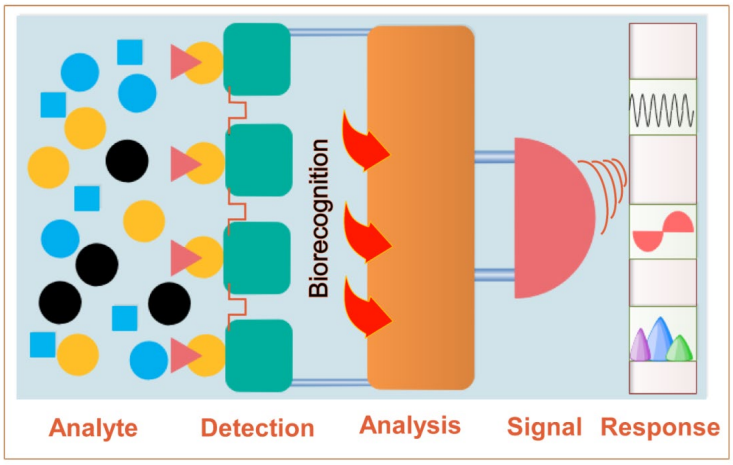

Fig. 1.7 Basic mechanism of a biosensor, where, analyte can be recognized and analyzed followed by the signal response.

Biosensors' efficacy can be determined through the determination step of an analyte. Reproducibility, cross-sensitivity, and stability are performed to establish the biosensor more

practical rather than the commercially available techniques in a diagnostic laboratory. The selectivity of a biocomponent within a biosensor has a keen level of interest but susceptible to such conditions as pH, temperature, and ionic strength (Reshetilov and Bezborodov, 2008). In the solution phase, biological molecules like enzymes, antibodies, receptors, and cells, etc. generally have a very short lifetime. Surface area, porosity, reaction conditions, hydrophilic character of immobilizing matrix, and methodology are an important factor for the activity of immobilized molecules. Several techniques such as physical adsorption, gel entrapment (Dave *et al.*, 1994; Gupta and Chaudhury, 2007), cross-linking (Gregg and Heller, 1990; Miao and Tan, 2000), and covalent (Chu *et al.*, 2007; Williams and Blanch, 1994), etc. have been used to immobilize biological molecules on the materials. Biomolecules can be immobilized on various matrices such as gels, membranes, carbon, silica, graphite, polymeric films, etc. Designing a biosensing platform that is compatible with the biological component can lead to a sensitive and fast detection system. Different nanoparticles and nanocomposites are such attractive possible materials for the biosensing applications.

1.4.1 Classification of biosensor

Several types of biosensors are available for various measurement techniques which are as follows:

Optical biosensors: Optical biosensors are the most used methods based on light absorption or emission which can be measured as the significance of a biochemical reaction. In this type of optical biosensors, light waves are followed by the optical fibers for suitable detections (Li *et al.*, 2010; Liu *et al.*, 2018; Rajeev *et al.*, 2018).

Electrochemical biosensor: The principle of this type of biosensing system involves the transduction of different electrochemical signal produced after the interaction between the

substrate and analyte where the measurement will be performed by an electrical parameter such as voltage, current, impedance, resistance, conductance, etc.

Conductometric biosensors: the change in the conductance of the biological material in a pair of metal electrodes is measured in this type (Chouteau *et al.*, 2005; Muhammad-Tahir and Alocilja, 2003).

Amperometric biosensors: the current is measured at a persistent potential in this type of biosensor (Razola *et al.*, 2002; Xu *et al.*, 2003).

Impedimetric biosensors: Impedance change after immobilization is the parameter for measurement (Esseghaier *et al.*, 2008; Shamsipur *et al.*, 2008).

Potentiometric biosensors: This type of sensing system is rarely used for detection but can be used for detecting enzymes immobilized in the electrodeposited polymer layers (Adeloju *et al.*, 1993).

Piezoelectric biosensors: These can be applied for measuring the deformation that occurred on crystals when an electrical potential is applied. The alternating current (A.C.) generates a standing wave in the crystal at a certain frequency which is dependent on the properties of the crystal. A change in the resonance frequency can occur where a crystal is coated with a biological element for recognition and binds with a target analyte that gives a signal. The sensitivity will greatly increase while using the surface acoustic waves (SAW) (Haddada *et al.*, 2018; Han *et al.*, 2018).

Among all the biosensing systems, optical and electrochemical methods are mostly studied and useful techniques. Toxic and nontoxic metal ions such as As, Hg, Pd, Cu, Zn, Fe, etc. are determined by an optical sensor and the limit of detection is at a very low level of concentration in the range of nano, pico and femtomolar (He *et al.*, 2018; Kaur *et al.*, 2018). Various biomolecules like glucose, cholesterol, protein, DNA, virus, bacteria, etc. are also detected by

optical measurements by using UV-vis absorption, fluorescence spectroscopy, surface plasmon resonance (SPR) spectroscopy, fluorescence correlation spectroscopy (FCS), etc. (Khatri *et al.*, 2018; Zhao *et al.*, 2018).

1.4.2 Optical biosensors

Optical biosensors containing an optical transducer that transforms a biological response into an easily measurable and quantifiable signal, as same as other conventional biosensors that apply magnetic, electrochemical, or acoustic (Fan *et al.*, 2008). Optical methods have several advantages over other mechanical or electrical label-free methods such as high sensitivity, cost cost-effectiveness, specification, and a wide range of applications. Generally, an optical biosensing system contains a biorecognition layer (i.e., biological probe) which is placed on the sensor surface. A biorecognition layer can be either functional proteins, biomaterials like ligands, antibodies, or a biological system such as bacteria, living cells, or tissues (Fang and Ferrie, 2008; Szekacs *et al.*, 2018). A change in optical properties has been occurred in the system due to the interaction between the biorecognition layer and the target analyte which can be detected by the optical transducer and further can be used to measure the quantity of the bound target analytes in the sample.

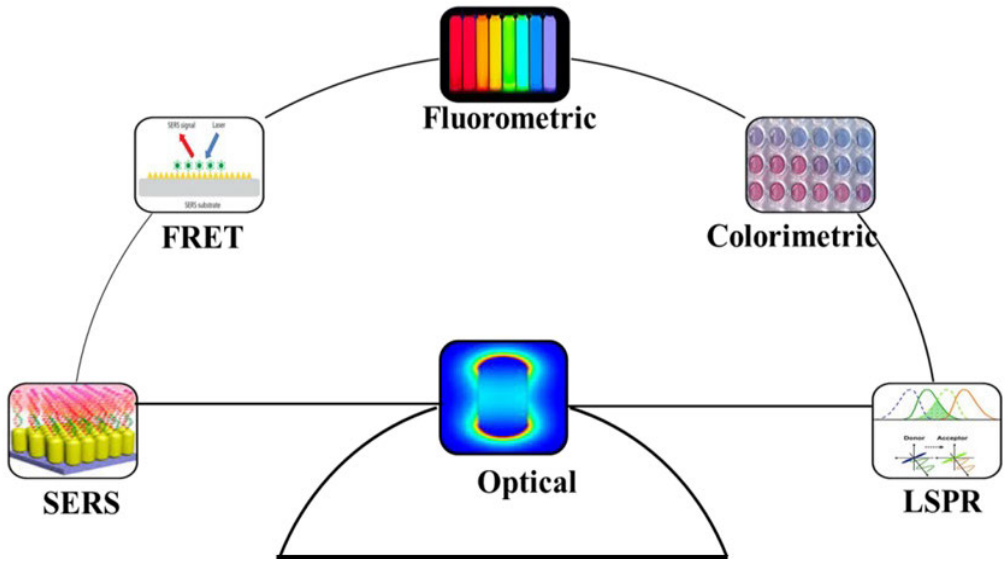

Fig. 1.8 Application of optical biosensor in various fields.

There are several optical sensing methods available (**Fig. 1.8**) such as surface-enhanced Raman spectroscopy (SERS), Förster resonance energy transfer (FRET), fluorometric, colorimetric, and localized surface plasmon resonance (LSPR). Typically, two detection methods are used to carry out the optical biosensing system which is label-free detection and fluorescence-based detection. The target molecule is usually labeled with different tags like fluorescence dye in the fluorescence-based method (Szekacs *et al.*, 2018). The presence of the target analyte can be determined quantitatively through the intensity of the fluorescent signal. These detection systems are very sensitive and able to detect as low as a single molecule, but the tagging process is very laborious and costly. On the other hand, a label-free detection system is easy to perform, cost-effective, and able to perform both quantitative and kinetic measurements. There is no need to label the target molecule so that the functionality remains the same in the label-free detection system (Ding *et al.*, 2018). In typical fluorescence-based detection, the signal generating based on the presence of the total number of analytes in the sample volume. In contrast, label-free sensing is based on the

change in the refractive index rather than the total sample mass which means the signal for detection is not depending on sample volume.

1.4.3 Electrochemical biosensors

Electrochemical biosensors are one of the basic research subjects along with their application for nearly fifty years. In 1962, the principle of the enzyme electrode with the glucose oxidase immobilization has been introduced at the New York Academy of Sciences Symposium by Leland C. Clark which was the first example of electrochemical biosensor (Clark Jr and Lyons, 1962). After the last three decade of research, now the biosensors can be explained in three different generations depending on the integration level. In the first-generation biosensor, the biocatalysts are either entrapped or bound in a membrane and fixed on the surface of the transducer. The second-generation biosensor involves the covalent fixation or adsorption of the biological component to the surface of transducer which permits to eliminate the semi-permeable membrane. In third generation biosensor, the biocatalyst can be directly bound to an electronic device that can transduces and amplifies the signal. Currently, there are many commercialized devices based on the chemical sensing method using for pathogens and toxic components. The most crucial part for the development of electrochemical biosensors is the incorporation of a suitable biomolecule in the biorecognition layer acting as an electroactive substance for detection by the physico-chemical transducer which can provide the signal for measurement. Generally, the surface of the biosensor has been functionalized with a biorecognition material for targeting species which can only interact with the analyte. Therefore, the sensor matrix is immobilized with monoclonal antibodies, specific enzymes, and specific DNA etc. The target specific binding between these two is very important in sensing application for generating a signal for detection with high specificity.

1.4.4 Liposome based biosensors

Liposomes having a unique structure, can possess both a hydrophilic and a hydrophobic region within it. For this reason, it can either encapsulate water-soluble molecules in the hydrophilic region of the liposome or immobilize water-insoluble molecules within hydrophobic region (Chen and Wang, 2015). Therefore, liposomes are often used as biological carriers of various chemicals, nanoparticles, and biomolecules, and can be used in different applications of drug delivery, chemical, and biological sensors. The surface of liposome can be modified to attach with target molecule which provide very specific binding to the receptor (Banerjee, 2001; Čeh and Lasic, 1998). Due to the structural advantage of liposome, it has received significant attention for use in sensing of biological and chemical detection. Various transduction technology like optical, fluorescence, and colorimetric can be combined with liposome, which can provide enormous signal amplification and therefore, achieve ultrasensitive assays (Ganganboina *et al.*, 2020). Due to the easy preparation, fabrication process, biocompatibility, and modification, liposomes proved to show superior advantages over other biostructures in biosensing system (Chen and Wang, 2015). It is also compatible to use with various sensing technology including nanoparticles, semiconductor quantum dots, immunoassay, fluorescence, electrochemical, and optical spectroscopy, etc. Target amplification is usually employed to achieve high sensitivity where a target attached with a single liposome, can produce intense signals by releasing their encapsulated signaling probes. Therefore, few numbers of target can generate immense signal for detection. In a previously reported single particle detection methods, liposome-QD complex could reach the detection at attomolar concentration of DNA without prior target amplification (Zhou *et al.*, 2013). Moreover, liposome-based detection system can easily be modified for multitarget detection and sensing by incorporating different sensing materials and target molecules (Chen and Wang, 2015).

In another report, a liposome-based dual-modality sensor containing colorimetric and electrochemical methods has been established to detect target virus with high sensitivity and accuracy (Ganganboina *et al.*, 2020). Though, many researchers have been working to establish highly sensitive methods, more effort is still needed to overcome the challenges for real application.

1.5 Application of biosensor for virus sensing

In recent years, virus sensing has been a challenging field in nanotechnology as there are several viral outbreaks taking place with accelerated mutation rates and creating huge economic loss (Weerathunge *et al.*, 2019; Ye *et al.*, 2017). Maybe the speedy infection rate of viruses occurs due to the easy traveling worldwide and has become a threat to public health (Bui *et al.*, 2015; Zang *et al.*, 2019). Recently, a very dangerous viral outbreak occurred and brutally affected people all over the world, the spread of COVID-19 transformed from the epicenter Wuhan, China to worldwide within few months and severely causing the death of people by transforming from one to another very fast (Liu *et al.*, 2020). Last few years of the database WHO also showed that 44,000 people have died due to hepatitis E virus infection in 2015, and annual death worldwide is almost 200,000 due to viral infection (Ganganboina *et al.*, 2020).

As the people from worldwide are suffering significantly from various viral infections, the development of fast and sensitive detection techniques has become a challenge to control this alarming situation. Therefore, biosensors having a low limit of detection is a vital issue (Chowdhury *et al.*, 2019; Dutta Chowdhury *et al.*, 2018; Hassanpour *et al.*, 2018; Tereshchenko *et al.*, 2017). Therefore, researchers are working devotedly to search for suitable techniques having enhanced sensitivity in the sensing platform including optical sensing (Ahmed *et al.*, 2014; Haes and Van Duyne, 2002; Qiu *et al.*, 2017). To obtain this, proper signal amplification of target should

be achieved where few numbers of viruses can generate a signal in high magnitude which is the key for early state detection.

For example, a fluorescent aptasensor system has been developed for sensitive detection of influenza virus by immobilization of guanine-enriched anti-rHA aptamers on the surface of the $Ag@SiO_2$ nanoparticles and performed as a sensing system based on metal-enhanced fluorescence (Pang *et al.*, 2015). Similarly, another sensing platform has been developed by the electrochemical and immune-sensing of an enzyme-induced bi-functional magnet for Influenza virus A (H7N9) detection (Wu *et al.*, 2015). Also, several efforts have been reported on optical sensing for virus detection (Chang *et al.*, 2010; Lee *et al.*, 2015; Takemura *et al.*, 2017). In a previously reported work, LSPR-induced optical transduction has been used for the detection of influenza virus A (H1N1) where AuNPs was conjugated with anti-NA and CdSeTeS QDs was conjugated with anti-HA antibody which can bind with the target influenza virus antigen NA and HA, respectively (Takemura *et al.*, 2017) (**Fig. 1.9)**. In this sensing system, the enhancement of fluorescence can be measured upon binding of the target virus which can trigger the LSPR effect from adjacent AuNPs. This system could detect the target virus successfully with high sensitivity.

However, these systems are quite expensive due to the double antibody needed to detect the target. Another disadvantage of this report showed the high background signal of fluorescence which hampers the surface plasmon signal.

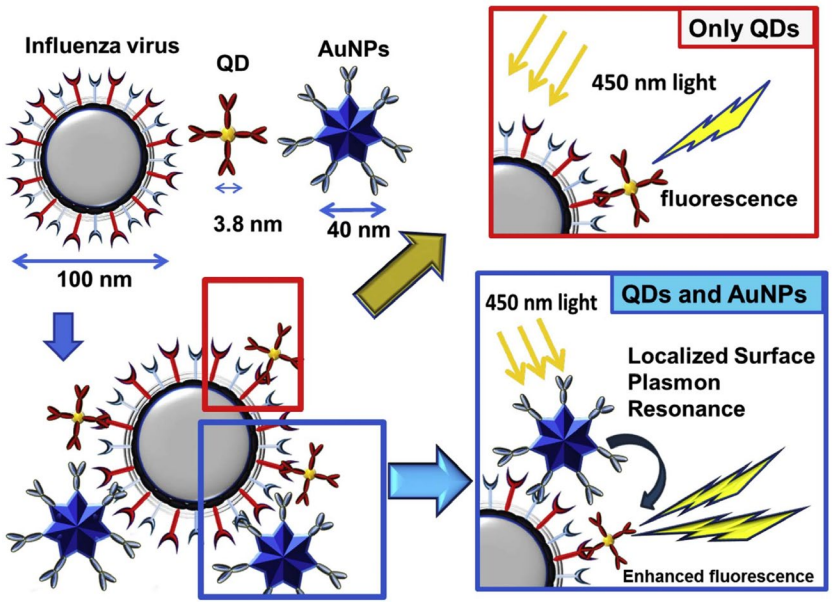

Fig. 1.9 Sensing principle for influenza virus using LSPR-induced fluorescence biosensor. (Takemura *et al.*, 2017) (Reprinted, with permission from Elsevier)

In the last few years, some researchers claimed to attain LSPR-based fluorometric sensors with having a very low limit of detection where they also used SPR-mediated fluorescence change (Feizpour *et al.*, 2015). Another report proposed a sensitive detection method for dengue DNA with its serotype identification which is also based on the change in the distance-dependent LSPR between AuNPs and QDs (Dutta *et al.*, 2019) (**Fig. 1.10**). In this work, four different nanoprobes were fabricated using a primer for individual serotype and covalently bonded with QDs. This sensor could identify dengue serotypes, in which fluorescence was enhanced in the case of dengue serotype 1 and 3 along with quenching phenomenon for the presence of dengue serotypes 2 and 4.

Here, without target DNA amplification, DNA was detected by applying the LSPR mechanism. Though this proposed sensor showed satisfactory results, still there is difficulty to perform this method for real sample analysis.

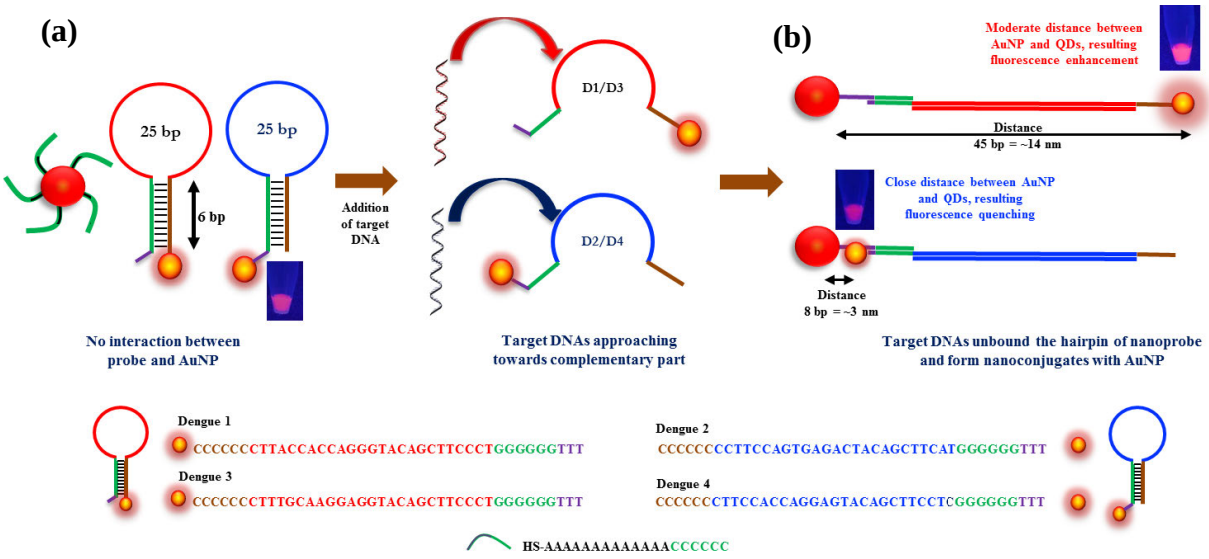

Fig. 1.10 Schematic representation for detecting dengue DNA with four different serotypes using distance dependent LSPR between AuNPs and hairpin ssDNA-CdSeTeS QDs **(a)** represents probe design and AuNPs functionalization, where, showing no interaction without target, **(b)** represents identification of target and fluorescence enhancement for dengue serotype 1 and 3 along with quenching for dengue serotype 2 and 4 due to the distance between AuNPs-dsDNA-CdSeTeS QDs (Dutta *et al.*, 2019). (Reprinted, with permission from The Royal Society of Chemistry)

However, these above reports also have limitations in the real application of clinical sample analysis, therefore, point-of-care detection is still difficult and rarely reported. Moreover, the reproducibility and reliability of these sensors have not still reached to the satisfactory level as all the parameters are not optimized well. A combined general biosensing system should have been introduced to detect analytes through optimized conditions.

1.6 Research objective

The development of ultrasensitive detection tools for virus sensing has emerged as the new challenge in ongoing nanotechnology in recent years. Several infectious viruses are circulating and keeping outbreaks with a continuous mutation which has become life-threatening all over the world. Therefore, a sensitive method for virus detection should be applied in the early stage of infection so that the probable survival rate can be increased.

Keeping this in mind, many researchers are aiming for the development of a biosensor system for virus detection, but the rapid and highly sensitive virus detection techniques have not yet been developed. There are several existing methods for virus detection such as virus isolation, enzyme-linked immunosorbent assay (ELISA), polymerase chain reaction (PCR), and next-generation sequencing, etc. which has many drawbacks including sensitivity, time, cost and equipment problems. Foremost, it is in extreme demand to establish a reliable biosensor to overcome all the lacking regarding the severity and challenges to face the emerging outbreak caused by viral infection where the prerequisite is to have the ability to determine the virus regardless of its low concentration.

The main objective of this thesis is to synthesize and establish different sensing methods for virus detection by using various nanocomposites that can be reliable, fast, cost-effective, and highly sensitive (**Fig. 1.11**). For this, various nanoparticles such as AuNPs, QDs, etc. have been incorporated to develop some optical and electrochemical techniques for virus detection with a low detection limit and high sensitivity.

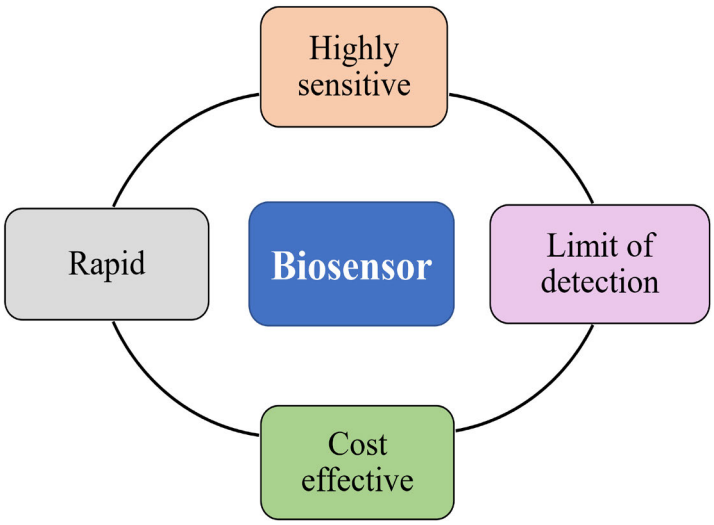

Fig. 1.11 A biosensor with desired target characteristics.

To achieve this, the specific objectives of this research are:

1. Preparation and construction of high throughput, low cost, and fast detection methods using gold nanoparticles, fluorescent semiconductor nanoparticles (i.e. QDs), etc.

2. Synthesis, characterization, and functionalization of the nanoparticles and nanocomposites to confirm their size, shape, and capability to conjugate with biomolecules.

3. Optimization and further application of the as-synthesized nanocomposites on various optical and electrochemical sensing platform for detecting several virulent viruses.

4. Confirmation and analysis of the signal restoration/enhancement/quenching effect regarding the sensing technique after accumulating target analyte or virus particles.

5. Quantification of a target analyte or virus from biomedical samples and further checking its applicability on clinical real samples.

Overall, this work provides some new ideas and an outlook on the synthesis of nanocomposites and advancement in applications towards sensing system for virus detection as well as other novel applications.

CHAPTER 2

EXPERIMENTAL SECTION

2. Experimental section

In this chapter, biological materials, chemicals, experimental techniques along with their instrumental specifications used in this thesis are described.

2.1 Materials

Table 2.1 List of biological reagents used in this work along with the supplier's name.

Biological Reagents	
Reagents	**Suppliers**
Anti-NoV antibody	Kindly provided by Prof. Tetsuro Suzuki, Hamamatsu University School of Medicine
Primary Ab for Hemagglutinin (HA) proteins of influenza virus A/H1N1 (New Caledonia/20/99) Mouse monoclonal antibody [B219M] Anti-white spot syndrome virus VP28 antibody [AB26935] Recombinant chikungunya virus protein (ab187240) Anti-chikungunya virus antibody [B1413M] (ab130889)	Abcam Inc. (Cambridge, UK)
Goat anti-rabbit IgG-horseradish peroxidase (HRP)	Santa Cruz Biotechnology (CA, USA)
Recombinant influenza virus A/H1N1 (New Caledonia/20/99)	Prospec-Tany Techno Gene Ltd. (Rehovot, Israel)
Norovirus-like particle (NoV-LP) HEV-like particle (HEV-LP) Anti-hepatitis E virus (HEV) antibody	Kindly provided by Dr. Tian-Cheng Li of Department of Virology, National Institute of Infectious Diseases
Zika virus	Kindly provided by Professor K. Morita, Institute of Tropical Medicine, Nagasaki University
White spot syndrome virus (WSSV)	Kindly provided by Dr. Jun Satoh, National Research Institute of Aquaculture of Japan Fisheries Research and Education Agency
Influenza virus A (H3N2)	Kindly provided by Dr. C. Kawakami, Yokohama City Institute of Health, Yokohama Japan
Norovirus (NoV)	Kindly provided by Mr. Fuyuki Abe, Shizuoka Institute of Environment and Hygiene, Shizuoka Japan

Table 2.2 List of chemicals used in this work along with the supplier's name.

Chemicals	**Suppliers**
Phosphate-buffered saline (PBS) buffer Sodium citrate Polyoxythylene Sorbitan monolaurate (Tween 20) Hydrogen peroxide (H_2O_2) Sulfuric acid (H_2SO_4) Methanol Potassium hydroxide (KOH) Trisodium citrate ($Na_3C_6H_5O_7$) Chloroform Acetone	Wako Pure Chemical Ind. Ltd. (Osaka, Japan)
$HAuCl_4$ *N*-(3-dimethylaminopropyl)-*N*-ethylcarbodiimide hydrochloride (EDC) *N*-hydroxysuccinimide (NHS) Bovine serum albumin (BSA) 11-mercaptoundecanoic acid (MUDA) 1-octadecene (ODE) Cadmium oxide (CdO) Thioglycolic acid (TGA) Tellurium (Te) L-cysteine Hexadecylamine (HDA) Zinc oxide (ZnO) Trioctylphosphine oxide (TOPO) Trioctylphosphine (TOP) Selenium (Se) Sulfur (S)	Sigma Aldrich Co., LLC (Saint Louis, MO, USA)
Tetramethylbenzidine (TMBZ)	Dojindo (Kumamoto, Japan)
Oleic acid	Nacalai Tesque Inc. (Kyoto, Japan)
1-palmitoyl-2-oleoyl-sn-glycero-3-phosphocholine (DOPC) 1,2-dioleoyl-sn-glycero-3-phospho-(1'-rac-glycerol) (DOPG) 1,2-distearoyl-sn-glycero-3-phosphoethanolamine-N-[amino(polyethylene glycol)-2000] (ammonium salt) (DSPE-PEG_{2000} amine)	Avanti Polar Lipids, Inc. (Alabama, AL, USA)

2.2 Methods

2.2.1 Synthesis of CdSeTeS QDs

Quaternary-alloyed CdSeTeS QDs were synthesized by the organometallic hot-injection method followed by our previously reported synthesis method in which the basic precursors were CdO, Se, and S (Adegoke *et al.*, 2015).

2.2.2 Preparation of L-cysteine-capped CdSeTeS QDs

As-synthesized hydrophobic CdSeTeS QDs were turned into hydrophilic QDs and the surface was functionalized with an amine group by conjugating the L-cysteine by a ligand exchange reaction. 2 g of L-cysteine and 3 g of KOH in 40 mL of methanol were dissolved to prepare a methanolic-KOH-L-cysteine solution. After that, the hydrophobic QDs in chloroform solution were added to the solution, and the hydrophilic QDs was precipitated from the solution by adding an appropriate volume of ultrapure deionized (DI) water. The solution was stimulated for a few minutes and was kept overnight to separate the water-soluble state and organic state. Finally, QDs were purified by using chloroform and acetone several times.

2.2.3 Preparation of AuNPs

A 35 µL of 2 mM $HAuCl_4$ and later on 300 µL of 100 mM tri-sodium citrate were added into a volumetric flask containing 25 mL of boiling water with the continuous stirring condition to synthesize AuNPs (Zhao *et al.*, 2008). The solution was continued to boil and stir for 15 min until the color was completely turned into pink.

2.2.4 Functionalized AuNPs by 11-mercaptoundecanoic acid (11-MUDA)

The Carboxyl group (-COOH) was generated on the surface of the AuNPs by making the attachment with 11-MUDA. 0.1 mM of MUDA (at pH 3) was added into AuNPs solution and

continued stirring for 2 h. The thiol group has been conjugated with AuNPs by a covalent bond with the through soft acid soft base reaction. After successfully functionalized the AuNPs with 11-MUDA, the solution was centrifuged at 6000 × g and cleaned with DI water to remove the excess MUDA from the solution.

2.2.5 Synthesis and preparation of solubilized CdZnSeS/ZnSeS QDs

CdZnSeS/ZnSeS QDs were synthesized by organometallic hot-injection synthesis method from the basic precursors like CdO, HDA, ODE, ZnO, TOP, Se, OA, and S followed by the previously reported method (Adegoke *et al.*, 2016).

QDs were made water solubilized by adding KOH-methanolic-TGA solution applying ligand exchange reaction (Adegoke *et al.*, 2016). Briefly, 2 mL of TGA and 3 g of KOH were added and dissolved together in 40 mL of methanol with continuous stirring. After that, this KOH-methanolic-TGA solution was combined with hydrophobic QDs solution which made the effective separation of the water-soluble state to the organic state with continuous stirring for 1 h and kept for overnight. The solution was centrifuged and washed with chloroform and acetone and finally dried in a fume hood to obtain high yield water-soluble QDs.

2.2.6 Synthesis and growth of different seeds of AuNPs

At 100°C, Na_3Ctr was dissolved for conducting the reduction steps of $HAuCl_4$ for the synthesis of various sizes of AuNPs (Leng *et al.*, 2015). Briefly, 200 μL of 1 M NaOH was added in 100 mL of 1 mM $HAuCl_4$ in a 250 mL of volumetric flask. The solution was continued to boil and stir and followed by adding 10 mL of 38.8 mM Na_3Ctr. After completing the reaction, the solution color was turned into wine-red. Finally, the reaction was stopped after 15 min and the final volume of the solution was made ~100 mL by adding deionized water into the solution.

The different volume of the above-synthesized seed solution was added with 227 μL of 44.7 mM $HAuCl_4 \cdot 3H_2O$ to obtain AuNPs growth solution. After that, 176 μL of 38.8 mM $Na_3Ctr \cdot 2H_2O$ was added to the solution and continued to stir until the color of the solution turned into wine red from colorless solution (Leng *et al.*, 2015).

2.2.7 Preparation of NoV-LPs and clinical sample of NoV

The standard method of VLP preparation was followed to obtain NoV-LPs (Ahmed *et al.*, 2016; Jiang *et al.*, 1992). Fecal samples of the patients containing foodborne illness, infectious gastroenteritis, were collected to detect clinical sample of NoVs by following the laws and ordinances. The proper guideline was followed for the sampling of NoV after receiving the approval of the Ethics Committee of Environment and Hygiene Institute in Shizuoka Prefecture (September 14, 2016).

2.2.8 Quantification of clinical sample of NoVs via real-time PCR

A 10 % suspension from feces in PBS was the starting material to collect RNA from Nov followed by extraction using QIAamp Viral RNA Mini Kit (QIAGEN, Tokyo Japan). Extracted RNA was treated with recombinant DNase (RNase-free) (TaKaRa Bio Inc., Shiga, Japan) and thereafter, Prime Script RT Reagent Kit (Perfect Real Time) (TaKaRa Bio Inc.) was performed for reverse transcription step. Finally, cDNAs were quantified by real-time PCR by using Premix EX Taq (Probe qPCR) (TaKaRa Bio Inc.) followed by the notice accordance with the Ministry of Health, Labor and Welfare, Japan (2003).

2.2.9 Synthesis of APTES coated Fe_3O_4 nanoparticles

Synthesis of Fe_3O_4 nanoparticle was followed by the previously reported standard method (Dutta Chowdhury *et al.*, 2017). In brief, 0.6 g of $FeSO_4 \cdot 7H_2O$ and 1.165 g of $FeCl_3 \cdot 6H_2O$ were

dispersed in 200 mL deionized water and heated at 60°C with vigorous stirring under nitrogen atmosphere. 20 mL of 8 M NH_4OH solution was added to precipitate surface immobilized Fe^{2+} and Fe^{3+} ions. The conversion of iron ions to iron oxides was ensured by maintaining the pH at about 11. A precipitate was observed and heated at 70°C for 6 h, and finally magnetic samples were washed by water and separated by magnetic separation. As synthesized Fe_3O_4 nanoparticles were coated with APTES by following the previously reported standard method (Ganganboina *et al.*, 2017). To dissolve the APTES, dry toluene was used as the reaction medium and finally the as synthesized Fe_3O_4 nanoparticles were added to it. To obtain the APTES-coated Fe_3O_4 nanoparticles, the mixture was then refluxed at 120°C for 20 h with continuous stirring. Finally, the APTES-coated Fe_3O_4 nanoparticles was washed by rinsing with fresh toluene to remove the excess APTES and was dried overnight and stored for further use.

2.2.10 Synthesis of liposome containing QDs and methylene blue (MB)

The as synthesized hydrophobic CdSe QDs were centrifuged at 10,000 rpm for 10 min and then re-dispersed in chloroform to measure the concentration. 10mM of MB solutions was prepared by dilution method in PBS. Dual functionalized amine liposomes were prepared according to our previous work (Ganganboina *et al.*, 2020). Briefly, 20 µL of hydrophobic CdSe QDs dissolved in chloroform and 200 µL mixture solution of 10 mM phospholipid of 1-palmitoyl-2-oleoyl-sn-glycero-3-phosphocholine (DOPC), 1,2-dioleoyl-sn-glycero-3-phospho-(1'-rac-glycerol) (DOPG), and 1 mM phospholipid of 1,2-distearoyl-sn-glycero-3-phosphoethanolamine-N-[amino(polyethylene glycol)-2000] (ammonium salt) (DSPE-PEG_{2000} amine) were taken as DOPC:DOPG:DSPE (molar ratio 50:40:10) in chloroform and added into 5 mL of glass vials. After that, it was evaporated by flowing stream of 99.9% nitrogen gas to produce a thin homogeneous lipid film layer on the glass wall. Then the vial was stored in a vacuum desiccator

for 12h to evaporate completely. To make the homogeneous lipid suspension, the lipid film was hydrated with 1 mL of the MB solutions and agitated on a vortex mixer until the lipid film had fully detached from the glass vial walls. Finally, a micro injection was used to get 200 nm unilamellar monodisperse QD-MB-liposomes by using extrusion for at least 5 times through a 200 nm pore size of polycarbonate membrane.

2.2.11 Quantum yield (QY) measurement of CdZnSeS/ZnSeS QDs

The measurement of quantum yield (QY) of QDs was carried out and calculated by using fluorescein as a standard fluorophore (Φ = 0.79) through the comparative fluorescence method. QDs and fluorescein solutions were prepared in five different concentrations using deionized water. After that, absorbance along with the corresponding fluorescence curve was obtained (**Fig. 2.1**) and calculated followed by the equation: $QY = Q_R\ [m/m_R][n^2/n_R^2]$. Here, m is the slope of line gained from the two calibration lines, n is the solvent refractive index and the reference fluorophore of known QY was shown as subscript R. $QY_{CdZnSeS/ZnSeS} = 0.79 \times 6.6/14.4 = 0.36$

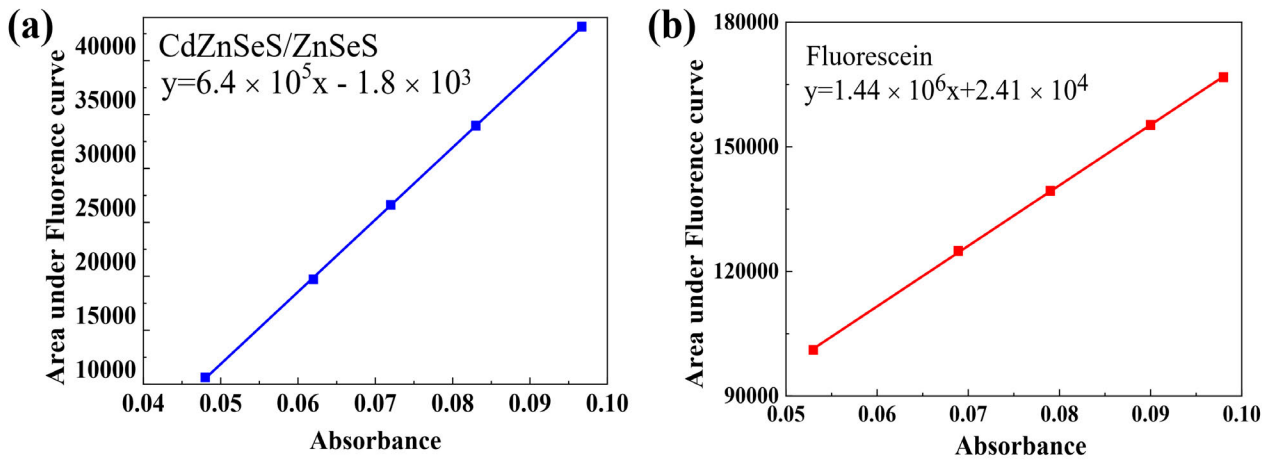

Fig. 2.1 The linear relationship between optical density and the corresponding area of the fluorescence curve from absorbance. **(a)** CdZnSeS/ZnSeS QDs and **(b)** fluorescein. (Nasrin *et al.*, 2020) (Reprinted with permission from Elsevier)

2.3 Instruments used for characterizations

In this chapter, the analytical techniques used for characterization (Transmission Electron Microscopy, X-ray Photoelectron Spectroscopy, X-ray Diffraction, Dynamic Light Scattering and UV-vis Spectroscopy) and detection (Fluorescence, electrochemical) have been described briefly. The detailed specification of the instruments has also been mentioned.

2.3.1 Transmission Electron Microscopy (TEM)

TEM images were obtained by using a TEM machine (JEOL, JEM-2100F, Tokyo, Japan) operated at 100 kV to check the size and surface morphology of the synthesized nanoparticles. High resolution transmission electron microscopic (HR-TEM) with energy dispersive spectroscopy (EDS) was performed by using a scanning electron microscopy system (JEM-16036, JEOL, Ltd., Tokyo, Japan) combined with JED-2300 EDS to observe the morphology, shape, and size of the prepared nanocomposites. The sample grid was prepared with fine dried samples which were prepared after proper sonication of the samples for 2 hr. A few drops of samples were placed on a copper grid and put in the incubator to dry well at 50ºC before observing by the microscope.

2.3.2 UV-vis Spectroscopy

Molecules containing non-bonding electrons (n-electrons) or π-electrons can absorb the energy in the form of visible or ultraviolet light to excite these electrons towards higher anti-bonding molecular orbitals. It can absorb a longer wavelength of light as the electrons are more easily excited. The spectrophotometer was used to measure this exciting light beam which refers to reflectance spectroscopy or absorption spectroscopy in the UV-visible region. UV-vis spectroscopy is commonly used in various fields for the quantitative measurement of different analytes such as highly conjugated organic compounds, transition metal ions, and biological

macromolecules. The measurements were taken by using a filter based multimode microplate reader (Infinite® F500; TECAN, Ltd, Männedorf, Switzerland).

2.3.3 X-ray Photoelectron Spectroscopy (XPS)

X-ray Photoelectron Spectroscopy (XPS) was carried out to determine the chemical, elemental states, and information of functional groups from the material surface. The chemical component in the nanocomposite was measured by X-ray photoelectron spectroscopy (XPS, ESCA1600 system, ULVAC-PHI Inc.) using an Al Ka X-ray source (1486.6 eV).

2.3.4 X-ray Diffraction (XRD)

Different mixtures of the nanocomposite were characterized by X-ray diffraction (XRD) studies which determine the crystalline structure of the sample. The measurement analysis was carried out using a RINT ULTIMA XRD (Rigaku Co., Tokyo, Japan) with a Cu-Kα source and Ni filter. Reference from JCPDS powder diffraction files was followed to compare the diffraction patterns of samples. Scherrer formula, $t = ¼\ k\ \lambda/\beta\ \cos\theta$, was used to calculate the particle size by a mathematical analysis of Bragg's peaks, where t is the size of crystalline, k is constant (k = 0.94, assuming the grains to be spherical), λ is the wavelength of X-ray radiation (λ = 1.5406 A˚), β is the full width at half-maxima stated in radians (gained after correction of an instrumental error) and θ is half of the diffraction angle.

2.3.5 Dynamic light scattering (DLS)

Dynamic light scattering (DLS) is the well-established and most common measurement technique for particle size analysis in the nanometer range. It has been used for the characterization of the nanoparticles for providing information about particle size and measured by using a Zetasizer Nano series (Malvern Inst. Ltd., Malvern, UK).

2.3.6 Confocal laser scanning microscopy (CLSM)

Liposome containing QDs were observed by using CLSM (FV-1000, Olympus, Tokyo, Japan) at 25 ± 1 °C with a stage thermocontrol system (Thermoplate, Tokai Hit, Shizuoka, Japan), in reference to a previously reported method (Hossain *et al.*, 2019). For CLSM measurements, fluorescence images of QDs (559 nm laser) and differential interference contrast (DIC) images were obtained by using a 60×objective (UPLSAPO060X0, Olympus) (NA = 1.35).

2.3.7 Optical measurements and Fluorescence (FL)

A specific wavelength of light emitted by fluorescent molecules while stroking by the light of shorter wavelength (Stokes shift). A single fluorescent molecule can generate one fluorescence photon (quantum of light). The intensity of the fluorescence emission spectrum is measured to calculate the quantity of fluorescent-labeled compounds. Here, fluorescence spectra for detection and analysis of nanocomposites were recorded by using a filter-based multimode microplate reader (Infinite F500, TECAN, Ltd, Mannedorf, Switzerland) with LED light as the excitation source. The fluorescence spectrum of the respective samples was measured at a 400 – 500 nm wavelength of excitation and 500 – 750 nm wavelength of emission.

2.3.8 Electrochemical measurements

Electrochemical experiments of differential pulse voltammetry (DPV) was performed by SP-150 (BioLogic.Inc., Tokyo, Japan) in a conventional three-electrode system. The carbon coated electrode was used as a working electrode, platinum wire was used as counter electrode, and Ag/AgCl used as the reference electrodes (EC frontier, Tokyo, Japan). The pulse was generated during the virus incubation time with two Pt wires as the electrodes. The CV was recorded at a scan rate of 20 mV s^{-1} in a potential range of 0–1 V for 10 cycles.

CHAPTER 3

CONCEPT OF THE SENSING MECHANISM

The whole work of this thesis is comprised of three sensing mechanism **(Principle 1, 2, and 3)** which are described in detail. In this chapter, only the principle of each sensing mechanism has been described along with their experimental scheme.

3.1 Principle 1 for the construction of the localized surface plasmon resonance-induced optical sensor

3.1.1 Introduction

In the optical sensing, fluorometric assays are the most used methods which come in a variety of use due to its easy application and consistent outcomes (Al-Ogaidi *et al.*, 2014; Huang *et al.*, 2014). There are a lot of parameters using in sensors which include fluorescence intensity, quenching efficiency, decay time, and regeneration of luminescence and fluorescence. Therefore, the most innovative optical biosensors among these are based on the SPR properties by using AuNPs (Kawaguchi *et al.*, 2008; Lee *et al.*, 2015; Singh and Strouse, 2010; Yeom *et al.*, 2013). Detection of so many infectious diseases including cells, viruses, and bacteria, has been widely used with these biosensors (Ahmed *et al.*, 2016; Guo *et al.*, 2015; Lee *et al.*, 2019; Oh *et al.*, 2017). Fluorescent properties of QDs have been widely used as the reporter in several LSPR-based biosensor in which the SPR created by AuNPs plays the vital role to stimulus the signal of fluorescence-based on a different size, shape, and distance (Lee *et al.*, 2015; Takemura *et al.*, 2017). It can change the position along with the distance between the two nanoparticles (QDs and AuNPs) by triggering with analytes, ensuing the variation in signal detection. Here, a new method has been established on LSPR-induced optical transduction system in a single-step process for the detection of NoV-LPs and Norovirus (NoV) which is the common cause of gastroenteritis disease which are transmitted through food and waterborne routes and shellfish consumption (Bitler *et al.*, 2013). In

this detection method, NoV-LPs was used as the initial target analyte as there is no vigorous cell culture system for this virus propagation to date.

3.1.2 Concept of this biosensor

The main goal of this work is to establish a new and simple detection system for viruses without performing any pretreatment process. Therefore, antibody-conjugated nanocomposite (Ab-CdSeTeS QDs/AuNPs) has been synthesized by covalent bonding between CdSeTeS QDs and AuNPs which act as the sensing probe and have the sensing ability to detect the NoV-LPs (as presented in **Fig. 3.1**).

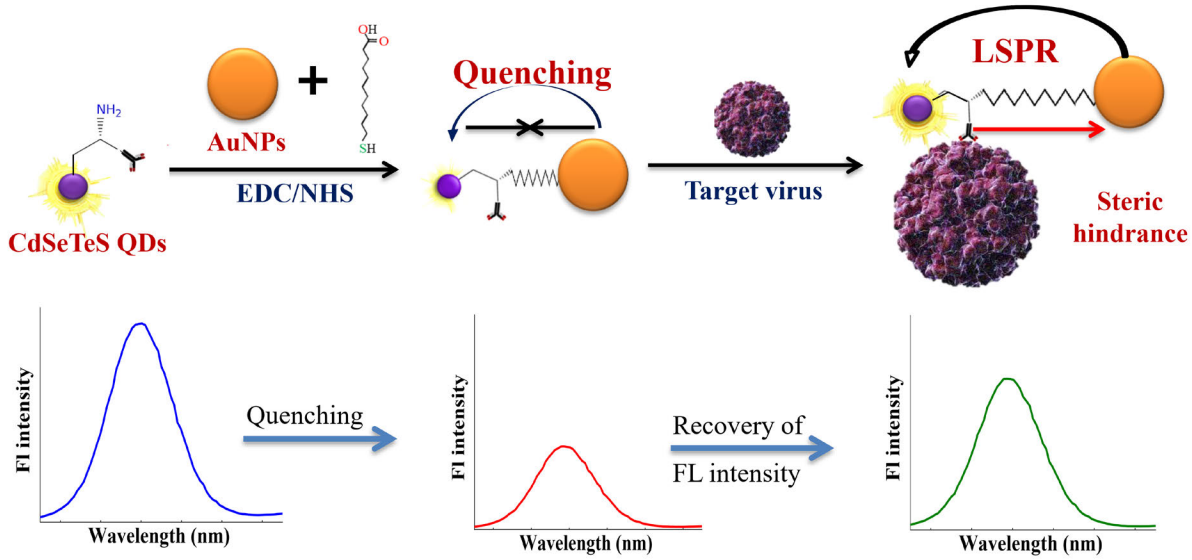

Fig. 3.1 Schematic illustration for the preparation of CdSeTeS QD/AuNPs nanocomposites along with the detailed mechanism of NoV-LPs detection. The covalent attachment between CdSeTeS QDs and AuNPs showed fluorescence quenching initially which has been recovered and showed enhancement upon the binding of target virus. (Nasrin *et al.*, 2018) (Reprinted with permission from Elsevier)

The covalently bound CdSeTeS QDs and AuNPs generated the sensing probe of nanocomposite which can make lower nonspecific interaction efficiently along with hampering the sensitivity. The covalent bond between AuNPs and CdSeTeS QDs initially creates quenching of fluorescence strongly. After addition of the virus in different concentrations, it has been attached on the nanoconjugate Ab-CdSeTeS QD/AuNPs due to the presence of the monoclonal antibody on this nanoconjugate. The interaction between antigen and antibody induces steric hindrance, therefore, a certain distance for LSPR occurred between two nanoparticles which causes enhancement of fluorescence. Here, the mechanism of detection encompasses the regeneration of quenched fluorescence due to the LSPR phenomena as the target virus generates a steric hindrance between two nanoparticles.

The construction of this biosensor along with the other parts including optimization, characterization, and application in sensing has been described in detail in **Chapter 4**.

3.2 Principle 2 for tuning of the localized surface plasmon resonance-based sensing platform

3.2.1 Introduction

The AuNPs are one of the noble-metal nanoparticles which have been used widely due to their versatility, chemical stability and exclusive optical properties such as localized surface plasmon resonance (LSPR), initiated to the enhancement of so many optical fields of local and nanoscale level (Liu *et al.*, 2015; Shang *et al.*, 2017; Ye *et al.*, 2014; Zhang *et al.*, 2016). As an advancement of these methods, LSPR-based biosensor has been used widely where fluorescence signal of fluorescent quantum dots (QDs) is directly influenced by the adjacent AuNPs which also depends on a different shape, distance, and size (Dutta Chowdhury *et al.*, 2017; Jans and Huo, 2012; Lee *et al.*, 2013; Takemura *et al.*, 2017). The background signal of the sensor remains high in the

conventional LSPR-based system because of the initial emission level of the fluorescent intensity of QDs, which causes a decrease in sensor sensitivity (Ahmed *et al.,* 2016). In addition to the conventional LSPR-based system, a new method can be established where very low dimensional viruses can cause small changes in the structural conformation which can lead to the analysis in an optimized condition. In this case, the analyte can cause quenching of the initial fluorescence signal gradually based on the concentration. This quenching phenomenon offers higher sensitivity because the highest level of fluorescent enhancement between two nanoparticles created by the LSPR effect can gradually decrease by the increasing concentration of the analytes. Here, the structural form is maintained by the distance which can be tuned by the specific length of the linker through the peptide chain. In the current work, the detection analysis was performed on influenza viruses which is the causative agent for infectious diseases in the respiratory tract and acts as a potential threat for human healthcare (Bedford *et al.*, 2015; Hushegyi *et al.*, 2016; Peiris *et al.*, 1999).

3.2.2 Concept of this biosensor

In this work, an LSPR based sensing platform was developed for the detection of viruses where all the parameters regarding the sensor can be optimized whenever needed of the analytes. To achieve this, the biosensor was developed by combining QD-peptide-AuNP nanocomposite in a new way. Here, the mechanism of detection provides quenching phenomena of the fluorescence of QDs as the LSPR signal is restricted due to the binding of AuNPs and QDs as depicted in **Fig. 3.2**.

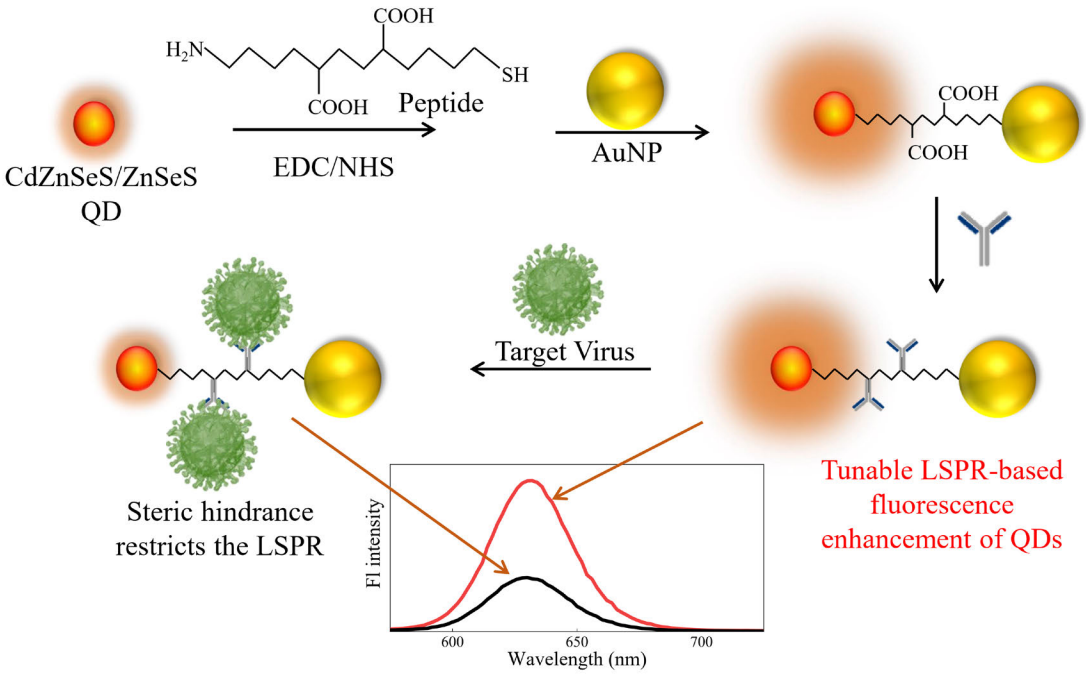

Fig. 3.2 Schematic representation for the synthesis of CdZnSeS/ZnSeS QD-peptide-AuNP nanocomposite along with its detection mechanism for sensing the influenza virus. Different lengths of peptide chains were applied in between AuNPs and QDs to get tunable LSPR effect, where, the enhanced signal of fluorescence showed quenching upon the addition of target virus. (Nasrin *et al.*, 2020) (Reprinted with permission from Elsevier)

The peptide was used in this work to make a stable sensor of CdZnSeS/ZnSeS QD-peptide-AuNP which has been designed and prepared according to the binding interaction with the QDs and AuNPs in its both ends. An antibody can bind with the peptide chain due to the presence of two aspartic acid residues on the peptide chain (**Fig. 3.3**). For the detection of the virus, the sensing probe (Ab-QD-peptide-AuNP) has been prepared by conjugating the anti-HA Ab for influenza virus in the peptide chain of the nanocomposite. The sensor generated a rigid structure as the QDs and AuNPs bound covalently via the peptide linker which can provide the reduction of the background noise and make the detection limit low. This linker length between two nanoparticles

can be tuned with the different chain length of peptides. Initially, the CdZnSeS/ZnSeS QD-peptide-AuNP sensor probe offers the fluorescence enhancement which later on showed quenching phenomena after binding of the target virus to the sensing probe as a strong steric hindrance has been generated by the interaction between antigen and antibody and caused the restricted LSPR between QDs and AuNPs. And, this quenching phenomenon is followed by the target virus concentration which confirms enough detection ability of the biosensor.

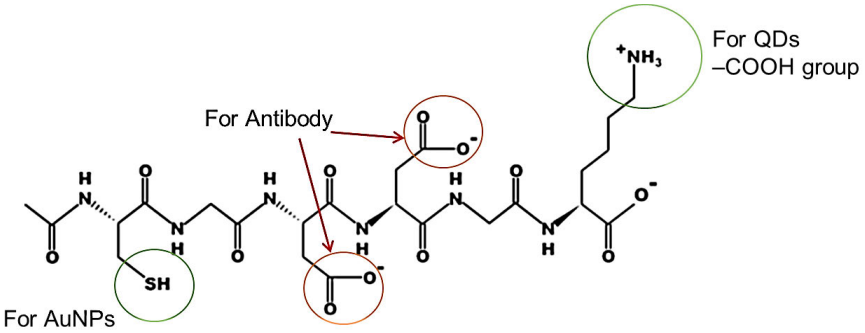

Fig. 3.3 The structure of the peptide chain used as a linker in the nanocomposite, containing two carboxyl groups, one amino group and one thiol group to attach with antibody, QDs, and AuNPs, respectively. (Nasrin *et al.*, 2020) (Reprinted with permission from Elsevier)

The construction of this biosensor along with the optimization, characterization, and application in sensing has been described in detail in **Chapter 5.**

3.3 Principle 3 for the advancement in sensing system by constructing dual functional liposome-based biosensor

3.3.1 Introduction

Recent studies are focusing on the development of nanomaterials for using in targeting huge number of analytes to get a high specificity. For this reason, the development of dual-functional biosensors has emerged as an advancement in the field of sensing application which can combine

two or more detection methods in a single platform and ensures better sensitivity and reliability for detection (Chuong *et al.*, 2017). Current amplification methods based on single detection systems often suffer from low sensitivity and selectivity which is not adequate for target detection and quantification (Ganganboina *et al.*, 2020). Therefore, it is necessary to work and develop dual-functional biosensors to overcome the limitations and challenges in the conventional methods. By using this, one method can be combined with the benefits of another method, which can minimize the disadvantages of both. Dual functional methods combined of two or more detection systems ensures the greater sensitivity and reliability for sensing target. Recent developments in establishing multifunctional nanomaterials have improved the detection methodology and allow the possibility to construct dual-functional detection methods (Xiong *et al.*, 2018). In this purpose, liposomes are one of the most attractive tools for their versatile and unique properties, which enables the encapsulation of various nanomaterials, providing both single and dual-sensing systems (Carboni *et al.*, 2019). Various reports are demonstrating the combination of fluorometric, colorimetric, and electrochemical responses by using liposomes (Holme *et al.*, 2018). Target amplification is usually employed to achieve high sensitivity where liposomal matrixes have emerged as an attractive approach where a target virus attached with a single liposome, can produce multiple signals, releasing their encapsulated signaling probes. Therefore, few numbers of viruses can produce the intense signal, encapsulated within the liposome. Another advantage of liposome-based systems is that the encapsulated probes remain protected until the external triggers appear which can reduce the background noise significantly (Ganganboina *et al.*, 2020). However, in the case of real-time application, to achieve the detectability in a very low level of virus concentration in sample medium where a lot of impurities can interfere with the sensing, the purification of the target virus from the medium should be extremely important. To serve this

purpose, the well-established Fe_3O_4 magnetic nanoparticles can be useful for the removal of the interferences from the virus loaded liposomal platform after proper conjugation (Chowdhury *et al.*, 2020). Therefore, a successful combination of the liposomal matrix with magnetic nanoparticles can be applied for the construction of a new class of biosensor for virus sensing. In this work, the chikungunya virus E1 protein (CHIKVE1) has been taken as a model to establish the sensing platform. The virus can spread to people by the bite of an infected mosquito. There is no vaccine has been developed yet to prevent chikungunya virus infection. Therefore, there is an increased demand for the development of this virus detection system which can detect the viruses in an early stage with high sensitivity and ability to perform in real-time monitoring.

3.3.2 Concept of this biosensor

In this study, a fluorescent QDs-embedded and MB-encapsulated dual-functional liposome has been synthesized for the detection of CHIKVE1. Initially, a hydrophobic red fluorescent CdSe QDs has been synthesized and embedded on the bilayer of the DOPC: DOPG: DSPE-PEG_{2000} liposome during its lipid layer synthesis process. A solution of MB as a redox indicator has been encapsulated in the liposome during its solvation process. Therefore, in this case, a new class of QDs-MB-liposome has been prepared which can be used for the fluorescent as well as electrochemical sensing **(Fig. 3.4)**. The APTES-coated Fe_3O_4 magnetic nanoparticles (MNP) has been used to separate the target-specific liposome form the solution mixture. The developed biosensor showed its ability to detect target virus in a broad range with a low detection limit which is the advancement of using a dual-functional sensing system.

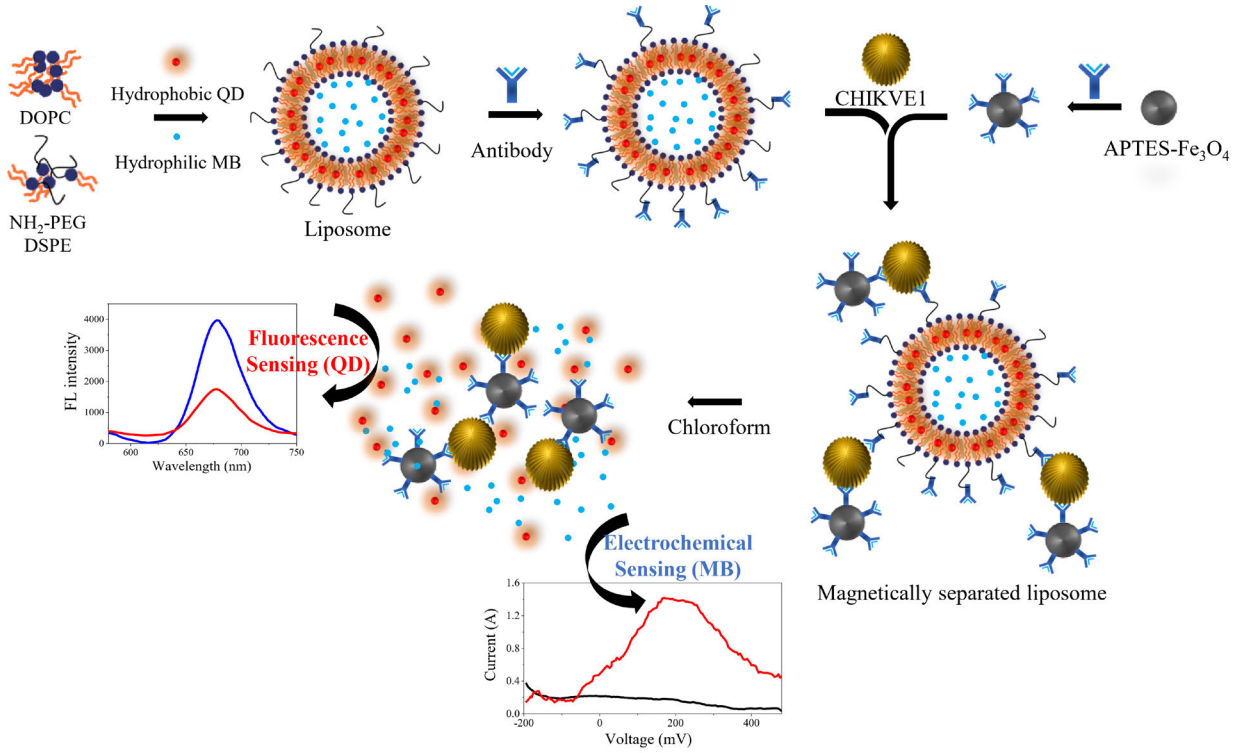

Fig. 3.4 Schematic representation for the synthesis of QDs-MB-liposome nanocomposite along with its optical and electrochemical detection mechanism for sensing CHIKVE1. The QDs and MB released from the magnetically separated target specific liposome act as the indicator of signal amplification for optical and electrochemical sensing, respectively.

The construction of this biosensor along with the optimization, characterization, and application in sensing has been described in detail in **Chapter 6.**

CHAPTER 4

CONSTRUCTION OF THE LOCALIZED SURFACE PLASMON RESONANCE-INDUCED OPTICAL SENSOR

As per the sensing mechanism (**Principle 1**) mentioned in chapter 3, the detailed construction of the sensor and the scope of the application in sensing has been described in this chapter.

4.1 Construction of the biosensor

4.1.1 Synthesis of sensing probe

At first, EDC/NHS chemistry was applied to conjugate anti-NoV antibody (anti-NoV) with CdSeTeS QDs on the carboxylic group of L-cysteine. AuNPs were functionalized with 11-MUDA which was later covalently bound with an amine group on the L-cysteine-capped QDs through the same reaction (Valeur and Bradley, 2009). Briefly, functionalized AuNPs were mixed with 100 µL of 0.1 M EDC, and 100 µL of 0.1 M NHS was added for activation and kept for 30 min and then antibody-conjugated QDs (Ab-QDs) were added in it. The solution was stirred at 7°C for overnight to form the nanocomposites (Ab-CdSeTeS QD/AuNPs). And finally purified by centrifuge at 3000 × g for 5 min and immediately 2 mL of ultrapure DI water was added to dissolve.

4.1.2 Preparation for the fluorometric sensing of NoV-LPs and clinical sample of NoVs

A 20 µL of the different concentrated target virus was added in the CdSeTeS QD/AuNPs nanocomposite and measurements of fluorescence were obtained after 1 min of incubation. The concentration range of target NoV-LPs was $1 \times 10^{-14} – 1 \times 10^{-7}$ g mL^{-1} in DI water. The solution of nanocomposite along with target analyte was excited at the wavelength of 450 nm and the measurement of fluorescence intensity was taken in the wavelength range of 500 – 700 nm. To investigate interfering effect of impure compounds, NoV-LPs was diluted in 10% of human serum for another analysis. For, clinical sample detection of NoVs, the same measurement procedure was performed with the sensor probe to get the response of fluorescence.

4.2 Characterization of nanoparticles and nanocomposites of the sensor

4.2.1 Characterization of CdSeTeS QDs and AuNPs

The synthesis of two nanoparticles was initially confirmed by checking morphology and size distribution. TEM analysis was performed to observe morphological properties and shape of the CdSeTeS QDs where spherical shaped and monodisperse particle distribution is obtained in the TEM image (**Fig. 4.1a**). Inset of the figure (**Fig. 4.1a**) showed particle size distribution of QDs and found particles are homogeneously distributed in the range of 3 – 9 nm while average particle size is about 5.9 ± 0.6 nm. UV-Vis spectrum of the CdSeTeS QDs in **Fig. 4.1b** showed the hump obtained for the absorption of QDs which remains to be observed after the conjugation of antibody. From **Fig. 4.1c**, AuNPs are shown to be spherical in size and distributed evenly in the range of 7 – 15 nm while the average particle size is about 11.4 ± 0.5 nm. From UV-vis spectra shown in **Fig. 4.1d**, the confirmation of capping with MUDA is observed as the agglomeration of AuNPs is reduced even after incorporating with MUDA.

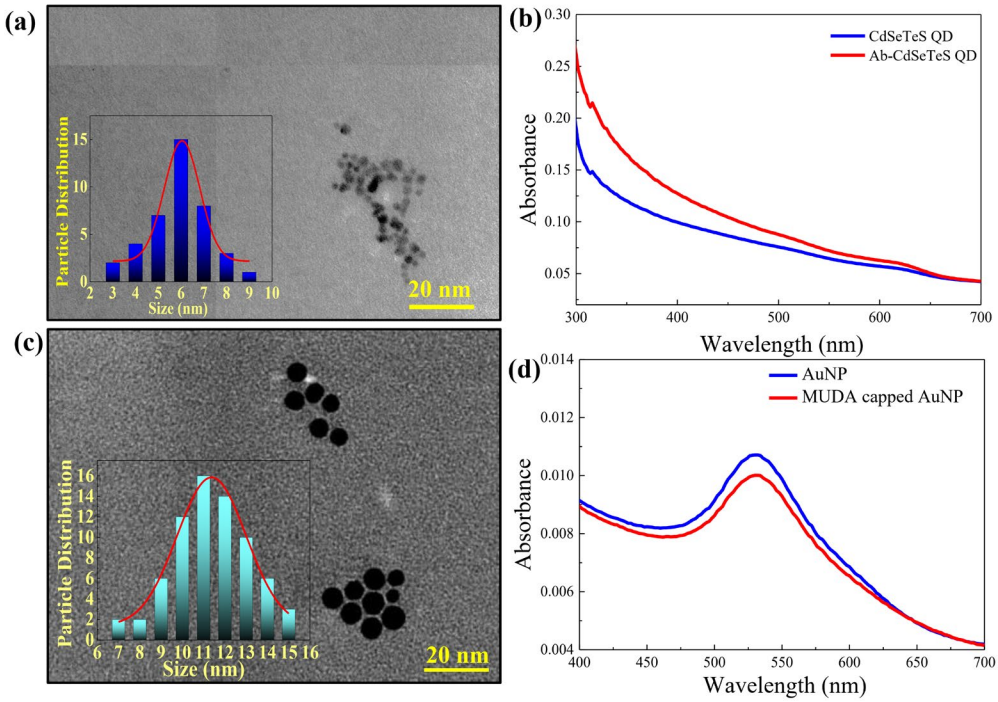

Fig. 4.1 (a) TEM image of CdSeTeS QDs (inset: particle size distribution, n=30), **(b)** UV-Vis spectra of QDs before and after the conjugation of antibody. **(c)** TEM image of AuNPs (inset particle size distribution, n=30), **(d)** UV-Vis spectra of AuNPs with or without capping of 11-mercaptoundecanoic acid. (Nasrin *et al.*, 2018) (Reprinted with permission from Elsevier)

4.2.2 Characterization of nanocomposites

The nanocomposite Ab-CdSeTeS QD/AuNPs was synthesized and conjugated with anti-Nov antibody and then observed by TEM image (**Fig. 4.2a**) which showed that the QDs (~5 nm) and AuNPs (~12 nm) are positioned very closely as they were covalently bound and linked by MUDA. ELISA was performed to confirm the conjugation of the anti-NoV antibody with the nanocomposites (**Fig. 4.2b**), which showed the absorbance peak is increased mostly in the case of Ab-CdSeTeS QD/AuNP nanocomposite compared to the bare QDs. The ELISA of Different stages of nanocomposite formation was supported by the ELISA where antibody conjugation was successfully observed.

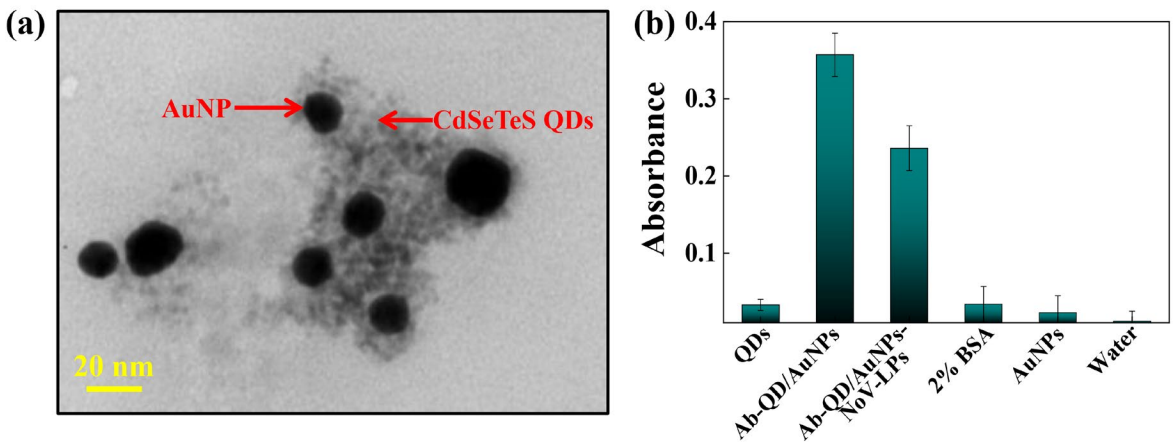

Fig. 4.2 (a) TEM image of CdSeTeS QDs/AuNPs nanocomposites, **(b)** ELISA result of QDs, the nanocomposite with and without NoV-LPs binding. (Nasrin *et al.*, 2018) (Reprinted with permission from Elsevier)

XRD spectra were also obtained to characterize the nanocomposites where the crystallized nature of the QD was illustrated. In **Fig. 4.3a**, it is shown that the diffraction pattern of QDs supports the crystalline and cubic nature of the QDs in which three characteristic peaks at 2theta of 24.9°, 42.3° and 50.6° for (111), (220) and (311) crystal planes are exhibited respectively (Adegoke *et al.*, 2015; Li *et al.*, 2016; Yang *et al.*, 2013). It is also observed that all these peak positions were unchanged even after functionalized with AuNPs and additionally a small peak at 2theta = 37.9° has been generated as AuNPs were incorporated with the nanocomposite to the characteristic (111) plane (Krishnamurthy *et al.*, 2014).

The dispersity and hydrodynamic diameter of the nanoparticle along with their nanocomposites were measured via DLS (**Fig. 4.3b**). The size distribution of the AuNP before and after capping with MUDA showed particle size of 8.5 ± 1.1 nm and 11.2 ± 1.2 nm, respectively. The bare QDs and after antibody-conjugation, the hydrodynamic diameter was 29.4 ± 2.3 and 54.2 ± 3.4 nm respectively. This result differs from the TEM images because QDs have a tendency to

agglomerate in the aqueous medium (Reghuram *et al.*, 2015). After the formation of the nanocomposite Ab-CdSeTeS QD/AuNPs, it showed 102.1 ± 3.2 nm of the diameter which is much higher than before the formation of nanocomposite which proved the successful conjugation of the nanocomposites even after addition of target virus.

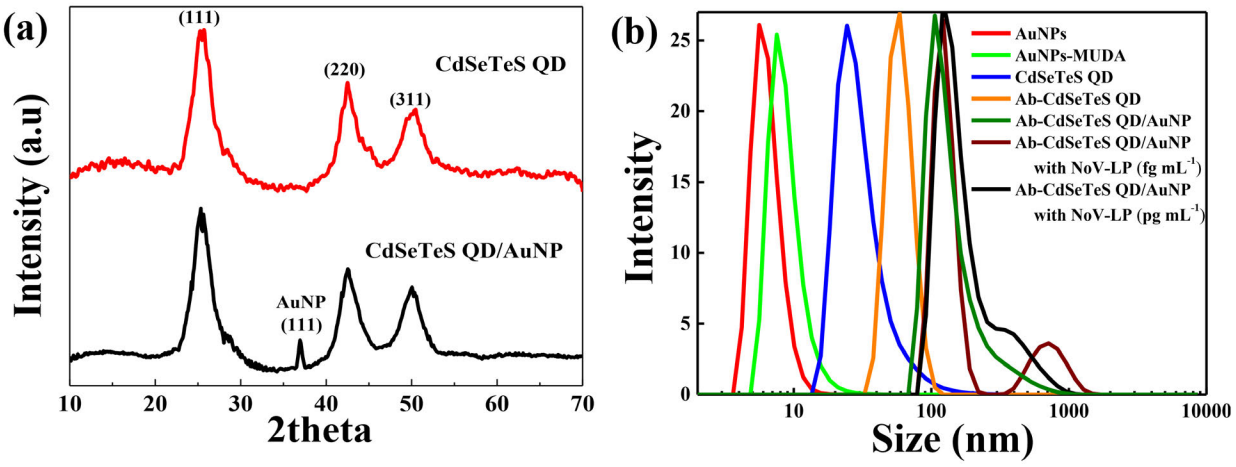

Fig. 4.3 (a) XRD analysis of CdSeTeS QDs and the synthesized nanocomposites, **(b)** Hydrodynamic diameter (DLS) of AuNPs, MUDA capped-AuNPs, bare QDs, Ab-conjugated QDs, the nanocomposite, and NoV-LPs loaded nanocomposite. (Nasrin *et al.*, 2018) (Reprinted with permission from Elsevier)

4.3 Optimization of the sensing mechanism

The as-synthesized Ab-CdSeTeS QD/AuNPs nanocomposite has been applied to the fluorometric sensing system for the detection of NoV-LPs. Initially, strong fluorescence was shown by the bare Ab-CdSeTeS QDs at 640 nm of wavelength while the excitation was at 450 nm (**Fig. 4.4a**). Due to the covalent conjugation with AuNPs, the QDs interact closely with AuNPs and consequently, the fluorescence intensity has been quenched about 65 %. In **Fig. 4.4a**, the quenching phenomena due to the close interaction was also confirmed by the spectral overlapping

between the spectrum of surface plasmon of AuNPs and emission of QDs (**Fig. 4.4b)**. However, a significant fluorescent enhancement has occurred after the addition of different concentrated NoV-LPs into the nanocomposite because of the enhanced distance generated between AuNPs and QDs due to the steric hindrance which is the key mechanism to detect a virus in this work (**Fig. 4.4a**). LSPR between any two nanoparticles is strongly dependent on their size and distance(Guo *et al.*, 2015). In this mechanism, the distance between the two nanoparticles playing the key role to alter fluorescence intensities as the size of AuNPs and QDs were kept constant, which initiated the LSPR induced fluorescence enhancement.

LSPR depends on several factors such as the properties, size, concentration, shape, and the ratio of AuNPs and QDs (Li *et al.*, 2011; Singh and Strouse, 2010). Here, for optimization, various sizes of AuNPs ranging from 5 to 100 nm were investigated while the size of QDs was kept constant and applied the system for 1×10^{-9} g mL^{-1} NoV-LPs detection. In **Fig. 4.5**, 12 nm size of AuNPs showed the highest quenching effect on QDs which afterward showed enhanced fluorescence compared to other sizes of AuNPs (5, 12, 20, 40, 80, 100 nm). The bigger sized AuNPs generates larger overlapping on the surface resonance orbital compared to small-sized AuNPs, therefore, small change generated by the NoV-LPs could not able to make enough distance for creating LSPR. Therefore, 10 – 12 nm size of AuNPs has been chosen to perform the rest of the work in this virus sensing system.

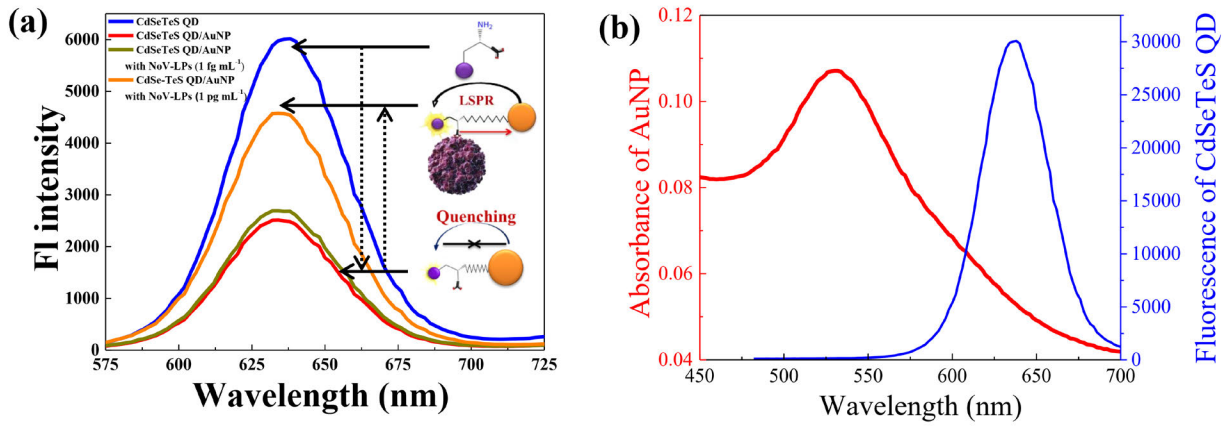

Fig. 4.4 (a) Fluorescence spectra of the bare CdSeTeS QDs along with after nanocomposite formation and the NoV-LPs loaded nanocomposites, **(b)** UV-absorption of AuNP and emission spectra of QDs to observe the SPR peak of AuNPs through spectral overlapping. (Nasrin *et al.*, 2018) (Reprinted with permission from Elsevier)

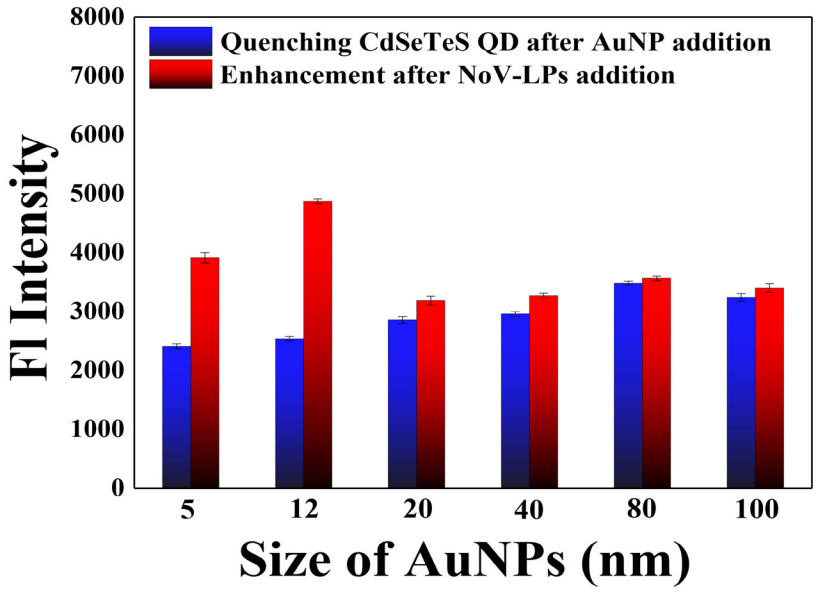

Fig. 4.5 Effect on the LSPR based enhancement and quenching of fluorescence depending on the size of AuNPs. (Nasrin *et al.*, 2018) (Reprinted with permission from Elsevier)

4.4 Application of the biosensor for virus detection

4.4.1 Control test for the applicability of the sensor

The sensitivity of the nanocomposite sensor probe was confirmed by a control test whether to check the proposed sensing system can verify the LSPR behavior by the influence of AuNPs or not. At first, the AuNPs were mixed physically rather than to bound covalently with Ab-CdSeTeS QDs. In **Fig. 4.6**, it is shown that the physically mixed AuNPs and the QDs have not affected the fluorescence emission spectra of the Ab-CdSeTeS QDs which indicated that the target virus cannot be detected without LSPR signal generated by the sensor.

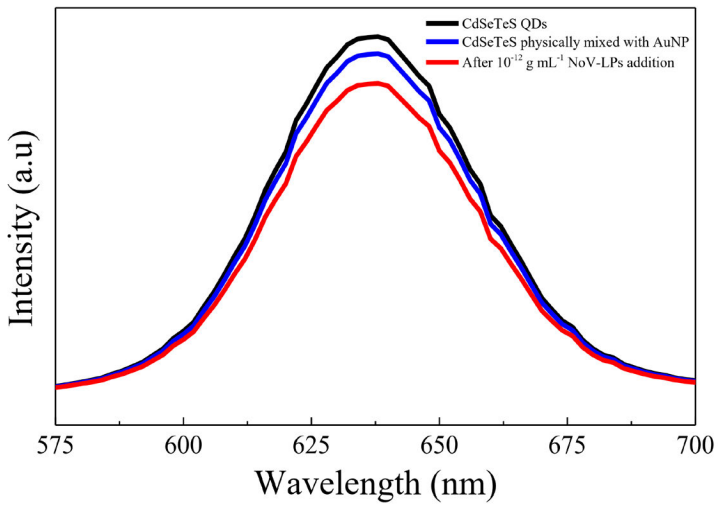

Fig. 4.6 Effect of non-covalently attached, physically mixed AuNPs on CdSeTeS QDs for NoV-LPs detection. (Nasrin *et al.*, 2018) (Reprinted with permission from Elsevier)

4.4.2 Fluorometric sensing of NoV-LPs using nanocomposite

The detection of NoV-LPs was performed by the nanocomposite sensor using the LSPR-induced fluorescence enhancement and the change of fluorescent intensities and its calibration curve is shown in **Figs. 4.7a** and **4.7b**, respectively. The intensity of the sensing fluorescence signal

of QDs was monitored at 640 nm which was quenched initially by the effect of adjacent AuNPs. After that fluorescence enhancement was achieved with successive addition of NoV-LPs concentrations without hampering the stability of QDs. The response time for detection is about 1 min after the addition of the target analyte. The calibration curve showed the detection limit (LOD) was found at 12.1 fg mL^{-1}, based on $L + 3\sigma$ (where σ is the standard deviation of the lowest signal, and L is the lowest concentration) (Shrivastava and Gupta, 2011).

The change in fluorescence intensity of the nanocomposite has been observed through bare eyes at the wavelength of 450 nm under UV light chamber (**Fig. 4.7d**). The highly intense fluorescence of Ab-CdSeTeS QDs was quenched strongly after the CdSeTeS QD/AuNPs nanocomposite formation. However, the fluorescence intensity was again enhanced after adding 1×10^{-9} g mL^{-1} of NoV-LPs, which confirms the LSPR induced fluorescence. In **Fig. 4.7c**, the TEM images showed the Ab-CdSeTeS QD/AuNPs nanocomposites were positioned on the surface of NoV-LPs (~40 nm), inset of **Fig. 4.7c** showing CdSeTeS QD/AuNPs/NoV-LPs image with higher magnification of an isolated particle which supports our phenomena.

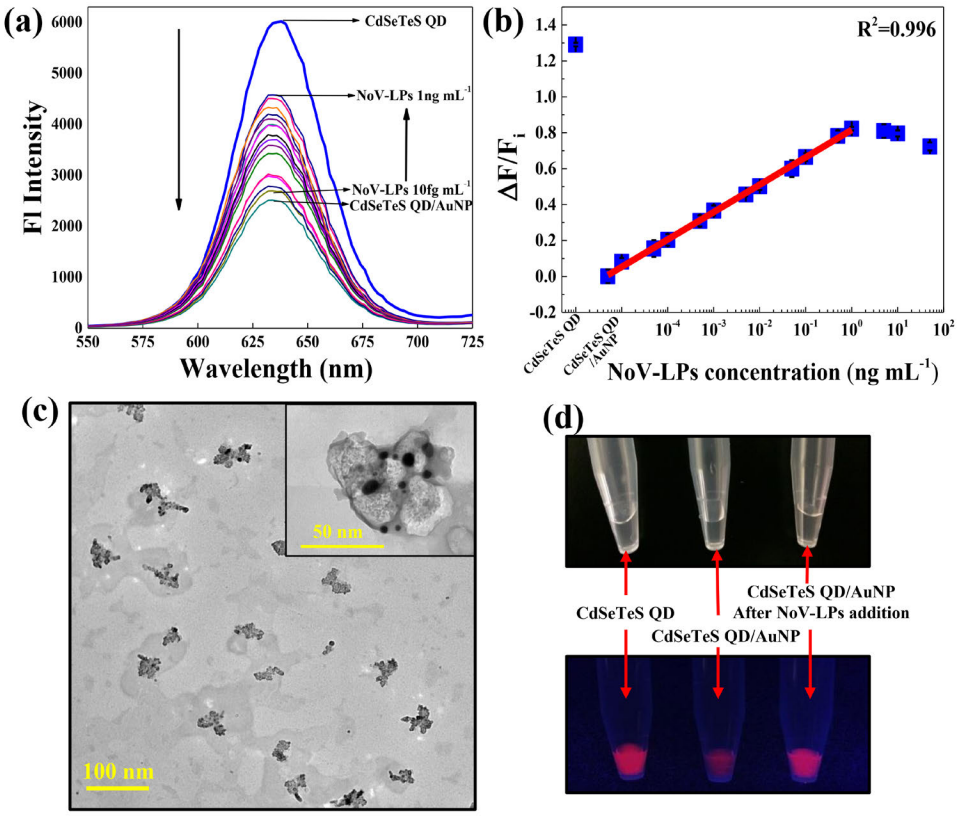

Fig. 4.7 (a) Fluorescence emission spectra for NoV-LP detection in the concentration range of 1 × 10^{-14} – 1 × 10^{-7} g mL^{-1} by using the nanocomposite, **(b)** Corresponding calibration curve for detecting NoV-LPs. Error bars represent the standard deviation of measuring 3 replicates, **(c)** TEM image of NoV-LPs loaded nanocomposites (inset: nanocomposite with NoV-LPs in higher magnification), **(d)** Fluorescence images of QDs, Ab-conjugated nanocomposites, and NoV-LPs loaded nanocomposites in normal light and the UV lamp at a wavelength of 450 nm. (Nasrin *et al.*, 2018) (Reprinted with permission from Elsevier)

4.4.3 Selectivity of the sensor

For the applicability of the real sample analysis, selectivity is the most important parameter. To check the selectivity of the proposed biosensor, it was also applied to the detection of other viruses like the Zika virus and Influenza virus A (H3N2) along with 2 % BSA solution, human

serum, and 10 % human serum as the negative control to check the matrix effect. In **Fig. 4.8**, the result showed the matrix effect is negligible in most of the interferences while 100% human serum affects a little due to the presence of huge interfering agents in it. The proposed biosensor for the target NoV-LPs showed a much higher signal than any other viruses. Additionally, some metal ions (1×10^{-4} g mL^{-1}) and amino acids (2 mM mL^{-1}) were also investigated and found a negligible signal, confirming enough specificity of the biosensor.

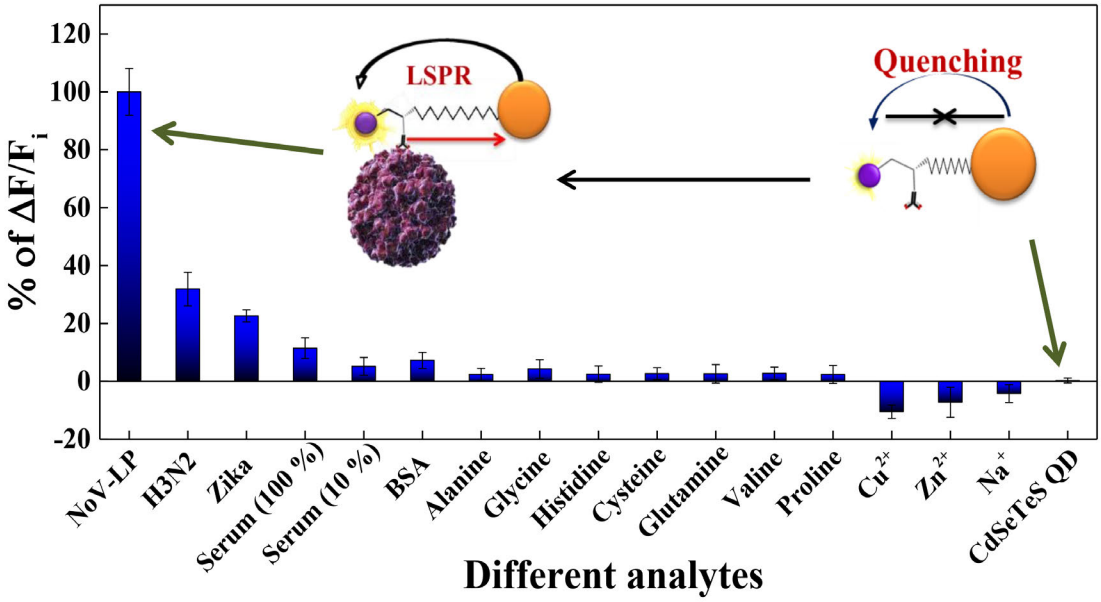

Fig. 4.8 The selectivity of the sensor nanocomposite comparing with 10^4 PFU mL^{-1} of the Zika virus, 30 μg mL^{-1} of Influenza virus, and other common interfering agents. (Nasrin *et al.*, 2018) (Reprinted with permission from Elsevier)

4.4.4 Sensing performance in serum sample

The proposed biosensor was demonstrated in the 10 % of human serum as working to check the ability to perform in a complex biological medium. In **Fig. 4.9a**, the detection pattern showed a similar trend for sensing the different concentrations of NoV-LP which proved that the real sample can be analyzed through this sensor. The calibration curve in **Fig. 4.9b** showed that the

detection slope is a little flattered compared to the detection performed in DI water. However, the sensitivity is still appreciable with little decreased LOD of 15.6 fg mL^{-1}.

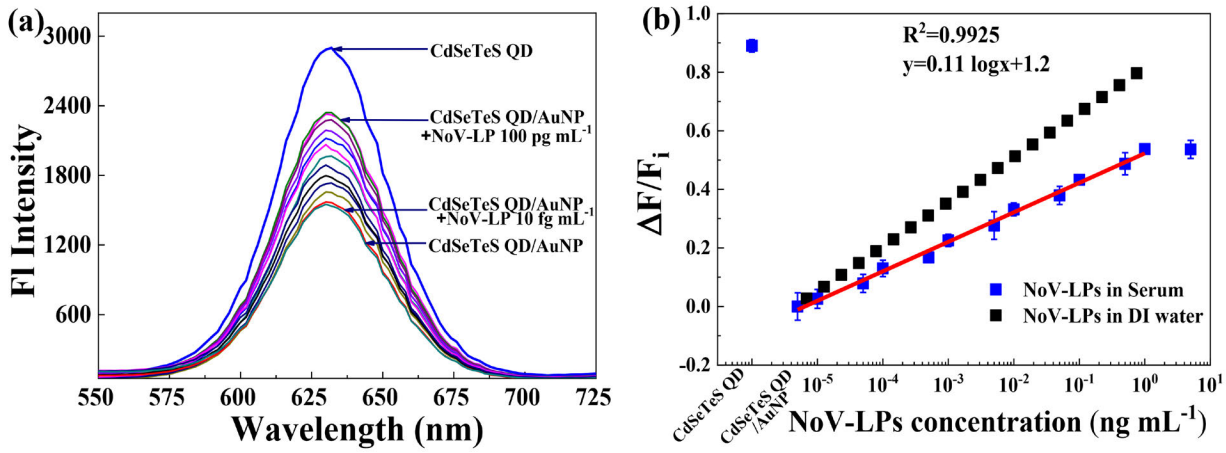

Fig. 4.9 (a) Fluorescence emission spectra for NoV-LPs detection using the sensor nanocomposite while in 10% human serum and **(b)** the corresponding calibration curve along with additional calibration line (black dots) which was found in DI water (shown in **Fig. 4.7b**). Error bars represent the standard deviation for measuring 3 replicates. (Nasrin *et al.*, 2018) (Reprinted with permission from Elsevier)

4.4.5 Sensing of clinical sample of NoV

The real NoV sample was collected from patient feces and applied to carry out the detection by the nanocomposites. After the addition of different concentrated NoV, the intensity of fluorescence was increased gradually which followed the same trend as NoV-LPs (**Fig. 4.10a**). From **Fig. 4.10b**, the calibration curve obtained the detection in the range of 10^2 – 10^4 copies mL^{-1} followed by the detection limit of 95.0 copies mL^{-1}. This result implies that the proposed biosensor can successfully detect clinical NoV without hampering efficiency. The TEM images in **Fig. 4.10c** showed the nanocomposites positioned closely with the NoVs which confirms the

successful conjugation with ~40–80 nm size of NoVs. Inset of **Fig. 4.10c** presented the magnified image of a nanocomposite which supports our proposed hypothesis.

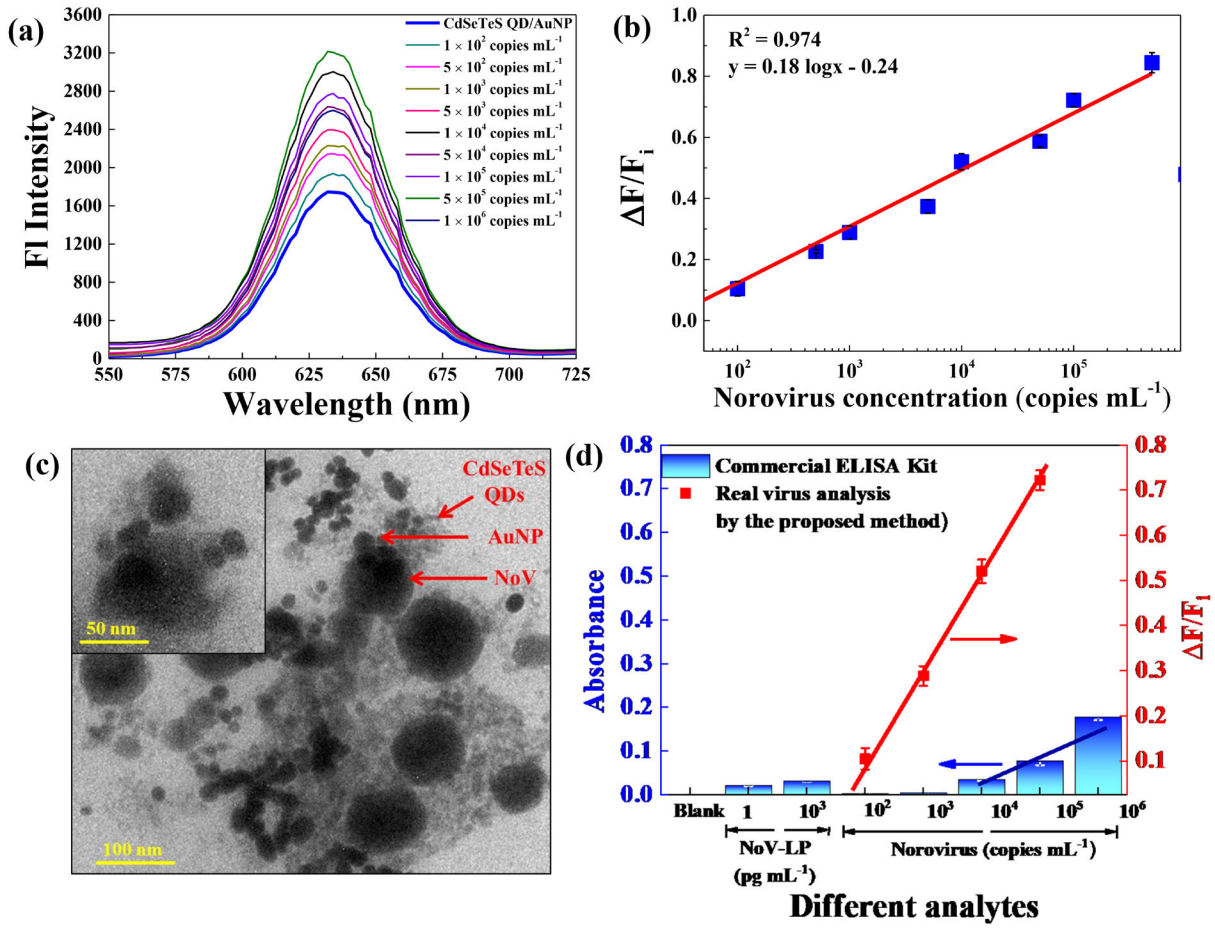

Fig. 4.10 (a) Fluorescence emission spectrum for detecting clinical sample of NoV in the concentration range of 10^2 to 10^6 copies mL^{-1} by using this LSPR-induced biosensor, **(b)** Corresponding calibration curve for NoV detection, **(c)** TEM image of NoV loaded nanocomposites (inset: NoV loaded nanocomposite in higher magnification), and **(d)** Comparison of the performance for detection of the target analyte by this proposed sensor (red line) and the commercially available ELISA kit (indicated blue line and bars). (Nasrin *et al.*, 2018) (Reprinted with permission from Elsevier)

For further confirmation, the applicability of the sensor was checked by comparing the detection of NoV-LP and clinical sample of NoV with a commercial ELISA kit and analyzed the results to compare the obtained result with our proposed biosensor. In **Fig. 4.10d**, it is observed that the proposed sensor showed outstanding detectability even in low concentration of NoV (10^2 – 10^5 copies mL^{-1}) whereas commercial kit is only applicable to detect higher concentration range for NoV (10^4 – 10^6 copies mL^{-1}).

4.5 Conclusion

In this chapter, a successful synthesis, preparation, and applicability of a new class of nanocomposites have been presented which can detect target analyte with a rapid fluorescence-based technique. The LSPR-based steric hindrance induced fluorescence is the key mechanism in this work for virus detection with higher sensitivity compared to other conventional LSPR-based biosensors. The proposed sensor can detect the target NoV-LPs with a linear range from 10^{-14} to 10^{-9} g mL^{-1} and the LOD is 12.1 fg mL^{-1} in DI water and 15.6 fg mL^{-1} in human serum which confirms efficient detection of the target analyte. The detection of clinical sample of NoV from infected patients showed a high sensitivity of 95.0 copies mL^{-1}. These results showed the evidence of easy applicability and detectability of target analytes which can serve as an efficient platform in the wide range of sensing applications in the future.

CHAPTER 5

TUNING OF THE LOCALIZED SURFACE PLASMON RESONANCE-BASED SENSING PLATFORM

As per the sensing mechanism (**Principle 2**) mentioned in chapter 3, the detailed construction of the sensor and the scope of the application in sensing has been described in this chapter.

5.1 Construction of the biosensor

5.1.1 Synthesis of sensing probe

Initially, the free carboxylic group of TGA-capped CdZnSeS/ZnSeS QDs was covalently conjugated with the peptide containing an amino group in one side and thiol group in another side through the EDC/NHS reaction (Adegoke *et al.*, 2016). After that, the thiol group of peptides was conjugated to AuNPs followed by the synthesis of the QD-peptide-AuNP nanocomposite. Anti-HA antibody for influenza virus A/H1N1 was attached covalently with the peptides containing the free carboxyl group by EDC/NHS reaction. This solution mixture was continued to stir for 2–3 h at 7°C to create the sensing probe QD-peptide-AuNP nanocomposite and purified by centrifugation for 5 min at 3000 g followed by dissolving in 2 mL of ultrapure water. A total set of six different nanocomposites containing the different lengths of the peptide (4 to 34 amino acids) has been prepared to optimize the sensor probe. Here, **Fig. 5.1** presented the structures of six peptides used in the sensor.

5.1.2 Preparation for sensing by fluorometric detection

20 µL volume of the virus with different concentrations was added in a 180 µL solution of QD-peptide-AuNP nanocomposite sensing probe and the measurement of fluorescence intensity was taken after incubating for 3 min. For the optimization, the six-chain length of peptides was applied to the nanocomposites keeping a similar condition. The excitation and emission wavelength for the detection was 450 nm and 500 – 700 nm respectively for measuring the intensity of fluorescence.

1. AcO-CGGGGGGGGGGDGGGGGGGGGGDGGGGGGGGGGK (34) (~15.5 nm)

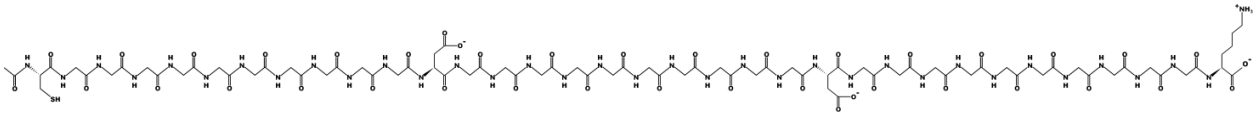

2. AcO-CGGGGGGGDGGGGGGDGGGGGGGK (24) (~11 nm)

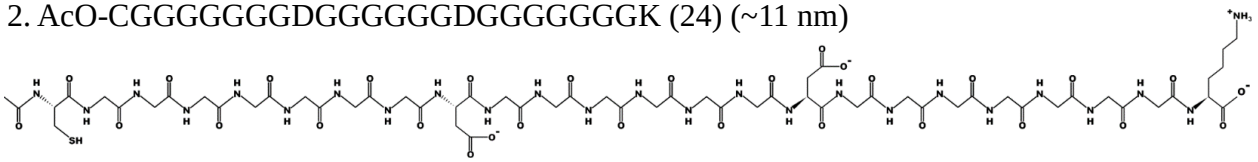

3. AcO-CGGGGGDGGGGDGGGGGK (18) (~8.5 nm)

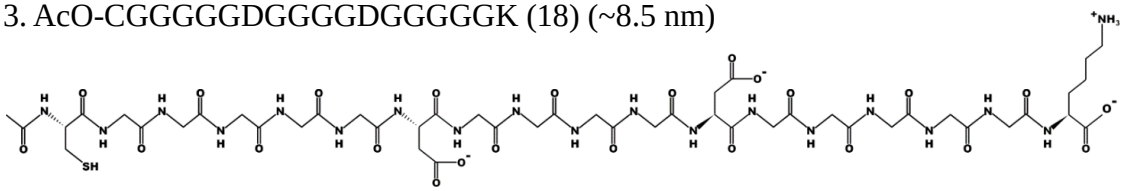

4. AcO-CGGGDGGDGGGK (12) (~6nm)

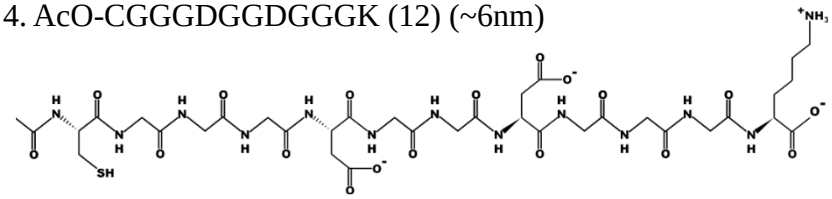

5. AcO-CGDDGK (6) (~3 nm)

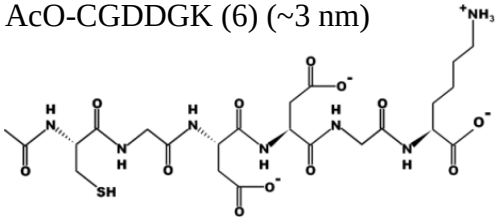

6. AcO-CDDK (4) (~1.8 nm)

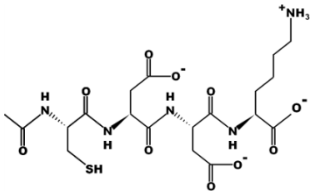

Fig. 5.1 The structure of six different lengths of peptides used as a linker. (Nasrin *et al.*, 2020) (Reprinted with permission from Elsevier)

5.2 Characterizations of the nanoparticles and nanocomposites used in the sensing probe

5.2.1 Characterization of CdZnSeS/ZnSeS QDs and AuNPs

Size distribution and morphology of QDs and AuNPs were examined first. In **Fig. 5.2a and 5.2b**, TEM image and particle distribution respectively, showed the spherical shape and evenly distributed AuNPs in the range of 20 – 35 nm with an average particle size of 26.5 ± 0.5 nm. In **Fig. 5.2c** and **5.2d** also confirmed the consistent spherical shaped QDs in TEM image with a particle as 4.8 ± 0.6 nm respectively. In this study, a medium quantum yield (QY) of 0.36 QDs has been selected to interact with a bigger size (25 nm) of AuNP to avoid background noise of high fluorescence signal. From **Fig. 5.3**, UV-Vis absorption of AuNPs and QDs along with the fluorescence spectra of QDs has been observed.

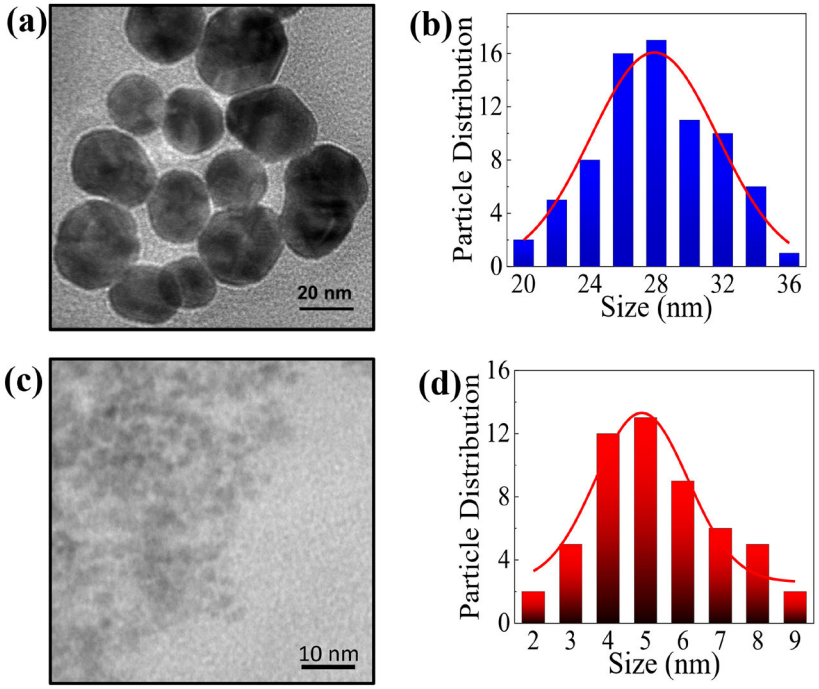

Fig. 5.2 (a) TEM images and **(b)** particle size distributions of AuNPs. **(c)** TEM image and **(d)** particle size distribution of CdZnSeS/ZnSeS QDs. (Nasrin *et al.*, 2020) (Reprinted with permission from Elsevier)

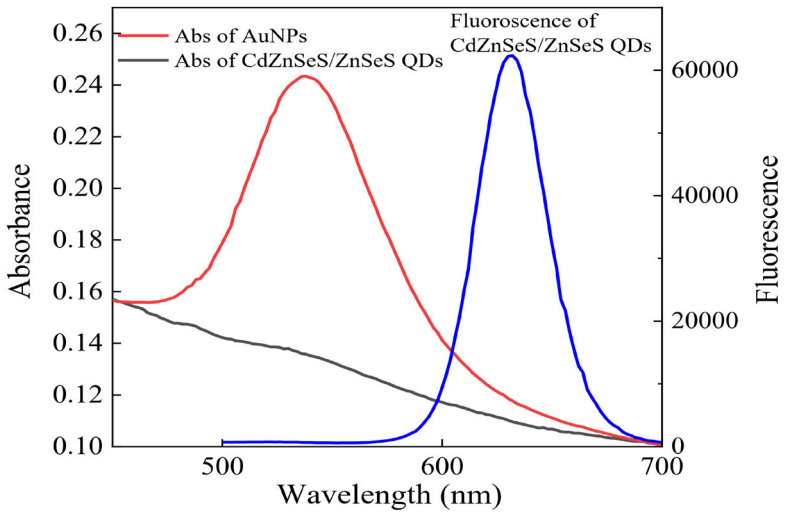

Fig. 5.3 UV-Visible spectra of AuNPs and after the formation of the nanocomposite along with the fluorescence emission spectra of QDs. (Nasrin *et al.*, 2020) (Reprinted with permission from Elsevier)

5.2.2 Characterization of the nanocomposite prepared for the sensor

The nanocomposite QD-peptide-AuNP was characterized after successful synthesis and the formation was confirmed by EDS mapping (**Fig. 5.4**), which presented a cluster of nanocomposites along with individual nanoparticles. For AuNPs and QDs mapping, Cd and Au were used respectively, for the nanocomposite and the result proved that these two nanoparticles were linked successfully.

The measurement of hydrodynamic diameter (DLS) was also performed to verify the nanocomposite formation. In **Fig. 5.5a** showed the determination of the different size of individual nanoparticles along with the nanocomposites where AuNPs and QDs show the hydrodynamic size of 28.4 ± 1.5 nm and 5 ± 0.5 nm, respectively as same as the result found in the TEM image.

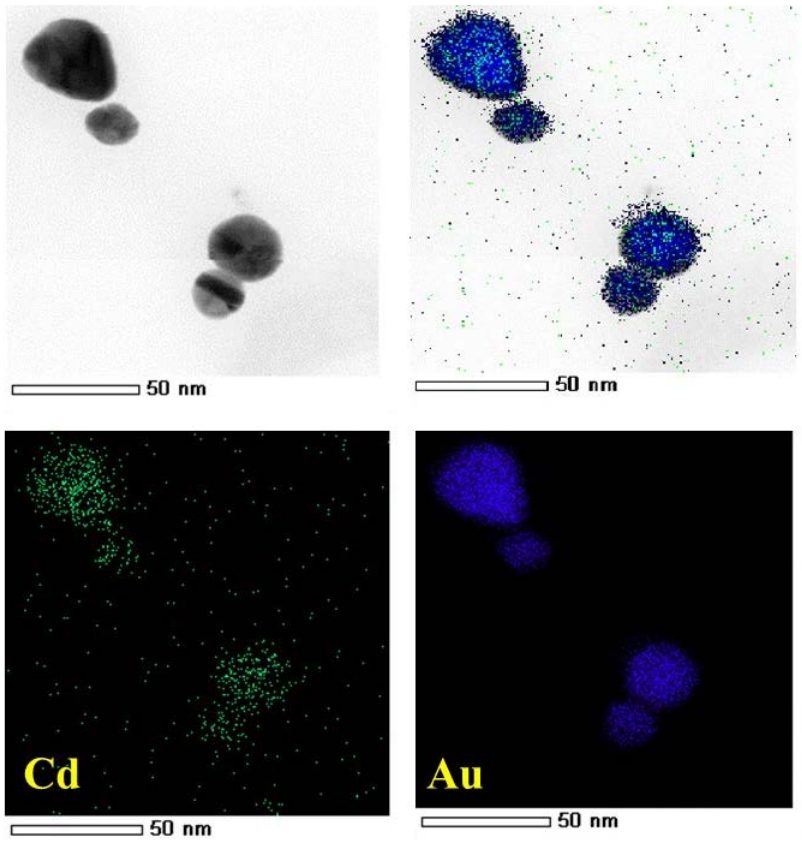

Fig. 5.4 EDS mapping analysis of the synthesized CdZnSeS/ZnSeS QD-peptide-AuNP nanocomposites of Cd, Au individually along with and merged image. (Nasrin *et al.*, 2020) (Reprinted with permission from Elsevier)

After the formation of the nanocomposite, the diameter showed a size of 57 ± 0.5 nm which confirms the conjugation of nanoparticles. Additionally, after binding of the influenza virus with the sensing nanocomposite, the size increased up to 172 ± 0.5 nm which suggests the successful binding with the sensing probe. XRD analysis was also performed to confirm the nanocomposite formation presented in **Fig. 5.5b**, in which the combination of two crystalline individual peaks from nanoparticles showed the summation while forming the nanocomposite.

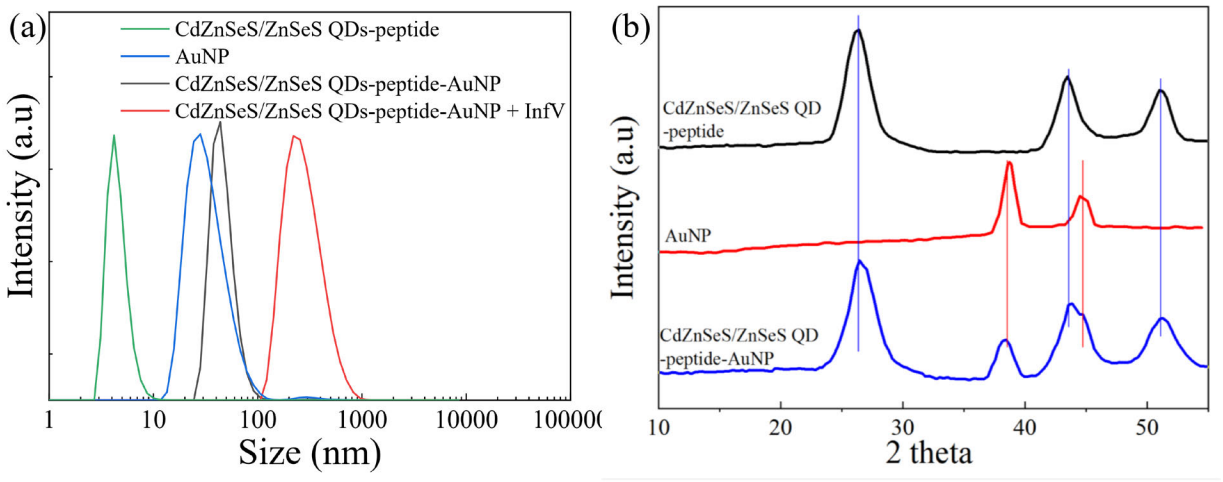

Fig. 5.5 (**a**) Hydrodynamic size diameter (DLS) of the QD-peptide-AuNP nanocomposites and its nanoparticles of QDs, AuNPs, along with Influenza virus loaded nanocomposite, (**b**) XRD analysis patterns of QDs, AuNP, and the nanocomposites. (Nasrin *et al.*, 2020) (Reprinted with permission from Elsevier)

Later, the XPS analysis also confirmed the formation of the nanocomposites. In **Fig. 5.6a**, the survey spectrum of QD-peptide-AuNP nanocomposite showed the induction of Au peak which indicates the AuNPs conjugation while in **Fig. 5.6b and 5.6c**, the deconvoluted Au4f spectra of nanocomposite have been compared with bare QDs where a strong Au peak was seen in nanocomposite only, confirming the conjugation. In **Fig. 5.6d and 5.6e**, the deconvoluted spectra of C1s have also confirmed the nanocomposite formation as the intensity of carbon is extremely increased in the case of nanocomposites rather than in QDs only, which indicates that the large carbon moiety comes from the peptide chain linkage.

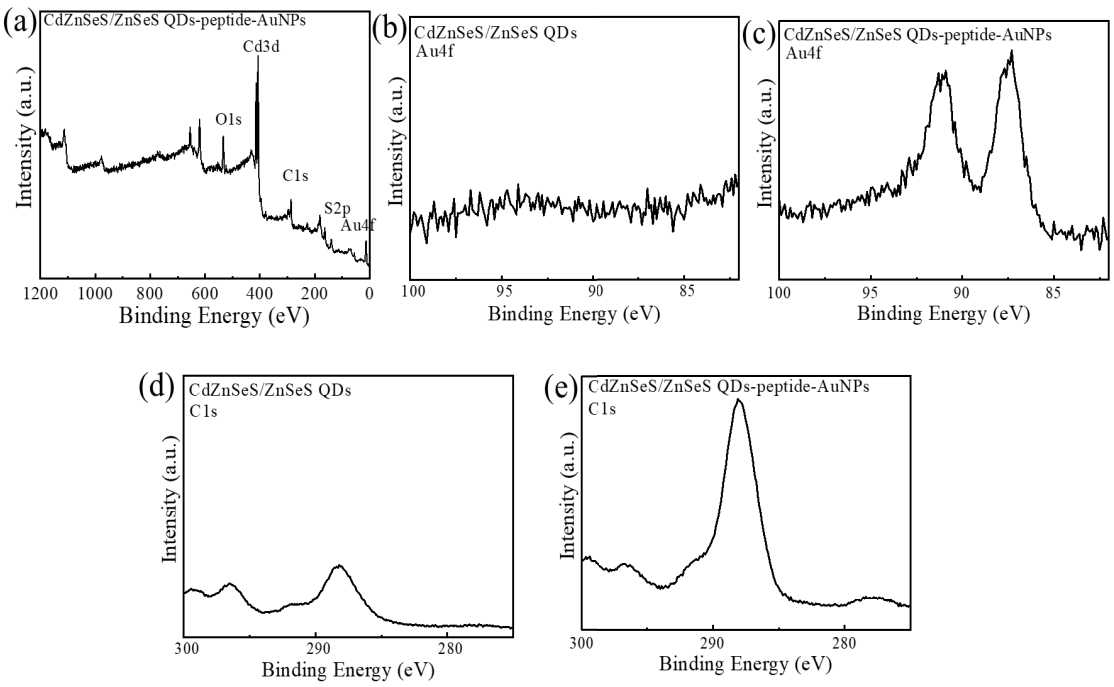

Fig. 5.6 (**a**) XPS analysis scan of the QD-peptide-AuNP nanocomposite and deconvoluted Au4f spectra of **(b)** QDs and **(c)** the QD-peptide-AuNP nanocomposite and deconvoluted C1s spectra of **(d)** QDs and **(e)** the nanocomposite. (Nasrin *et al.*, 2020) (Reprinted with permission from Elsevier)

5.3 Optimization of the sensing mechanism

In this work, the measurement of LSPR-mediated fluorescent generated by CdZnSeS/ZnSeS QDs is the key mechanism for sensing. Initially, the QD-peptide-AuNP nanocomposites provided the enhancement of fluorescence intensity due to the LSPR-induced effect as here, ~8.5 nm distance was maintained by the peptide linker between two nanoparticles. The possible structure after nanocomposite formation is shown in **Fig. 5.7**.

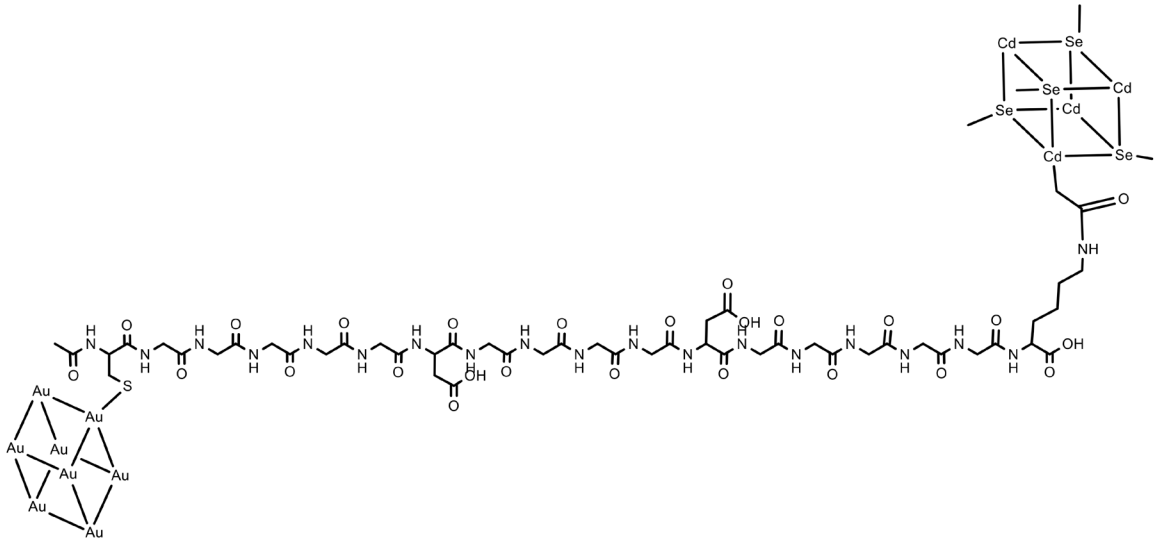

Fig. 5.7 Possible structure after formation of the CdZnSeS/ZnSeS QD-peptide-AuNP nanocomposite. (Nasrin *et al.*, 2020) (Reprinted with permission from Elsevier)

According to previously reported other LSPR-based phenomena, 8 – 12 nm distance between two nanoparticles are perfect for enhancing fluorescence intensity (Feng *et al.,* 2015; Li *et al.,* 2016; Nasrin *et al.,* 2018). Two aspartic acid moieties are present in the peptide where two antibodies can be conjugated. Therefore, after the addition of the target virus, they can bind to these antibodies via the antigen-antibody interaction which can provide enough steric repulsion in LSPR from AuNPs towards QDs. In this work, the concentration, size of AuNPs along with peptide length was varied and applied to the sensing system to get the best-optimized condition.

In **Fig. 5.8 (a**–**f)**, the distance dependency in LSPR was verified, where it is shown that the change in fluorescence signal was occurred according to the change in distance between two nanoparticles, keeping other parameters constant. While the distance is about 1.8 nm, strong quenching was observed. However, when the distance was increased from 1.8 to 6 nm, the enhancement of fluorescence observed gradually (**Fig. 5.8g)**. This observation can be elucidated

by the previously reported phenomenon where the emission intensity and quantum efficiency of QDs can be changed towards enhancement or quenching by the balance of two ways of electron transfer process like local field enhancement effect and non-radiative energy transfer (Feng *et al.*, 2015; Hao *et al.*, 2014). The maximum enhancement here was observed at a distance of about 15.5 nm. In this sensing mechanism, the system needs to be flexible as the addition of a small number of viruses should provide alteration in the electron transfer process. In case of higher distance (11 or 15.5 nm), it would be difficult to change in quenching effect, therefore, the 8.5 nm length of the peptide was chosen for the sensing application as it showed the best results for changing fluorescence properties from enhancement to quenching while after adding target virus.

The simple construction of the QD-peptide-AuNP nanocomposite containing 8.5 nm peptide linker has been obtained by performing the energy minimization (**Fig. 5.9**) which showed a most possible structure of the nanocomposite. From the obtained result, the peptide length has been calculated by the theoretical analysis which showed a distance of 7.9 nm which provides the same distance of the constructed peptide.

5.4 Application of the biosensor for virus detection

5.4.1 Control test for the applicability of the sensor

To check the performance of the sensing system, QDs were mixed physically with AuNPs rather than chemical binding for detecting viruses. In **Fig. 5.10**, it is shown that there was no change in the intensity of fluorescence of CdZnSeS/ZnSeS QD-peptide even after adding AuNPs due to the physical mixing which confirms the biosensor only work followed by LSPR mechanism to detect target analytes.

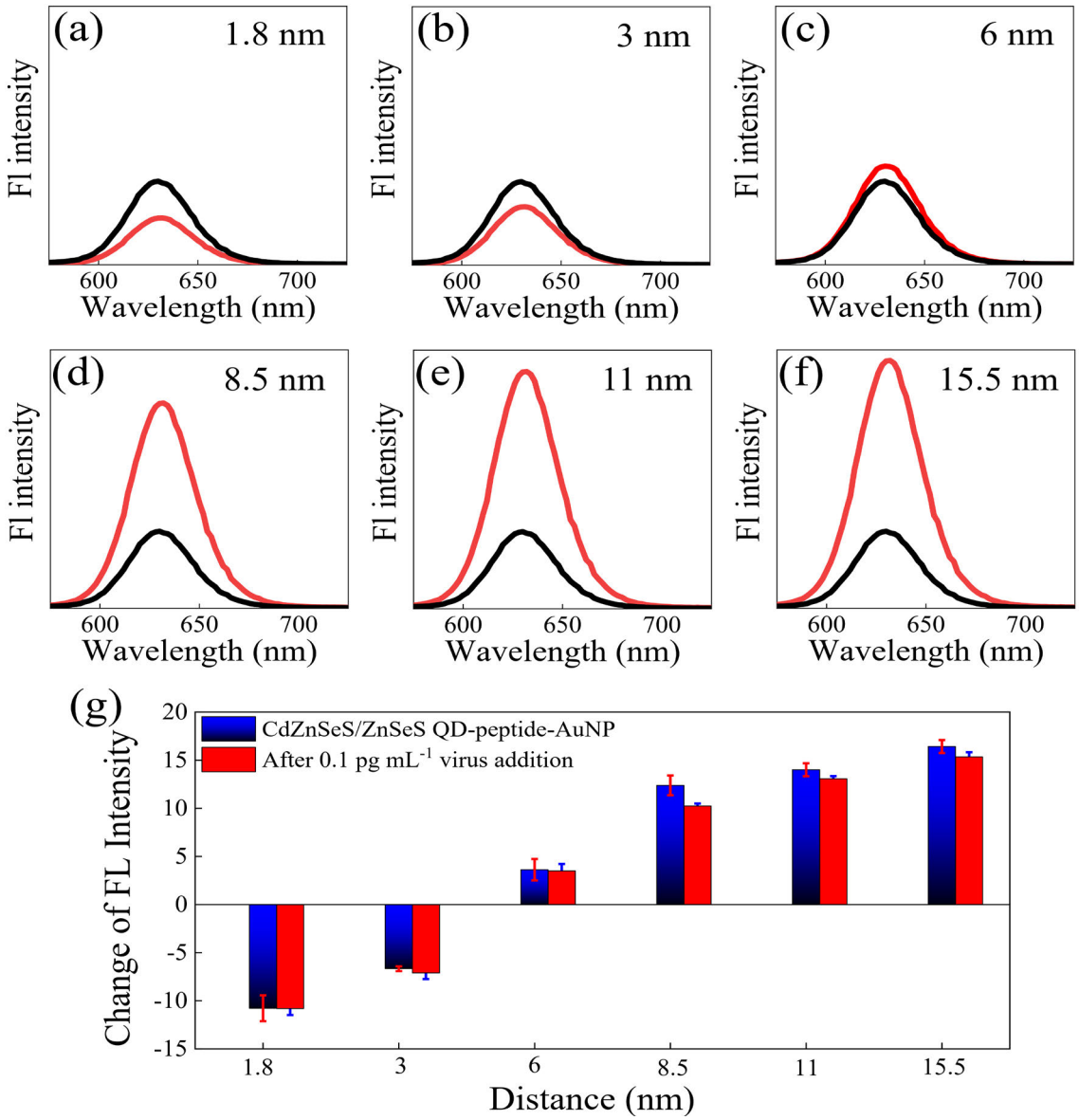

Fig. 5.8 Fluorescence spectra depending of various distance where the peptide chain length was varied from **(a)** 1.8, **(b)** 3, **(c)** 6, **(d)** 8.5, **(e)** 11 and **(f)** 15.5 nm. Here, fluorescence showed before (black) and after (red lines) AuNP conjugation with nanocomposites and **(g)** comparison of the fluorescence change based on the chain length variation of the peptide after adding target virus. (Nasrin *et al.*, 2020) (Reprinted with permission from Elsevier)

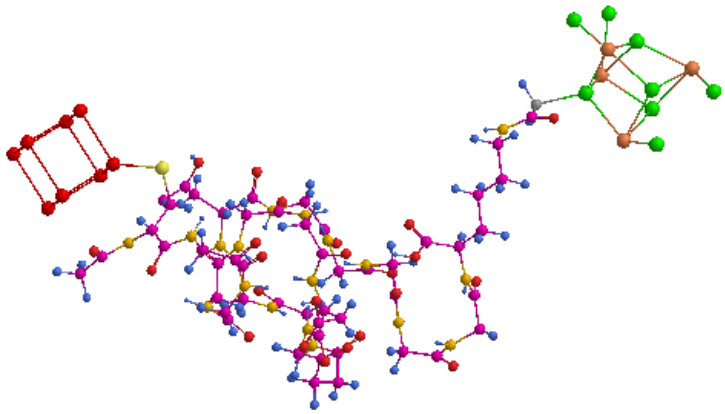

Fig. 5.9 Probable structure of the QD-peptide-AuNP nanocomposites with the peptide chain length of 8.5 nm obtained after simulation. (Nasrin *et al.*, 2020) (Reprinted with permission from Elsevier)

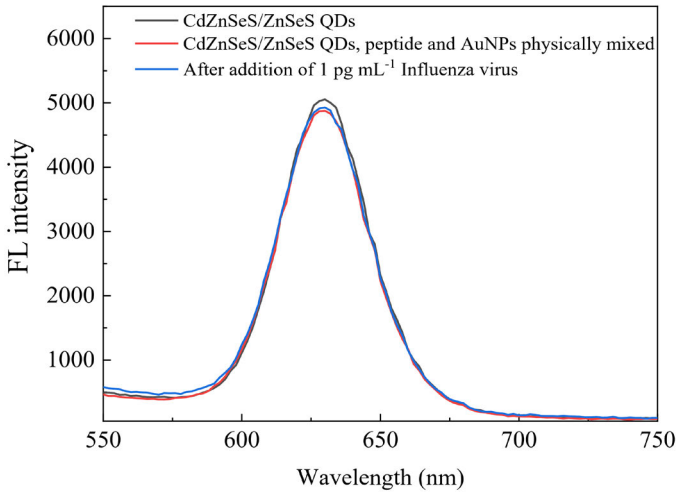

Fig. 5.10 The fluorescence intensities remained unchanged while the nanoparticles were physically mixed for sensing. (Nasrin *et al.*, 2020) (Reprinted with permission from Elsevier)

5.4.2 Fluorometric sensing of influenza virus

This biosensor was applied to detect the influenza virus based on the LSPR-induced fluorescence measurement. Fluorescence of QDs was obtained at a wavelength of 630 nm for detection. Initially, the fluorescence intensity of CdZnSeS/ZnSeS QD-peptide was at a level of

26780 which was increased to 47320 after the CdZnSeS/ZnSeS QD-peptide-AuNP nanocomposite formation (**Fig. 5.11a)**. After that, the quenching of fluorescence took place while after addition different concentrated influenza viruses. The calibration curve was plotted as the fluorescence quenching by their initial fluorescence ($\Delta F/F_i$) against the different concentrations of the virus (**Fig. 5.11b).** The plot showed excellent linearity up to 100 ng mL^{-1} and become saturated after that, providing the corresponding linearity from femto to 100 ng mL^{-1} range of concentration and the limit of detection (LOD) was calculated as 17.02 fg mL^{-1}, based on L + 3σ (where, σ is the standard deviation of the lowest signal and L is the lowest concentration used (Shrivastava and Gupta, 2011). This proposed sensing system has advantages over other conventional LSPR-based sensors that formed a rigid structure for the sensing probe which makes a lower possibility of nonspecific interaction and resulted in a very low background signal.

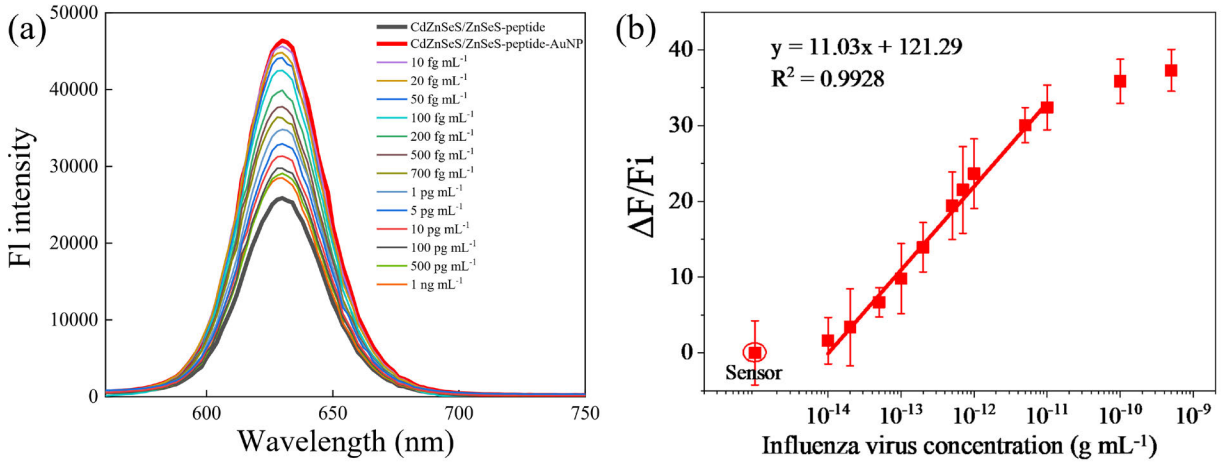

Fig. 5.11 (a) Fluorescence emission spectra for influenza virus detection in the concentration range of 10^{-14} – 10^{-9} g mL^{-1} using this LSPR-based sensing probe along with its **(b)** corresponding calibration curve for influenza virus detection. Error bar represents the standard deviation of measuring three replicates. (Nasrin *et al.*, 2020) (Reprinted with permission from Elsevier)

5.4.3 Sensing performance with a modified peptide linker

Also, the peptide linker was modified by varying the antibody binding sites. To obtain this, three different peptides of having one, two, and three antibody binding sites were used individually with the nanocomposites for the sensing (**Fig. 5.12a**). Therefore, three different sensing system was synthesized with having single, double, and triple antibody, and performed to detect virus sample in the same way. In **Fig. 5.12b**, it is showed that the patterns of fluorescence change are almost similar in the sensing probe having single- and double-antibody, while in the case of the sensor having triple antibody, the earlier saturation was observed from 100 pg mL^{-1} to 10 pg mL^{-1}. This may be because the sensor having a triple antibody was unable to provide enough steric influence on LSPR interaction.

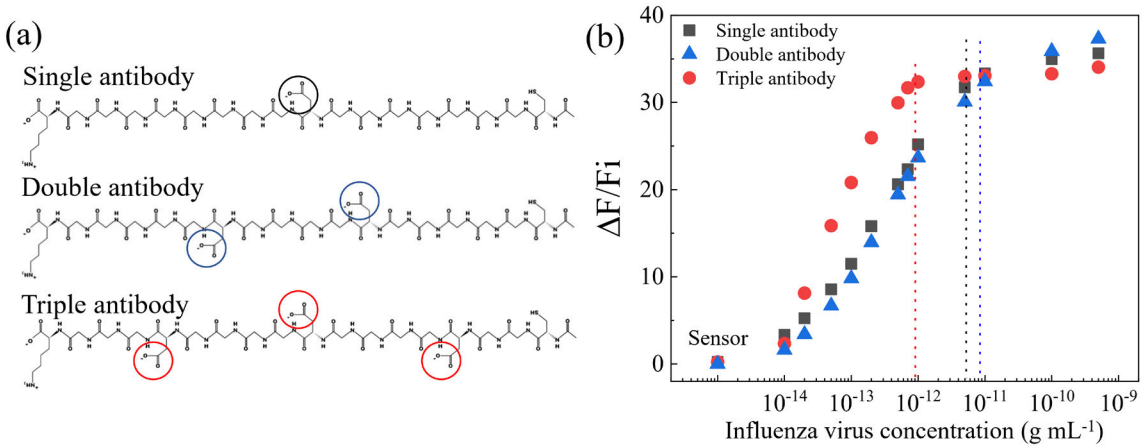

Fig. 5.12 (a) Three different peptides containing one, two, and three numbers of the carboxyl group. (**b**) Effect of these three different peptides containing nanocomposite for sensing performance. (Nasrin *et al.*, 2020) (Reprinted with permission from Elsevier)

5.4.4 Selectivity and stability of the sensor

Selectivity is one of the most important parameters to verify sensor applicability, therefore, this sensing system was performed for detecting target analyte along with other viruses and various interfering agents like phosphate ions, sodium, potassium, alanine, glycine, arginine, etc. in **Fig.**

5.13a. The result showed that no significant interaction occurred with other biomolecules except the target analyte. In this case, various viruses such as NoV-LP, Zika, HEV-LP, dengue, and WSSV virus were taken in the concentration of 10 and 50 pg mL^{-1} or 10^4 and 10^5 copies mL^{-1}, where the response was almost ignorable which indicates enough specificity of the biosensor for target virus.

For long term use, the sensor should be stable and therefore, this sensing QD-peptide-AuNP nanocomposites was stored at 4°C after antibody conjugation and performed to detect target virus at every interval of one week. In **Fig. 5.13b**, the result showed that the sensor performed efficiently for over 3 weeks, confirming the excellent applicability of this sensing system.

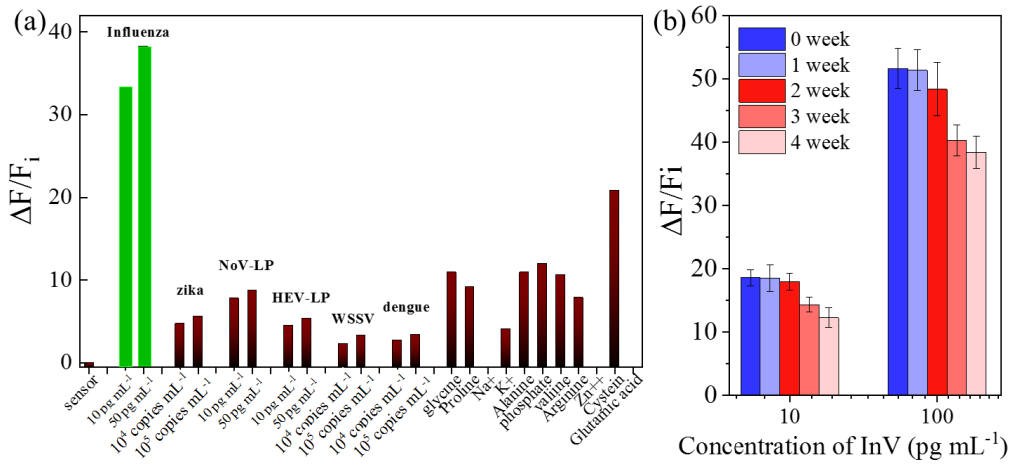

Fig. 5.13 (**a**) Selectivity test of the nanocomposite sensing probe for target influenza virus along with HEV-LP and NoV-LP, WSSV, Zika, and Dengue virus and some interfering agents like metal ions and amino acids. (**b**) Stability of the proposed sensor nanocomposite for detecting influenza virus over the one-month duration. (Nasrin *et al.*, 2020) (Reprinted with permission from Elsevier)

5.4.5 Sensing performance on different size of virus and effect on serum matrix

Three different sensing platform has been fabricated with three different antibodies of HEV-LP, influenza, and WSSV individually and performed to verify the dependency on virus size.

These three sensors having different antibodies corresponding to different sizes of target analytes including HEV-LP (30 nm), influenza (100 nm), and WSSV (200 nm). In **Fig. 5.14a**, the result showed there are no significant changes in sensing performance regarding virus sizes which proves the excellent performance of the proposed sensor.

To check the matrix effect of the sensor, the QD-peptide-AuNP nanocomposite has been applied to detect the influenza virus in 10 % human serum instead of DI water (**Fig. 5.14b**) and the calibration curve has been compared with performance in DI water which was obtained in **Fig. 5.11b**. The result showed little lower performances of the sensor in 10 % serum as the serum interferences are present in solution. However, the calculated LOD of the sensor is 65.1 fg mL^{-1} which is satisfactory for the applicability of the sensor in real samples.

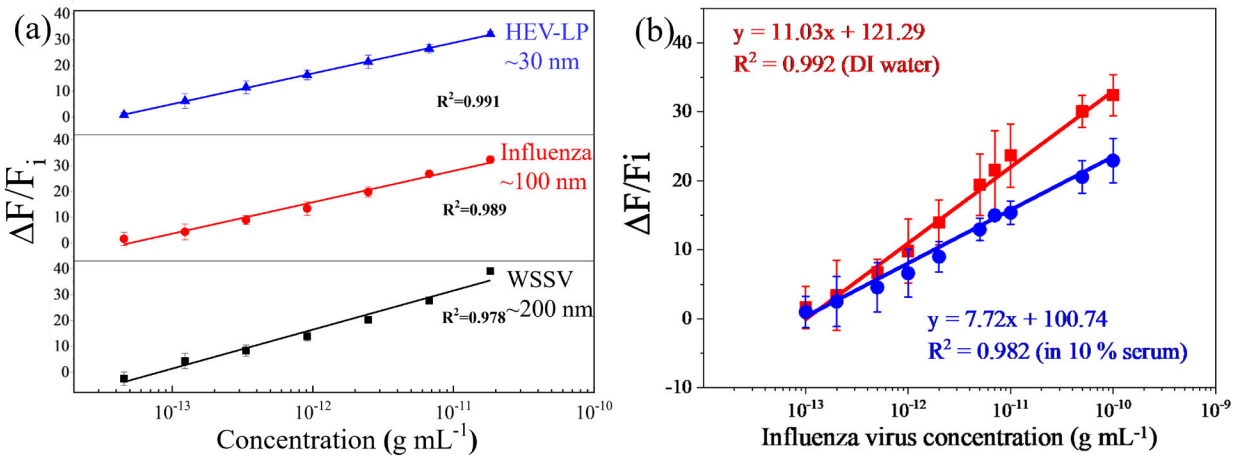

Fig. 5.14 (**a**) Comparison of three calibration lines obtained from the detection performance of three different viruses individually. (**b**) Comparison of calibration lines for detecting target influenza virus with this proposed sensor while performing in DI water and serum. (Nasrin *et al.*, 2020) (Reprinted with permission from Elsevier)

5.5 Conclusion

A new combination of nanocomposites has been synthesized in this work which can detect target analyte efficiently by a tunable LSPR-based fluorometric method. The detection mechanism was studied well where the distance-dependent LSPR can be tuned through the peptide linker. The result has been obtained a linear range of 10^{-14} to 10^{-9} g mL^{-1} with a detection limit of 17.02 fg mL^{-1} in water and 65.1 fg mL^{-1} in human serum for the target virus. As the linearity of this biosensor has been obtained from femtomolar to a nanomolar range which indicates the potential detectability and applicability for the detection of real sample analysis as a promising tool in the future.

CHAPTER 6

ADVANCEMENT IN SENSING SYSTEM BY CONSTRUCTING DUAL FUNTIONAL LIPOSOME-BASED BIOSENSOR

As per the sensing mechanism (**Principle 3**) mentioned in chapter 3, the detailed construction of the dual functionalized sensing system and the application for detection have been described in this chapter.

6.1 Construction of the biosensor

6.1.1 Synthesis of the sensing probe

Antibody for chikungunya was conjugated on the liposome and APTES-coated Fe_3O_4 nanoparticles separately, according to the previously reported protocol (Chowdhury *et al.*, 2020). Initially, the carboxyl group of the specific antibody to the CHIKVE1 was activated using EDC/NHS chemistry. After that, the as-synthesized amino-functionalized liposome-QD-MB complexes and APTES-coated Fe_3O_4 were added to activated antibody separately and incubated for 1 h at room temperature. The amine group of DSPE in liposome and APTES on Fe_3O_4 nanoparticles conjugates with the carboxylic group of the antibody and the solution were purified by centrifugation at 10,000 rpm for 10 min to remove the unreacted antibody and the coupling agents, separately.

6.1.2 Preparation of optical sensing for virus detection

Antibody-conjugated liposomes and Fe_3O_4 nanoparticles were mixed with various concentrations of the CHIKVE1 which made a sandwich structure and incubated for 30 min. After the hybridization, an external magnet was placed to the mixture solution for 1 min to separate the excess reactants from the solution and purify the sandwich nanocomposite structure. After separating, the sandwich mixture solution was re-dispersed in buffer and put in a microplate reader, and 5 µL of 0.1 mM chloroform was added to burst out the liposome which made releasing of encapsulated QDs. Finally, the sandwich nanocomposite solution was excited at 400 nm, and

measured the fluorescence intensity in a range of 600 – 750 nm before and after the addition of chloroform.

6.1.3 Preparation of electrochemical sensing for virus detection

For the electrochemical sensing, similar reaction procedure as mentioned above was performed in a separate tube and after disrupting, MB was released from the captured liposomes which were further deposited on graphene-modified electrodes and Differential pulse voltammetry (DPV) was carried out on a potentiostat/galvanostat workstation to record the electrochemical output signal of MB depending on the target virus concentration.

6.2 Characterization of nanoparticles and nanocomposites of the sensor

6.2.1 Characterization of CdSe QDs and APTES-coated MNP

As synthesized hydrophobic QDs were used to get encapsulated in the lipid bilayer of liposomes. These QDs nanoparticles were characterized by TEM images as showed in **Fig. 6.1a**. QDs were presented as uniformly dispersed with the range of 5 – 7 nm in diameter, where particle distribution showed in **Fig. 6.1b**. The fluorescence spectra and UV-absorption peak of QDs indicate that the emission peak and absorbance were at 670 nm and 650nm of wavelength, respectively (**Fig. 6.1c**). QDs were dark red in color as expected under UV light **(Fig. 6.1d**).

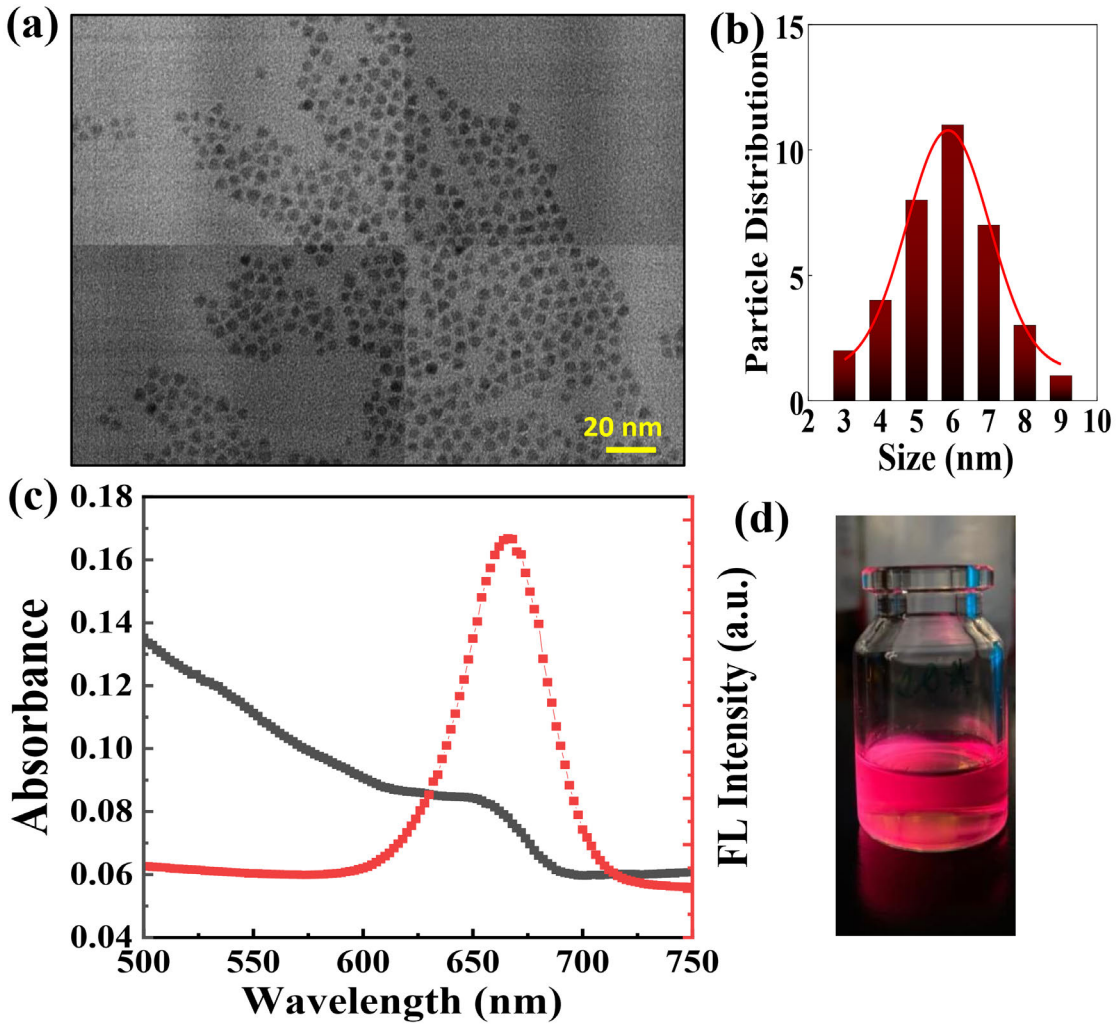

Fig. 6.1 Characterizations of the as-synthesized QDs nanoparticle showing, **(a)** the TEM image, **(b)** particle size distribution, **(c)** UV-vis absorption and fluorescence emission spectra, and **(d)** image under UV light.

At the same time, Fe_3O_4 nanoparticles were also obtained by sol-gel method and APTES was coated on it. The Fe_3O_4 nanoparticles were characterized by TEM image (**Fig. 6.2a**) and showed the size in between 10 – 25 nm with an average diameter of 16 nm (**Fig. 6.2b**).

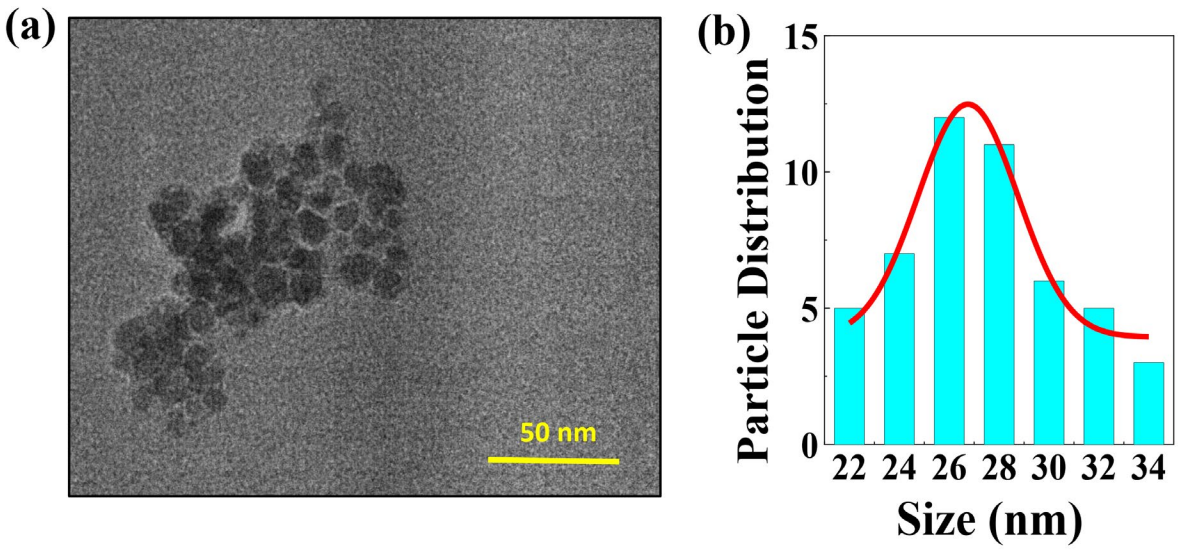

Fig. 6.2 Characterizations of the as-synthesized APTES-coated MNP showing, **(a)** TEM image, and **(b)** particle size distribution.

6.2.2 Characterization of the QDs and MB encapsulated liposome

Confocal analysis was performed to characterize the liposome structures. The phase-contrast (**Fig. 6.3a**) and fluorescent images (**Fig. 6.3b**) of liposome shows the perfectly spherical formation while emitting the intense red fluorescence of QDs in their lipid bilayer area. The liposomes were homogeneously distributed in the circular shape with the range of 200 – 300 nm in size, as shown in **Fig. 6.3c**. Hydrodynamic radius by DLS confirmed the size of the liposome, Fe_3O_4 nanoparticles, and nanocomposite after virus binding which forms the QD-MB-liposome/CHIKVE1/Fe_3O_4 sandwich nanoconjugates, as shown in **Fig. 6.3d**. The average size of the as-prepared Fe_3O_4 and QD-MB-liposome were found of 15 and 200 nm, respectively which resembles the size from the TEM image. However, after the formation of QD-MB-liposome/CHIKVE1/Fe_3O_4 sandwich nanoconjugates, the size of the nanoconjugates structure increased to 1000 nm, indicating the successful formation of the QD-MB-liposome/CHIKVE1/Fe_3O_4 sandwich structure.

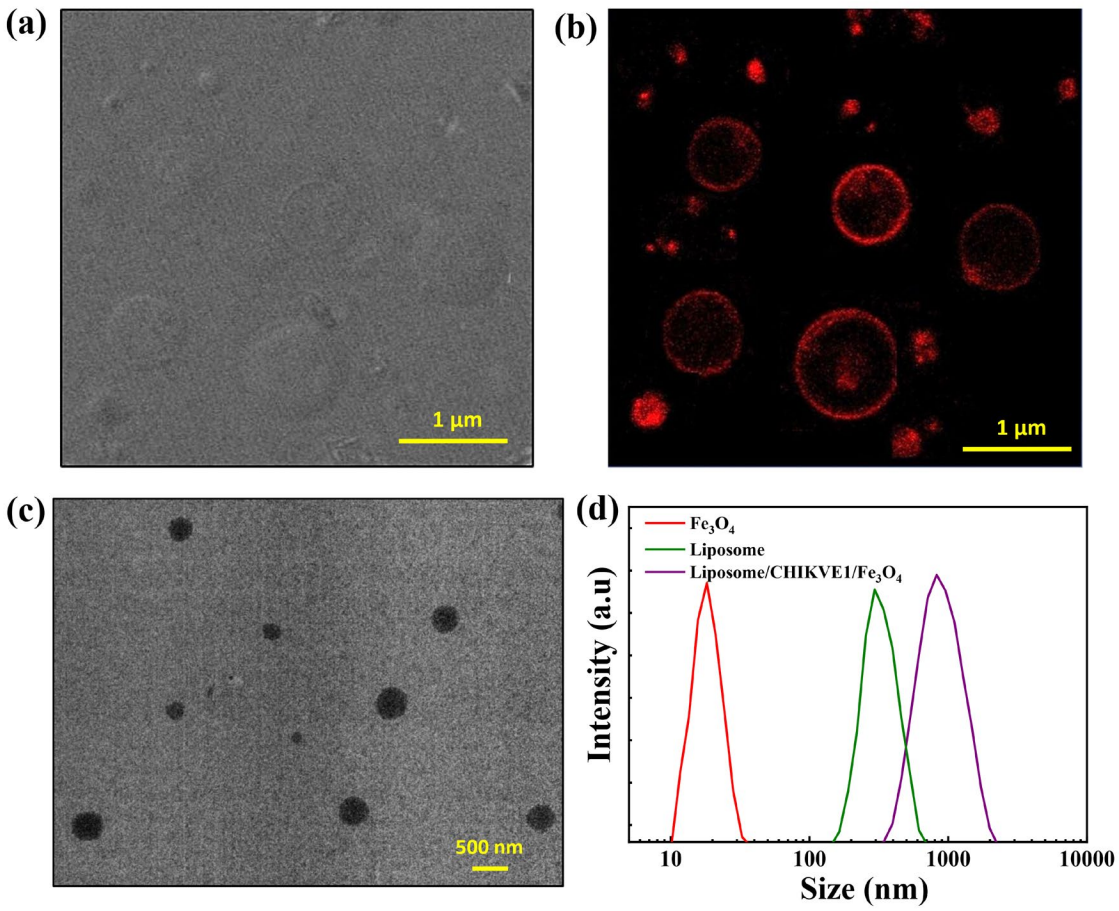

Fig. 6.3 Characterizations of the as-synthesized QD-MB-liposome nanocomposite. Confocal image for QD-MB-liposome showing **(a)** differential interference contrast (DIC) and **(b)** fluorescence images. TEM image showing for **(c)** QD-MB-liposomes. And, **(d)** hydrodynamic radius of as obtained Fe_3O_4 nanoparticles, liposomes, and QD-MB-liposome/CHIKVE1/Fe_3O_4 sandwich nanoconjugates.

6.3 Optimization of the sensing mechanism

The as-synthesized liposome has been initially investigated for the suitable agent to release of embedded fluorescent molecules. Among the different surfactants as presented in **Fig. 6.4a**, chloroform showed the best result compared to Triton X and Tween 20. In the case of 1:1 mixture of chloroform and methanol, the initial perturbation of the liposome may be a little higher than

only chloroform. However, after some time, the release of QDs has been noticed highest in the previous one. As the dissolving the lipid layer in the chloroform is a slow process, the optimized time for the complete release has chosen for 10 min as presented in **Fig. 6.4b**. After that the fluorescence enhancement has reached its saturation, confirming the dissolution time for liposome was for 10 min.

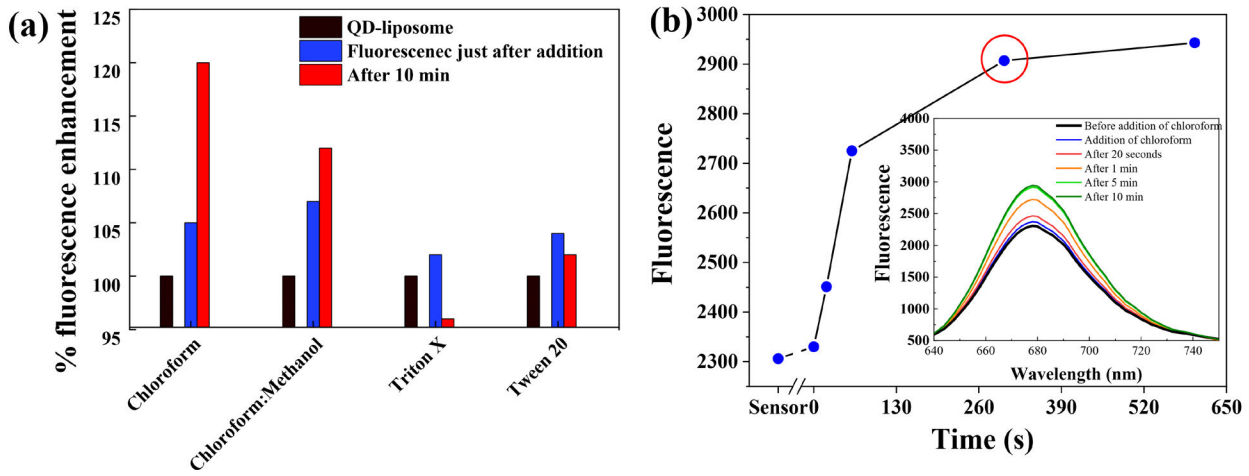

Fig. 6.4 Optimization of the QD-MB-liposome and Fe_3O_4 nanocomposites for sensing of CHIKVE1 detection. **(a)** Effect of the various chemical agents to burst out liposomes for releasing QDs. **(b)** Effect of time on showing the highest fluorescence level after liposome burst out.

The amount of CdSe QDs has been optimized with the fixed amount of liposome of 10^3 particles mL^{-1}. Three concentrations of QDs have been taken to check the optimum condition where the QDs can be perfectly embedded on the hydrophobic surface of the liposome. In the case of 0.5 and 1 mg mL^{-1} QDs concentration, the fluorescence enhancement is quite satisfactory compared to the low concentration of 0.1 mg mL^{-1}. However, in the case of 1 mg mL^{-1}, the QDs is not only embedded on the surface but also penetrated inside the liposome, as shown in the inset of **Fig. 6.5a**.

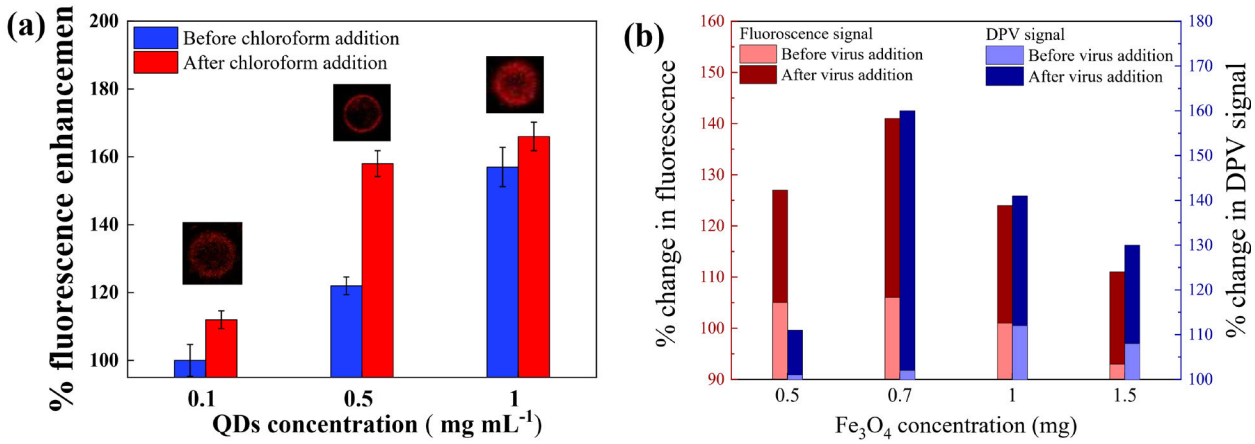

Fig. 6.5 Optimization of the QD-MB-liposome and Fe_3O_4 nanoconjugates for the detection of CHIKVE1. **(a)** Effect of different concentrations of QDs embedded in the liposome. **(b)** Effect of using different concentrations of Fe_3O_4 nanoparticles on signal amplification.

After optimizing the composition of liposome with the concentration of the embedded-QDs and encapsulated-MB, the formation of the QDs-MB-liposome/CHIKVE1/Fe_3O_4 nanoconjugates has been finally investigated with different ratio of the magnetic Fe_3O_4 nanoparticles and QDs-MB-liposome. In this work, the analyte of CHIKVE1 must be bound with antibody-conjugated QDs-MB-liposome and Fe_3O_4 in a sandwich structure and then isolated by the magnetic separation. Therefore, it is obvious that the higher number of Fe_3O_4 nanoparticles can enhance the possibility of better separation. However, optimization of the Fe_3O_4 nanoparticle is also a crucial parameter in this work. A concentration range of 10^{-13} – 10^{-9} g mL^{-1} of CHIKVE1 has tested with different amounts of Fe_3O_4 nanoparticles with a fixed concentration of QDs-MB-liposome. As shown in **Fig. 6.5b**, the magnetically separated QDs-MB-liposome/CHIKVE1/Fe_3O_4 nanoconjugates has tested on fluorometric and Differential pulse voltammetry (DPV), both method before and after the addition of chloroform. In the case of a low amount of Fe_3O_4, the magnetic nanoconjugates contain a lesser amount of virus particle as compared to the 0.7 mg which indicates the partial attachment

of viruses. On the other hand, a high amount of Fe_3O_4 of 1 and 1.5 mg, though the magnetic adduct successfully separated the viruses, however, it self-quenched the signal due to the MB-Fe_3O_4 and QDs-Fe_3O_4 interaction. Therefore, analyzing all the results, 0.7 mg of Fe_3O_4 showed the best-optimized condition for virus detection.

6.4 Application of the biosensor for virus detection

6.4.1 Fluorometric sensing of CHIKVE1 using liposome

The QDs-MB-liposome and Fe_3O_4 system has applied for the detection of different concentrations of CHIKVE1, as shown in **Fig. 6.6**. Before the addition of CHIKVE1, there is no interaction between antibody-conjugated QDs-MB-liposome and Fe_3O_4 in the reaction medium. After the addition of different concentrations of CHIKVE1 and incubated for 10 min, the nanoparticles have been bound with the virus by conjugating with the antibody on their surfaces and make the QDs-MB-liposome/CHIKVE1/Fe_3O_4 sandwich structure. Then these magnetically separated nanoconjugates have been tested on a fluorometric assay which showed a strong signal of the QDs after the burst out of the liposomes by chloroform. As shown in **Fig. 6.6a**, the fluorescence signal for different concentration of CHIKVE1 in the range of 10^{-13} – 10^{-8} g mL^{-1}, showed the increasing signal intensities of released QDs. The calibration line has been plotted in **Fig. 6.6b**, calculated from the intensity of fluorescence of QDs which showed the linearity over the wide concentration range. After calculating from the calibration line, the limit of detection has been shown with higher sensitivity which is 0.56 pg mL^{-1}.

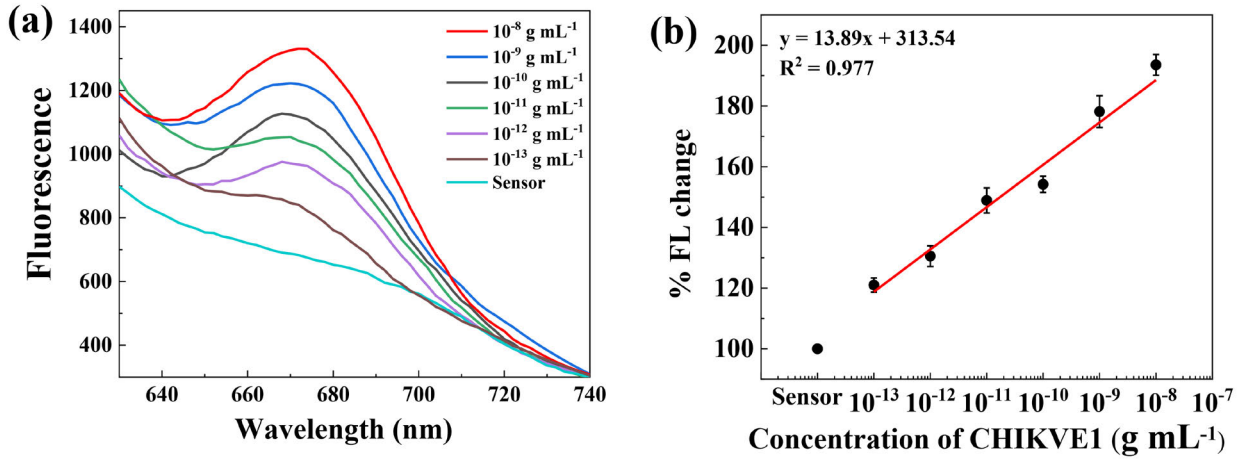

Fig. 6.6 Detection of CHIKVE1. **(a)** Fluorescence of QDs, released from the QD-MB-liposome/CHIKVE1/Fe_3O_4 nanoconjugates with different concentration of CHIKVE1 ranging from 10^{-8} – 10^{-13} g mL^{-1}, by treating with chloroform. **(b)** Calibration line of fluorescence intensities by successive concentration of CHIKVE1.

6.4.2 Electrochemical sensing of CHIKVE1 using liposome

Simultaneously, the QDs-MB-liposome/CHIKVE1/Fe_3O_4 nanoconjugates also tested in the electrochemical DPV for the measurement of the released MB. After the addition of the chloroform into the liposome nanocomposite solution, the released MB comes into the buffer solution. As shown in **Fig. 6.7a**, the DPV signal of MB at – 0.22 V represents the concentration of CHIKVE1 in the range of 10^{-14} – 10^{-8} g mL^{-1}. In **Fig. 6.7b**, the calibration line has been plotted from the peak current in DPV which showed the linearity with the correlation coefficient of 0.993. The limit of detection has been found of 32.7 fg mL^{-1}, calculated from 3σ/s method (Chowdhury and Park, 2019) (three times of the standard deviation of the lowest concentration of target/slope of the calibration line).

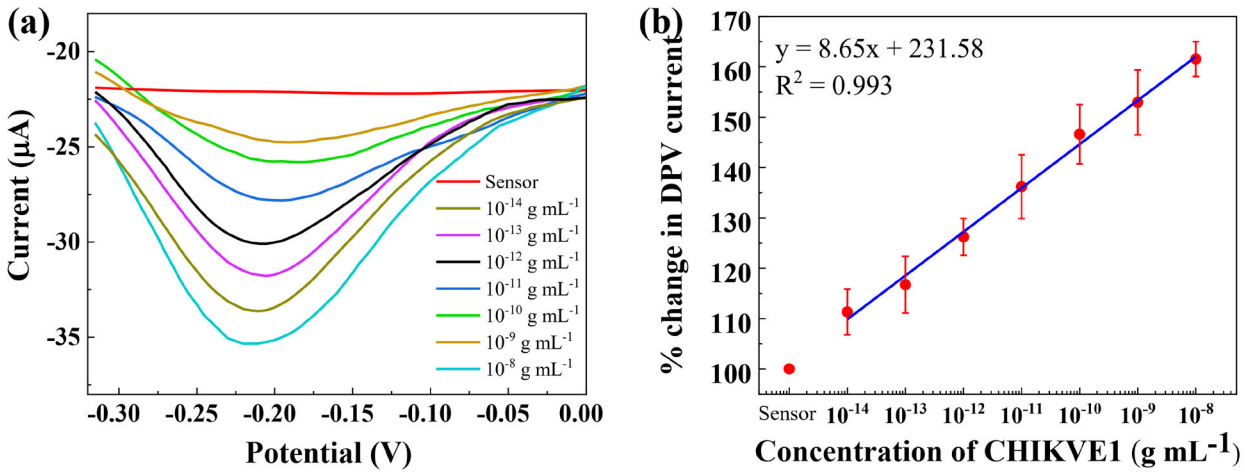

Fig. 6.7 Detection of CHIKVE1 in DPV. **(a)** redox peak of MB, released from the QD-MB-liposome/CHIKVE1/Fe_3O_4 nanoconjugates with different concentration of CHIKVE1 ranging from 10^{-8} – 10^{-14} g mL^{-1}, by treating with chloroform. **(b)** Calibration line of MB intensities by successive concentration of CHIKVE1.

6.5 Selectivity and specificity of the dual-functional sensing system

As the main interaction between the target CHIKVE1 and the QDs-MB-liposome and Fe_3O_4 nanoparticles is controlled by the antibody conjugation, therefore, the sensor has possessed high specificity. The selectivity test was carried out to confirm any non-specific binding of the sensor, in presence of BSA as negative matrix and different viruses like WSSV, Zika, and influenza viruses (10^5 copies mL^{-1}) and hepatitis E virus-like particle (10^{-9} g mL^{-1}). The sensor in BSA does not show any significant signal in both the detection method of fluorometric and DPV (**Fig. 6.8**). Also, other interfering viruses also do not show any significant signal as the sensing method contains a separation step through magnetic Fe_3O_4. Small signal from fluorometric response has been observed which may be due to some nonspecific interaction with the membrane of the liposome, however, it is significantly low compared to the target virus of CHIKVE1. Therefore,

from this selective study, it can be noted that the fluorescence as well as DPV signal comes only in presence of the specific target virus, confirming its practical applicability for the virus detection purpose.

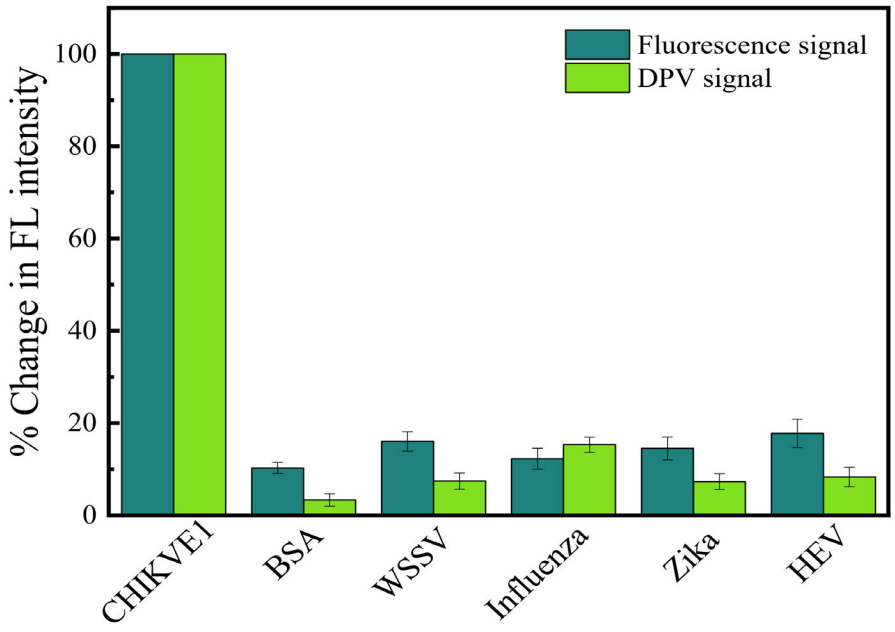

Fig. 6.8 Selectivity test of the QD-MB-liposome and Fe_3O_4 system. Fluorometric and electrochemical enhancement of QDs and MB, respectively in presence of the target CHIKVE1, BSA, WSSV, H1N1 influenza virus, Zika virus, and Hepatitis E virus-like particles.

6.6 Conclusion

In this study, a dual functional liposome-based biosensor encapsulating QDs and MB has been developed for the detection of virus by combining optical and electrochemical methods. The QD-MB-liposome composite was bound to target specific viruses and then the whole composites were magnetically separated from its medium and then burst out. Therefore, a large number of fluorescent QDs as well as the redox probe MB come out from few numbers of target analytes and amplify the detection signal in both processes of the fluorescence and electrochemical differential

pulse voltammetry (DPV). The detection limit has been found as 0.56 pg mL^{-1} and 32.7 fg mL^{-1} in the fluorometric and DPV processes, respectively. Besides, negligible cross-reactivity with similar viruses confirms the specific nature of the sensor with low background signal, indicating its potential application in different virus sensing approaches in the near future.

CHAPTER 7

CONCLUSIONS AND FUTURE PERSPECTIVE

7.1 Conclusions

To summaries, in the current thesis, the synthesis and application of different nanocomposites have been discussed in detail. A new combination of nanocomposites has been fabricated successfully for use in biosensors to detect different viruses.

All these sensing probes including nanomaterials are cost-effective, easy, and rapid which is based on reliable methods of optical and electrochemical techniques which are very important for the clinical diagnosis. All biosensors showed a satisfactory range of detection and could identify biological samples with a very low limit of detection. However, in this work, especially optical and electrochemical sensing process was applied and for this, different nanomaterials, nanocomposites, and liposomes have been synthesized by incorporating QDs, AuNPs, etc. and optimized their condition in nanocomposite for best sensing performance and thereafter applied to detect the virus.

In this thesis, initially described the fabrication of a new LSPR based method for label-free sensing system with higher selectivity and sensitivity. Here, LSPR behavior of AuNPs and fluorescent QDs were incorporated. Initially, these two duos were covalently attached to generate the sensing probe nanocomposites. And, based on LSPR response, the distance-dependent analysis was performed while adding the target virus and this sensing system could detect target NoV-LPs in the femtomolar level with a LOD of 12.1 fg mL^{-1} in DI water and 15.6 fg mL^{-1} in human serum. Even on performing real norovirus, the detection limit showed a satisfactory result which is 95.0 copies mL^{-1}. Therefore, this developed biosensor showed a possible application to detect the real virus in the future.

Another work in this research also described the fabrication of a nanocomposite based on tunable distance-based LSPR where the distance between fluorescent QDs and AuNPs was

optimized in a controlled manner. To maintain the distance, a peptide chain of 18 amino acids was applied. The main advantage of this work is the tuning capability of this distance between two duos which can result in the steric hindrance on the LSPR, the key mechanism to detect a virus. The detection performance reached in femtomolar level with a detection limit of 17.02 fg mL^{-1} in water and 65.1 fg mL^{-1} in human serum.

For the advancement in the sensing system, a dual functional liposome-based amplification technique has been established for target virus detection. In this work, both fluorescence of QDs and redox indicator MB have been used to generate the immense signals for specific target binding. The QD-MB-liposome composite was bound to target specific viruses and then the whole composites were magnetically separated from its medium and then burst out. Therefore, a large number of fluorescent QDs as well as the redox probe MB come out from few numbers of target analytes and amplify the detection signal, providing highly sensitive detection. The detection limit has been found as 0.56 pg mL^{-1} and 32.7 fg mL^{-1} in the fluorometric and DPV processes, respectively.

Overall, from these above results obtained in this thesis work, it can be concluded that the developed biosensor can be a potential candidate in the practical fields for application. The easy fabrication procedure, cost-effectiveness, and simple application procedures with higher sensitivity proved to show excellent performance in the biosensing field.

7.2 Future scope of the work

Recently, different nanocomposites have emerged as a new class of sensing probe for application in various fields. Through this research work, various biosensors have been developed by synthesizing different nanocomposites and optimizing them to get the best results for

demonstrating applicability in virus sensing. In this thesis, a detailed discussion has been made for the synthesis along with their properties. The work presented in this thesis provides some new opportunities for the development of optical and electrochemical biosensors.

The achievement of this research is to step forward in the field of nanotechnology which has been given the effort to develop a new combination of nanocomposites as a sensing probe. In terms of nanocomposite sensing development, strategies for combining nanomaterials are still in need.

The unique properties of different nanomaterials suggest that the ongoing research on developing biosensors is still at a very early stage and so many directions still need to be opened for exploration. Since the nanostructure has certain properties favorable for other applications, it can be used in bio-imaging as well as drug delivery systems.

Although many advancements have been achieved in the field of biosensing, the real-life applications are still unsatisfactory and having a lot of remaining challenges. Moreover, the development of therapeutic nanomaterials for use in biosensors may provide new thinking of generating smart devices for therapy and diagnostics use.

References

Aberl, F., Kößlinger, C., Biosensor-based methods in clinical diagnosis, Molecular diagnosis of infectious diseases, Springer1998, pp. 503–17.

Acimovic, S.S., Ortega, M.A., Sanz, V., Berthelot, J., Garcia-Cordero, J.L., Renger, J., et al., LSPR chip for parallel, rapid, and sensitive detection of cancer markers in serum, Nano Lett., 14(2014) 2636–41.

Adegoke, O., Morita, M., Kato, T., Ito, M., Suzuki, T., Park, E.Y., Localized surface plasmon resonance-mediated fluorescence signals in plasmonic nanoparticle-quantum dot hybrids for ultrasensitive Zika virus RNA detection via hairpin hybridization assays, Biosens. Bioelectron., 94(2017) 513–22.

Adegoke, O., Nyokong, T., Forbes, P.B., Structural and optical properties of alloyed quaternary CdSeTeS core and CdSeTeS/ZnS core–shell quantum dots, J. Alloys Compd., 645(2015) 443–9.

Adegoke, O., Seo, M.-W., Kato, T., Kawahito, S., Park, E.Y., Gradient band gap engineered alloyed quaternary/ternary CdZnSeS/ZnSeS quantum dots: an ultrasensitive fluorescence reporter in a conjugated molecular beacon system for the biosensing of influenza virus RNA, J. Mater. Chem. B, 4(2016) 1489–98.

Adegoke, O., Seo, M.-W., Kato, T., Kawahito, S., Park, E.Y., An ultrasensitive SiO_2-encapsulated alloyed CdZnSeS quantum dot-molecular beacon nanobiosensor for norovirus, Biosens. Bioelectron., 86(2016) 135–42.

Adeloju, S., Shaw, S., Wallace, G., Polypyrrole-based potentiometric biosensor for urea part 1. Incorporation of urease, Anal. Chim. Acta, 281(1993) 611–20.

Ahmed, S.R., Hossain, M.A., Park, J.Y., Kim, S.-H., Lee, D., Suzuki, T., et al., Metal enhanced fluorescence on nanoporous gold leaf-based assay platform for virus detection, Biosens. Bioelectron., 58(2014) 33–9.

Ahmed, S.R., Kim, J., Suzuki, T., Lee, J., Park, E.Y., Enhanced catalytic activity of gold nanoparticle-carbon nanotube hybrids for influenza virus detection, Biosens. Bioelectron., 85(2016) 503–8.

Ahmed, S.R., Oh, S., Baba, R., Zhou, H., Hwang, S., Lee, J., et al., Synthesis of gold nanoparticles with buffer-dependent variations of size and morphology in biological buffers, Nanoscale Res. Lett., 11(2016) 65.

Al-Ogaidi, I., Gou, H., Aguilar, Z.P., Guo, S., Melconian, A.K., Al-Kazaz, A.K.A., et al., Detection of the ovarian cancer biomarker CA-125 using chemiluminescence resonance energy transfer to graphene quantum dots, Chem. Commun., 50(2014) 1344–6.

Anderson, R.E., Chan, W.C., Systematic investigation of preparing biocompatible, single, and small ZnS-capped CdSe quantum dots with amphiphilic polymers, ACS Nano, 2(2008) 1341–52.

Anh, N.T.N., Chowdhury, A.D., Doong, R.-a., Highly sensitive and selective detection of mercury ions using N, S-codoped graphene quantum dots and its paper strip based sensing application in wastewater, Sens. Actuators, B, 252(2017) 1169–78.

Banerjee, R., Liposomes: applications in medicine, J. Biomater. Appl., 16(2001) 3-21.

Bedford, T., Riley, S., Barr, I.G., Broor, S., Chadha, M., Cox, N.J., et al., Global circulation patterns of seasonal influenza viruses vary with antigenic drift, Nature, 523(2015) 217–20.

Biju, V., Chemical modifications and bioconjugate reactions of nanomaterials for sensing, imaging, drug delivery and therapy, Chem. Soc. Rev., 43(2014) 744–64.

Biju, V., Itoh, T., Ishikawa, M., Delivering quantum dots to cells: bioconjugated quantum dots for targeted and nonspecific extracellular and intracellular imaging, Chem. Soc. Rev., 39(2010) 3031–56.

Bitler, E., Matthews, J., Dickey, B., Eisenberg, J., Leon, J., Norovirus outbreaks: a systematic review of commonly implicated transmission routes and vehicles, Epidemiol Infect, 141(2013) 1563–71.

Bohren, C.F., Huffman, D.R., Absorption and Scattering of, Light by Small, (1983).

Brolo, A.G., Plasmonics for future biosensors, Nat. Photonics, 6(2012) 709.

Bruchez, M., Moronne, M., Gin, P., Weiss, S., Alivisatos, A.P., Semiconductor nanocrystals as fluorescent biological labels, science, 281(1998) 2013–6.

Bui, M.-P.N., Ahmed, S., Abbas, A., Single-digit pathogen and attomolar detection with the naked eye using liposome-amplified plasmonic immunoassay, Nano Lett., 15(2015) 6239–46.

Campbell, C.T., Kim, G., SPR microscopy and its applications to high-throughput analyses of biomolecular binding events and their kinetics, Biomaterials, 28(2007) 2380–92.

Carboni, V., Maaliki, C., Alyami, M., Alsaiari, S., Khashab, N., Synthetic vehicles for encapsulation and delivery of CRISPR/Cas9 gene editing machinery, Adv. Ther., 2(2019) 1800085.

Čeh, B., Lasic, D.D., Kinetics of accumulation of molecules into liposomes, The J. of Phys. Chem. B, 102(1998) 3036-43.

Chan, W.C., Nie, S., Quantum dot bioconjugates for ultrasensitive nonisotopic detection, Science, 281(1998) 2016–8.

Chang, Y.-F., Wang, S.-F., Huang, J.C., Su, L.-C., Yao, L., Li, Y.-C., et al., Detection of swine-origin influenza A (H1N1) viruses using a localized surface plasmon coupled fluorescence fiber-optic biosensor, Biosens. Bioelectron., 26(2010) 1068–73.

Chen, C., Wang, Q., Liposome-based nanosensors, Am. J. Nano Res. Appl., 3(2015) 13-7.

Chen, S., Svedendahl, M., Van Duyne, R.P., Käll, M., Plasmon-enhanced colorimetric ELISA with single molecule sensitivity, Nano Lett., 11(2011) 1826–30.

Chouteau, C., Dzyadevych, S., Durrieu, C., Chovelon, J.-M., A bi-enzymatic whole cell conductometric biosensor for heavy metal ions and pesticides detection in water samples, Biosens. Bioelectron., 21(2005) 273–81.

Chowdhury, A.D., Agnihotri, N., De, A., Sarkar, M., Detection of positional mismatch in oligonucleotide by electrochemical method, Sens. Actuators, B, 202(2014) 917–23.

Chowdhury, A.D., Ganganboina, A.B., Tsai, Y.-c., Chiu, H.-c., Doong, R.-a., Multifunctional GQDs-Concanavalin A@Fe_3O_4 nanocomposites for cancer cells detection and targeted drug delivery, Anal. Chim. Acta, 1027(2018) 109–20.

Chowdhury, A.D., Park, E.Y., Methylene blue-encapsulated liposomal biosensor for electrochemical detection of sphingomyelinase enzyme, Sens. Actuators, B, 301(2019) 127153.

Chowdhury, A.D., Sharmin, S., Nasrin, F., Yamazaki, M., Abe, F., Suzuki, T., et al., Use of Target Specific Liposome and Magnetic Nanoparticles Conjugation for the Amplified Detection of Norovirus, ACS Appl. Bio Mater., (2020).

Chowdhury, A.D., Takemura, K., Li, T.-C., Suzuki, T., Park, E.Y., Electrical pulse-induced electrochemical biosensor for hepatitis E virus detection, Nat. Commun., 10(2019) 1–12.

Chu, X., Duan, D., Shen, G., Yu, R., Amperometric glucose biosensor based on electrodeposition of platinum nanoparticles onto covalently immobilized carbon nanotube electrode, Talanta, 71(2007) 2040–7.

Chuong, T.T., Pallaoro, A., Chaves, C.A., Li, Z., Lee, J., Eisenstein, M., et al., Dual-reporter SERS-based biomolecular assay with reduced false-positive signals, Proc Natl Acad Sci, 114(2017) 9056-61.

Clapp, A.R., Medintz, I.L., Mattoussi, H., Förster resonance energy transfer investigations using quantum-dot fluorophores, ChemPhysChem, 7(2006) 47–57.

Clark Jr, L.C., Lyons, C., Electrode systems for continuous monitoring in cardiovascular surgery, Ann. N.Y. Acad. Sci., 102(1962) 29-45.

Cornell, B.A., Braach-Maksvytis, V., King, L., Osman, P., Raguse, B., Wieczorek, L., et al., A biosensor that uses ion-channel switches, Nature, 387(1997) 580–3.

Dabbousi, B.O., Rodriguez-Viejo, J., Mikulec, F.V., Heine, J.R., Mattoussi, H., Ober, R., et al., (CdSe) ZnS core− shell quantum dots: synthesis and characterization of a size series of highly luminescent nanocrystallites, J. Phys Chem B, 101(1997) 9463–75.

Dave, B.C., Dunn, B., Valentine, J.S., Zink, J.I., Sol-gel encapsulation methods for biosensors, Anal. Chem., 66(1994) 1120A–7A.

Ding, L., Yang, H., Ge, S., Yu, J., Fluorescent carbon dots nanosensor for label-free determination of vitamin B_{12} based on inner filter effect, Spectrochim. Acta, Part A, 193(2018) 305–9.

Dutta, C.A., Kenshin, T., Memdi, K.I., Fahmida, N., Tun, N., Myat, M., et al., The detection and identification of dengue virus serotypes with quantum dot and AuNP regulated localized surface plasmon resonance, Nanoscale Adv., (2019).

Dutta Chowdhury, A., Agnihotri, N., Doong, R.-a., De, A., Label-free and nondestructive separation technique for isolation of targeted DNA from DNA–protein mixture using magnetic Au–Fe_3O_4 nanoprobes, Anal. Chem., 89(2017) 12244–51.

Dutta Chowdhury, A., Ganganboina, A.B., Nasrin, F., Takemura, K., Doong, R.-a., Utomo, D.I.S., et al., Femtomolar detection of dengue virus DNA with serotype identification ability, Anal. Chem., 90(2018) 12464–74.

Esseghaier, C., Helali, S., Fredj, H.B., Tlili, A., Abdelghani, A., Polypyrrole–neutravidin layer for impedimetric biosensor, Sens. Actuators, B, 131(2008) 584–9.

Eum, N.-S., Lee, S.-H., Lee, D.-R., Kwon, D.-K., Shin, J.-K., Kim, J.-H., et al., K_+-ion sensing using surface plasmon resonance by NIR light source, Sens. Actuators, B, 96(2003) 446–50.

Eustis, S., El-Sayed, M.A., Why gold nanoparticles are more precious than pretty gold: noble metal surface plasmon resonance and its enhancement of the radiative and nonradiative properties of nanocrystals of different shapes, Chem. Soc. Rev., 35(2006) 209–17.

Fan, X., White, I.M., Shopova, S.I., Zhu, H., Suter, J.D., Sun, Y., Sensitive optical biosensors for unlabeled targets: A review, Anal. Chim. Acta, 620(2008) 8–26.

Fang, Y., Ferrie, A.M., Label-free optical biosensor for ligand-directed functional selectivity acting on β2 adrenoceptor in living cells, FEBS Lett., 582(2008) 558–64.

Feizpour, A., Yu, X., Akiyama, H., Miller, C.M., Edmans, E., Gummuluru, S., et al., Quantifying lipid contents in enveloped virus particles with plasmonic nanoparticles, Small, 11(2015) 1592–602.

Feng, A.L., You, M.L., Tian, L., Singamaneni, S., Liu, M., Duan, Z., et al., Distance-dependent plasmon-enhanced fluorescence of upconversion nanoparticles using polyelectrolyte multilayers as tunable spacers, Sci. Rep., 5(2015) 7779.

Feng, L., Wu, X., Ren, L., Xiang, Y., He, W., Zhang, K., et al., Well-Controlled Synthesis of Au@ Pt Nanostructures by Gold-Nanorod-Seeded Growth, Chem. Eur. J, 14(2008) 9764–71.

Freeman, R., Girsh, J., Willner, I., Nucleic acid/quantum dots (QDs) hybrid systems for optical and photoelectrochemical sensing, ACS Appl. Mater. Interfaces, 5(2013) 2815–34.

Ganganboina, A.B., Chowdhury, A.D., Doong, R.-a., Nano assembly of N-doped graphene quantum dots anchored Fe_3O_4/halloysite nanotubes for high performance supercapacitor, Electrochim. Acta, 245(2017) 912-23.

Ganganboina, A.B., Chowdhury, A.D., Khoris, I.M., Nasrin, F., Takemura, K., Hara, T., et al., Dual modality sensor using liposome-based signal amplification technique for ultrasensitive norovirus detection, Biosens. Bioelectron., (2020) 112169.

Ganganboina, A.B., Doong, R.-a., The biomimic oxidase activity of layered V_2O_5 nanozyme for rapid and sensitive nanomolar detection of glutathione, Sens. Actuators, B, 273(2018) 1179–86.

Geißler, D., Charbonnière, L.J., Ziessel, R.F., Butlin, N.G., Löhmannsröben, H.G., Hildebrandt, N., Quantum dot biosensors for ultrasensitive multiplexed diagnostics, Angew. Chem. Int. Ed., 49(2010) 1396–401.

Gerard, M., Chaubey, A., Malhotra, B., Application of conducting polymers to biosensors, Biosens. Bioelectron., 17(2002) 345–59.

Ghosh, D., Chattopadhyay, N., Gold nanoparticles: acceptors for efficient energy transfer from the photoexcited fluorophores, Opt. Photonics J., 3(2013) 18–26.

Gowri, A., Sai, V., Development of LSPR based U-bent plastic optical fiber sensors, Sens. Actuators, B, 230(2016) 536–43.

Gregg, B.A., Heller, A., Cross-linked redox gels containing glucose oxidase for amperometric biosensor applications, Anal. Chem., 62(1990) 258–63.

Guo, L., Jackman, J.A., Yang, H.-H., Chen, P., Cho, N.-J., Kim, D.-H., Strategies for enhancing the sensitivity of plasmonic nanosensors, Nano Today, 10(2015) 213–39.

Guo, X., Surface plasmon resonance based biosensor technique: a review, J. Biophotonics, 5(2012) 483–501.

Gupta, R., Chaudhury, N., Entrapment of biomolecules in sol–gel matrix for applications in biosensors: Problems and future prospects, Biosens. Bioelectron., 22(2007) 2387–99.

Haddada, M.B., Salmain, M., Boujday, S., Gold colloid-nanostructured surfaces for enhanced piezoelectric immunosensing of staphylococcal enterotoxin A, Sens. Actuators, B, 255(2018) 1604–13.

Haes, A.J., Van Duyne, R.P., A nanoscale optical biosensor: sensitivity and selectivity of an approach based on the localized surface plasmon resonance spectroscopy of triangular silver nanoparticles, J. Am. Chem. Soc., 124(2002) 10596–604.

Han, J., Tong, F., Chen, P., Zeng, X., Duan, Z., Study of inflammatory factors' effect on the endothelial barrier using piezoelectric biosensor, Biosens. Bioelectron., 109(2018) 43–9.

Hansen, P.M., Bhatia, V.K., Harrit, N., Oddershede, L., Expanding the optical trapping range of gold nanoparticles, Nano Lett., 5(2005) 1937–42.

Hao, E., Schatz, G.C., Hupp, J.T., Synthesis and optical properties of anisotropic metal nanoparticles, J. Fluoresc., 14(2004) 331–41.

Hao, Q., Du, D., Wang, C., Li, W., Huang, H., Li, J., et al., Plasmon-induced broadband fluorescence enhancement on Al-Ag bimetallic substrates, Sci. Rep., 4(2014) 6014.

Hassanpour, S., Baradaran, B., de la Guardia, M., Baghbanzadeh, A., Mosafer, J., Hejazi, M., et al., Diagnosis of hepatitis via nanomaterial-based electrochemical, optical or piezoelectrical biosensors: a review on recent advancements, Microchim. Acta, 185(2018) 568.

He, W., Luo, L., Liu, Q., Chen, Z., Colorimetric sensor array for discrimination of heavy metal ions in aqueous solution based on three kinds of thiols as receptors, Anal. Chem., 90(2018) 4770–5.

Holme, M.N., Rana, S., Barriga, H.M., Kauscher, U., Brooks, N.J., Stevens, M.M., A robust liposomal platform for direct colorimetric detection of sphingomyelinase enzyme and inhibitors, ACS Nano, 12(2018) 8197-207.

Homola, J., Surface plasmon resonance sensors for detection of chemical and biological species, Chem. Rev., 108(2008) 462–93.

Hossain, F., Moghal, M.M.R., Islam, M.Z., Moniruzzaman, M., Yamazaki, M., Membrane potential is vital for rapid permeabilization of plasma membranes and lipid bilayers by the antimicrobial peptide lactoferricin B, J. Biol. Chem., 294(2019) 10449-62.

Hossain, M.K., Huang, G.G., Kaneko, T., Ozaki, Y., Characteristics of surface-enhanced Raman scattering and surface-enhanced fluorescence using a single and a double layer gold nanostructure, PCCP, 11(2009) 7484–90.

Huang, Y., Hu, F., Zhao, R., Zhang, G., Yang, H., Zhang, D., Tetraphenylethylene Conjugated with a Specific Peptide as a Fluorescence Turn-On Bioprobe for the Highly Specific Detection and Tracing of Tumor Markers in Live Cancer Cells, Chem. Eur. J, 20(2014) 158–64.

Hushegyi, A., Pihíková, D., Bertok, T., Adam, V., Kizek, R., Tkac, J., Ultrasensitive detection of influenza viruses with a glycan-based impedimetric biosensor, Biosens. Bioelectron., 79(2016) 644–9.

Jaiswal, J.K., Mattoussi, H., Mauro, J.M., Simon, S.M., Long-term multiple color imaging of live cells using quantum dot bioconjugates, Nat. Biotechnol., 21(2003) 47–51.

Jans, H., Huo, Q., Gold nanoparticle-enabled biological and chemical detection and analysis, Chem. Soc. Rev., 41(2012) 2849–66.

Jeon, J., Uthaman, S., Lee, J., Hwang, H., Kim, G., Yoo, P.J., et al., In-direct localized surface plasmon resonance (LSPR)-based nanosensors for highly sensitive and rapid detection of cortisol, Sens. Actuators, B, 266(2018) 710–6.

Jeong, E.-J., Jeong, Y.S., Park, K., Yi, S.Y., Ahn, J., Chung, S.J., et al., Directed immobilization of DNA-binding proteins on a cognate DNA-modified chip surface, J. Biotechnol., 135(2008) 16–21.

Jiang, X., Wang, M., Graham, D.Y., Estes, M.K., Expression, self-assembly, and antigenicity of the Norwalk virus capsid protein, J. Virol., 66(1992) 6527–32.

Kaur, B., Kaur, N., Kumar, S., Colorimetric metal ion sensors–a comprehensive review of the years 2011–2016, Coord. Chem. Rev., 358(2018) 13–69.

Kawaguchi, T., Shankaran, D.R., Kim, S.J., Matsumoto, K., Toko, K., Miura, N., Surface plasmon resonance immunosensor using Au nanoparticle for detection of TNT, Sens. Actuators, B, 133(2008) 467–72.

Kelly, K.L., Coronado, E., Zhao, L.L., Schatz, G.C., The optical properties of metal nanoparticles: the influence of size, shape, and dielectric environment, ACS Publications2003.

Khatri, A., Punjabi, N., Ghosh, D., Maji, S.K., Mukherji, S., Detection and differentiation of α-Synuclein monomer and fibril by chitosan film coated nanogold array on optical sensor platform, Sens. Actuators, B, 255(2018) 692–700.

Krishnamurthy, S., Esterle, A., Sharma, N.C., Sahi, S.V., Yucca-derived synthesis of gold nanomaterial and their catalytic potential, Nanoscale Res. Lett., 9(2014) 627.

Kulakovich, O., Strekal, N., Yaroshevich, A., Maskevich, S., Gaponenko, S., Nabiev, I., et al., Enhanced luminescence of CdSe quantum dots on gold colloids, Nano Lett., 2(2002) 1449–52.

Lee, J.-H., Kim, B.-C., Oh, B.-K., Choi, J.-W., Highly sensitive localized surface plasmon resonance immunosensor for label-free detection of HIV-1, Nanomed. Nanotechnol. Biol. Med., 9(2013) 1018–26.

Lee, J., Adegoke, O., Park, E.Y., High-Performance Biosensing Systems Based on Various Nanomaterials as Signal Transducers, Biotechnol. J., 14(2019) 1800249.

Lee, J., Ahmed, S.R., Oh, S., Kim, J., Suzuki, T., Parmar, K., et al., A plasmon-assisted fluoro-immunoassay using gold nanoparticle-decorated carbon nanotubes for monitoring the influenza virus, Biosens. Bioelectron., 64(2015) 311–7.

Leng, W., Pati, P., Vikesland, P.J., Room temperature seed mediated growth of gold nanoparticles: mechanistic investigations and life cycle assesment, Environ. Sci. Nano, 2(2015) 440–53.

Li, M.-X., Zhao, W., Qian, G.-S., Feng, Q.-M., Xu, J.-J., Chen, H.-Y., Distance mediated electrochemiluminescence enhancement of CdS thin films induced by the plasmon coupling of gold nanoparticle dimers, Chem. Commun., 52(2016) 14230–3.

Li, M., Cushing, S.K., Wang, Q., Shi, X., Hornak, L.A., Hong, Z., et al., Size-dependent energy transfer between CdSe/ZnS quantum dots and gold nanoparticles, J. Phys. Chem, 2(2011) 2125–9.

Li, Y., Schluesener, H.J., Xu, S., Gold nanoparticle-based biosensors, Gold Bull., 43(2010) 29–41.

Li, Z., Wang, Y., Wang, J., Tang, Z., Pounds, J.G., Lin, Y., Rapid and sensitive detection of protein biomarker using a portable fluorescence biosensor based on quantum dots and a lateral flow test strip, Anal. Chem., 82(2010) 7008–14.

Lim, D.-K., Jeon, K.-S., Hwang, J.-H., Kim, H., Kwon, S., Suh, Y.D., et al., Highly uniform and reproducible surface-enhanced Raman scattering from DNA-tailorable nanoparticles with 1-nm interior gap, Nat. Nanotechnol., 6(2011) 452.

Liu, C., Zhou, Q., Li, Y., Garner, L.V., Watkins, S.P., Carter, L.J., et al., Research and development on therapeutic agents and vaccines for COVID-19 and related human coronavirus diseases, ACS Publications2020.

Liu, J., Lu, Y., Colorimetric biosensors based on DNAzyme-assembled gold nanoparticles, J. Fluoresc., 14(2004) 343–54.

Liu, J., Zhou, X., Shi, H., An optical biosensor-based quantification of the microcystin synthetase a gene: early warning of toxic cyanobacterial blooming, Anal. Chem., 90(2018) 2362–8.

Liu, S., Zhao, N., Cheng, Z., Liu, H., Amino-functionalized green fluorescent carbon dots as surface energy transfer biosensors for hyaluronidase, Nanoscale, 7(2015) 6836–42.

Liu, Y., Zhang, L., Wei, W., Zhao, H., Zhou, Z., Zhang, Y., et al., Colorimetric detection of influenza A virus using antibody-functionalized gold nanoparticles, Analyst, 140(2015) 3989–95.

Malic, L., Sandros, M.G., Tabrizian, M., Designed biointerface using near-infrared quantum dots for ultrasensitive surface plasmon resonance imaging biosensors, Anal. Chem., 83(2011) 5222–9.

Miao, Y., Tan, S.N., Amperometric hydrogen peroxide biosensor based on immobilization of peroxidase in chitosan matrix crosslinked with glutaraldehyde, Analyst, 125(2000) 1591–4.

Monošík, R., Streďanský, M., Šturdík, E., Biosensors-classification, characterization and new trends, Acta Chimica Slovaca, 5(2012) 109–20.

Moskovits, M., Surface roughness and the enhanced intensity of Raman scattering by molecules adsorbed on metals, J Chem Phys, 69(1978) 4159–61.

Muhammad-Tahir, Z., Alocilja, E.C., A conductometric biosensor for biosecurity, Biosens. Bioelectron., 18(2003) 813–9.

Mulvaney, P., Surface plasmon spectroscopy of nanosized metal particles, Langmuir, 12(1996) 788–800.

Murray, C., Norris, D.J., Bawendi, M.G., Synthesis and characterization of nearly monodisperse CdE (E= sulfur, selenium, tellurium) semiconductor nanocrystallites, J. Am. Chem. Soc., 115(1993) 8706–15.

Nasrin, F., Chowdhury, A.D., Takemura, K., Kozaki, I., Honda, H., Adegoke, O., et al., Fluorometric virus detection platform using quantum dots-gold nanocomposites optimizing the linker length variation, Anal. Chim. Acta, (2020).

Nasrin, F., Chowdhury, A.D., Takemura, K., Lee, J., Adegoke, O., Deo, V.K., et al., Single-step detection of norovirus tuning localized surface plasmon resonance-induced optical signal between gold nanoparticles and quantum dots, Biosens. Bioelectron., 122(2018) 16–24.

Nie, S., Emory, S.R., Probing single molecules and single nanoparticles by surface-enhanced Raman scattering, science, 275(1997) 1102–6.

Oh, S.Y., Heo, N.S., Shukla, S., Cho, H.-J., Vilian, A.E., Kim, J., et al., Development of gold nanoparticle-aptamer-based LSPR sensing chips for the rapid detection of Salmonella typhimurium in pork meat, Sci. Rep., 7(2017) 1–10.

Oldenburg, S.J., Genick, C.C., Clark, K.A., Schultz, D.A., Base pair mismatch recognition using plasmon resonant particle labels, Anal. Biochem., 309(2002) 109–16.

Pang, Y., Rong, Z., Wang, J., Xiao, R., Wang, S., A fluorescent aptasensor for H5N1 influenza virus detection based-on the core–shell nanoparticles metal-enhanced fluorescence (MEF), Biosens. Bioelectron., 66(2015) 527–32.

Park, J., Joo, J., Kwon, S.G., Jang, Y., Hyeon, T., Synthesis of monodisperse spherical nanocrystals, Angew. Chem. Int. Ed., 46(2007) 4630–60.

Patskovsky, S., Jacquemart, R., Meunier, M., De Crescenzo, G., Kabashin, A.V., Phase-sensitive spatially-modulated surface plasmon resonance polarimetry for detection of biomolecular interactions, Sens. Actuators, B, 133(2008) 628–31.

Peiris, M., Yuen, K., Leung, C., Chan, K., Ip, P., Lai, R., et al., Human infection with influenza H9N2, The Lancet, 354(1999) 916–7.

Peng, X., Luo, G., Wu, Z., Wen, W., Zhang, X., Wang, S., Fluorescent-Magnetic-Catalytic Nanospheres for Dual-Modality Detection of H9N2 Avian Influenza Virus, ACS Appl. Mater. Interfaces, 11(2019) 41148-56.

Petryayeva, E., Algar, W.R., Multiplexed homogeneous assays of proteolytic activity using a smartphone and quantum dots, Anal. Chem., 86(2014) 3195–202.

Qiu, S., Zhao, F., Zenasni, O., Li, J., Shih, W.-C., Catalytic assembly of DNA nanostructures on a nanoporous gold array as 3D architectures for label-free telomerase activity sensing, Nanoscale Horiz., 2(2017) 217–24.

Rajeev, G., Xifre-Perez, E., Simon, B.P., Cowin, A.J., Marsal, L.F., Voelcker, N.H., A label-free optical biosensor based on nanoporous anodic alumina for tumour necrosis factor-alpha detection in chronic wounds, Sens. Actuators, B, 257(2018) 116–23.

Ramanathan, K., Bangar, M.A., Yun, M., Chen, W., Myung, N.V., Mulchandani, A., Bioaffinity sensing using biologically functionalized conducting-polymer nanowire, J. Am. Chem. Soc., 127(2005) 496–7.

Razola, S.S., Ruiz, B.L., Diez, N.M., Mark Jr, H., Kauffmann, J., Hydrogen peroxide sensitive amperometric biosensor based on horseradish peroxidase entrapped in a polypyrrole electrode, Biosens. Bioelectron., 17(2002) 921–8.

Reghuram, S., Arivarasan, A., Kalpana, R., Jayavel, R., CdSe and CdSe/ZnS quantum dots for the detection of C-reactive protein, J. Exp. Nanosci., 10(2015) 787–802.

Reiss, P., Protiere, M., Li, L., Core/shell semiconductor nanocrystals, small, 5(2009) 154–68.

Reshetilov, A., Bezborodov, A., Nanobiotechnology and biosensor research, Appl. Biochem. Microbiol., 44(2008) 1–5.

Reynolds, R.A., Mirkin, C.A., Letsinger, R.L., Homogeneous, nanoparticle-based quantitative colorimetric detection of oligonucleotides, J. Am. Chem. Soc., 122(2000) 3795–6.

Rogers, K., Recent advances in biosensor techniques for environmental monitoring, Anal. Chim. Acta, 568(2006) 222–31.

Saha, K., Agasti, S.S., Kim, C., Li, X., Rotello, V.M., Gold nanoparticles in chemical and biological sensing, Chem. Rev., 112(2012) 2739–79.

Satija, J., Tharion, J., Mukherji, S., Facile synthesis of size and wavelength tunable hollow gold nanostructures for the development of a LSPR based label-free fiber-optic biosensor, RSC Adv., 5(2015) 69970–9.

Schreiber, R., Do, J., Roller, E.-M., Zhang, T., Schüller, V.J., Nickels, P.C., et al., Hierarchical assembly of metal nanoparticles, quantum dots and organic dyes using DNA origami scaffolds, Nat. Nanotechnol., 9(2014) 74–8.

Sepúlveda, B., Angelomé, P.C., Lechuga, L.M., Liz-Marzán, L.M., LSPR-based nanobiosensors, Nano Today, 4(2009) 244–51.

Shamsipur, M., Kazemi, S.H., Mousavi, M.F., Impedance studies of a nano-structured conducting polymer and its application to the design of reliable scaffolds for impedimetric biosensors, Biosens. Bioelectron., 24(2008) 104–10.

Shang, L., Liu, C., Watanabe, M., Chen, B., Hayashi, K., LSPR sensor array based on molecularly imprinted sol-gels for pattern recognition of volatile organic acids, Sens. Actuators, B, 249(2017) 14–21.

Shi, J., Chan, C., Pang, Y., Ye, W., Tian, F., Lyu, J., et al., A fluorescence resonance energy transfer (FRET) biosensor based on graphene quantum dots (GQDs) and gold nanoparticles (AuNPs) for the detection of mecA gene sequence of Staphylococcus aureus, Biosens. Bioelectron., 67(2015) 595–600.

Shrivastava, A., Gupta, V.B., Methods for the determination of limit of detection and limit of quantitation of the analytical methods, Chron. Young Sci., 2(2011) 21.

Singh, M.P., Strouse, G.F., Involvement of the LSPR spectral overlap for energy transfer between a dye and Au nanoparticle, J. Am. Chem. Soc., 132(2010) 9383–91.

Szekacs, I., Orgovan, N., Peter, B., Kovacs, B., Horvath, R., Receptor specific adhesion assay for the quantification of integrin–ligand interactions in intact cells using a microplate based, label-free optical biosensor, Sens. Actuators, B, 256(2018) 729–34.

Takemura, K., Adegoke, O., Takahashi, N., Kato, T., Li, T.-C., Kitamoto, N., et al., Versatility of a localized surface plasmon resonance-based gold nanoparticle-alloyed quantum dot nanobiosensor for immunofluorescence detection of viruses, Biosens. Bioelectron., 89(2017) 998–1005.

Tate, J., Ward, G., Interferences in immunoassay, Clin Biochem Rev., 25(2004) 105.

Tereshchenko, A., Fedorenko, V., Smyntyna, V., Konup, I., Konup, A., Eriksson, M., et al., ZnO films formed by atomic layer deposition as an optical biosensor platform for the detection of Grapevine virus A-type proteins, Biosens. Bioelectron., 92(2017) 763–9.

Thévenot, D.R., Toth, K., Durst, R.A., Wilson, G.S., Electrochemical biosensors: recommended definitions and classification, Anal. Lett., 34(2001) 635–59.

Valeur, E., Bradley, M., Amide bond formation: beyond the myth of coupling reagents, Chem. Soc. Rev., 38(2009) 606–31.

Weerathunge, P., Ramanathan, R., Torok, V.A., Hodgson, K., Xu, Y., Goodacre, R., et al., Ultrasensitive colorimetric detection of murine norovirus using NanoZyme aptasensor, Anal. Chem., 91(2019) 3270–6.

Wei, H., Ratchford, D., Li, X., Xu, H., Shih, C.-K., Propagating surface plasmon induced photon emission from quantum dots, Nano Lett., 9(2009) 4168–71.

Wijaya, E., Lenaerts, C., Maricot, S., Hastanin, J., Habraken, S., Vilcot, J.-P., et al., Surface plasmon resonance-based biosensors: From the development of different SPR structures to novel surface functionalization strategies, Curr. Opin. Solid State Mater. Sci., 15(2011) 208–24.

Williams, R., Blanch, H., Covalent immobilization of protein monolayers for biosensor applications, Biosens. Bioelectron., 9(1994) 159–67.

Wu, J., Li, S., Wei, H., Multifunctional nanozymes: enzyme-like catalytic activity combined with magnetism and surface plasmon resonance, Nanoscale Horiz., 3(2018) 367–82.

Wu, Z., Zhou, C.-H., Chen, J.-J., Xiong, C., Chen, Z., Pang, D.-W., et al., Bifunctional magnetic nanobeads for sensitive detection of avian influenza A (H7N9) virus based on immunomagnetic separation and enzyme-induced metallization, Biosens. Bioelectron., 68(2015) 586–92.

Xia, L., Wei, Z., Wan, M., Conducting polymer nanostructures and their application in biosensors, J. Colloid Interface Sci., 341(2010) 1–11.

Xiong, L.-H., He, X., Zhao, Z., Kwok, R.T., Xiong, Y., Gao, P.F., et al., Ultrasensitive virion immunoassay platform with dual-modality based on a multifunctional aggregation-induced emission luminogen, ACS Nano, 12(2018) 9549-57.

Xu, J.Z., Zhu, J.J., Wu, Q., Hu, Z., Chen, H.Y., An amperometric biosensor based on the coimmobilization of horseradish peroxidase and methylene blue on a carbon nanotubes modified electrode, Electroanal, 15(2003) 219–24.

Xu, W., Xue, X., Li, T., Zeng, H., Liu, X., Ultrasensitive and selective colorimetric DNA detection by nicking endonuclease assisted nanoparticle amplification, Angew. Chem. Int. Ed., 48(2009) 6849–52.

Yang, F., Xu, Z., Wang, J., Zan, F., Dong, C., Ren, J., Microwave-assisted aqueous synthesis of new quaternary-alloyed CdSeTeS quantum dots; and their bioapplications in targeted imaging of cancer cells, Luminescence, 28(2013) 392–400.

Ye, H., Yang, K., Tao, J., Liu, Y., Zhang, Q., Habibi, S., et al., An enzyme-free signal amplification technique for ultrasensitive colorimetric assay of disease biomarkers, ACS Nano, 11(2017) 2052–9.

Ye, W.W., Tsang, M.K., Liu, X., Yang, M., Hao, J., Upconversion luminescence resonance energy transfer (LRET)-based biosensor for rapid and ultrasensitive detection of avian influenza virus H7 subtype, Small, 10(2014) 2390–7.

Yeom, S.-H., Han, M.-E., Kang, B.-H., Kim, K.-J., Yuan, H., Eum, N.-S., et al., Enhancement of the sensitivity of LSPR-based CRP immunosensors by Au nanoparticle antibody conjugation, Sens. Actuators, B, 177(2013) 376–83.

Zang, F., Su, Z., Zhou, L., Konduru, K., Kaplan, G., Chou, S.Y., Ultrasensitive Ebola virus antigen sensing via 3d nanoantenna arrays, Adv. Mater., 31(2019) 1902331.

Zeng, S., Yu, X., Law, W.-C., Zhang, Y., Hu, R., Dinh, X.-Q., et al., Size dependence of Au NP-enhanced surface plasmon resonance based on differential phase measurement, Sens. Actuators, B, 176(2013) 1128–33.

Zhang, C.-Y., Yeh, H.-C., Kuroki, M.T., Wang, T.-H., Single-quantum-dot-based DNA nanosensor, Nat. Mater., 4(2005) 826–31.

Zhang, H., Ma, X., Hu, S., Lin, Y., Guo, L., Qiu, B., et al., Highly sensitive visual detection of Avian Influenza A (H7N9) virus based on the enzyme-induced metallization, Biosens. Bioelectron., 79(2016) 874–80.

Zhao, F., Koo, B., Liu, H., Jin, C.E., Shin, Y., A single-tube approach for in vitro diagnostics using diatomaceous earth and optical sensor, Biosens. Bioelectron., 99(2018) 443–9.

Zhao, X., Cai, Y., Wang, T., Shi, Y., Jiang, G., Preparation of alkanethiolate-functionalized core/shell Fe_3O_4@Au nanoparticles and its interaction with several typical target molecules, Anal. Chem., 80(2008) 9091–6.

Zhou, J., Wang, Q.-x., Zhang, C.-y., Liposome–quantum dot complexes enable multiplexed detection of attomolar DNAs without target amplification, J. Am. Chem. Soc., 135(2013) 2056–9.